SHALLOW TRENCH ISOLATION PROCESS IN MICROFABRICATION FOR FLASH (NAND) MEMORY

A Thesis presented to
the Faculty of the Graduate School
at the University of Missouri-Columbia

In Partial Fulfillment
of the Requirements for the Degree
Master of Science

By

Niharika Garud

Dr. Gregory Triplett, Thesis Supervisor

May, 2008

The undersigned, appointed by
The dean of the Graduate
School, have examined the thesis entitled

Shallow Trench Isolation Process In Microfabrication For Flash (NAND) Memory

presented by Niharika Garud

a candidate for the degree of
Master of Science

and hereby certify that, in their opinion, it is worthy of acceptance.

Professor Gregory Triplett

Professor Jae W. Kwon

Professor Enos C. Inniss

I dedicate my thesis and my work to Mom, the most important person in my life.

ACKNOWLEDGEMENTS

I would like to thank my mentors, Dr. Gregory Triplett, Len Olmer, James Weil, for giving me support, encouragement and helping me out although my projects and my supervisors, John Moore, Brandon Eliason & Matt Miller. I would also like to thank all the members of Micron Technology who always stood by me during my stay at MTV, especially Joe Valliere, Brian Berry, Johnny Villanueva, Ananth for their cooperation.

I would like to thank my entire family for their unconditional support and my best friends for bearing with me.

TABLE OF CONTENTS

LIST OF TABLES

LIST OF FIGURES:

SUMMARY

Technology is steadily advancing where semiconductors and microelectronics have become such a huge source of revenue and area of technological interest, resulting in reduced device geometries and more complicated microelectronic fabrication methods. In this thesis, high density plasma oxide process has been discussed, which is widely used especially for shallow trench isolations on micro and nano-sized devices. The problem discussed here relates to the process and how it can be easily imbalanced due to inaccurate assumptions and process parameters. Etch-outs, as presented in this thesis, are the root cause of the problem and a model demonstrating various correlations with some noteworthy results has been developed.

CHAPTER 1

Introduction:

The semiconductor industry has been impacted by various issues in manufacturing. The gradual reduction in device geometries has driven fabrication processes towards alternative chemistry, chemical components and hardware setups, as well. The key driving force for manufacturability of devices with reducing geometries is continuous monitoring of the various excursions and scrap results. Most of the basic processes based on diffusion, etching, implantation, etc. are used in fabrication of almost all semiconductor devices. The process, which is studied extensively in this thesis, is high density plasma oxide process for shallow trench isolation - which comes under chemical vapor deposition processes. It is one of the most commonly used processes in a device fabrication environment. This chapter will include the introduction of effects due to reducing geometries and issues in high density plasma process.

Gordon Moore stated that the number of transistors on a semiconductor chip doubles about every two years [1]. Moore's Law is shown in Figure 1. Moore believed that the future of the integrated electronics is the future of electronics itself. By integrated electronics, Moore meant various technologies in microelectronics.

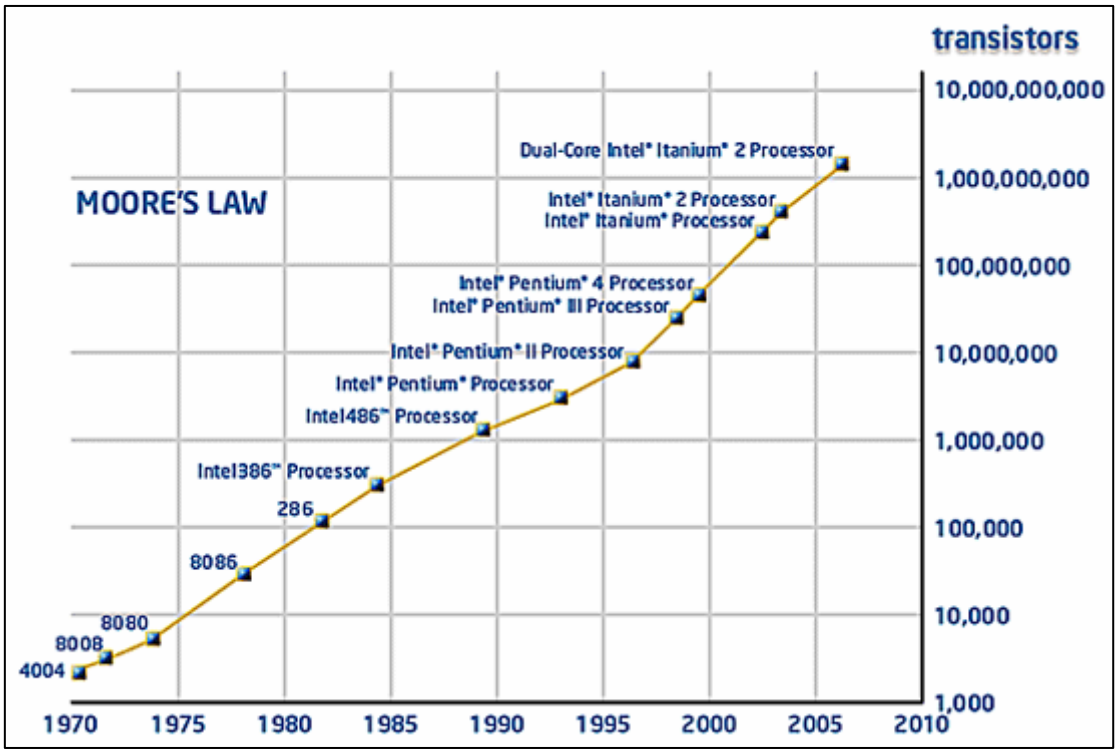

Figure 1. Moore's law: More Performance and Decrease in Costs.

Source: Intel Corporation, [20]

In scaling down device feature sizes,, there are numerous fabrication issues that come into play, for example, line edge roughness, dopant fluctuations, and device isolation. During various chemical vapor deposition processes while processing a silicon wafer, several barriers exist which hinder the uniform deposition of various compounds. It is challenging to determine processing conditions for achieving such uniformity for layers thinner than 4000Å, especially when it is a dynamic deposition-etching process. The research performed in this thesis explores a process where deposition and etching takes place together in order to attain perfect uniformity along with precise thickness. In such

processes, the balance between the two is crucial for maintaining uniformity as an end result.

In a deposition-etching process, equilibrium conditions can be challenging to control. When deposition or etching processes (due to sputtering) lose their direction, the surface becomes etched-out at random locations across the surface plane. In the case of high-density plasma silicon dioxide (SiO_2) process, silicon dioxide etches out near the edges of the structures. These anomalies are very small (in the range of 200Å) and cannot be discovered during immediate inspection steps until they are approximately 500Å or larger. Etch outs on the surfaces of the field oxide layer are further impacted by subsequent steps including chemical material planarization (CMP) step, CMP clean, CMP scrub for smoothing the top surface of the dioxide, and wet stripping of the field dioxide layer. The CMP steps and wet stripping cause the etch outs to enlarge, resulting in passage ways and short circuits in the product die.

The importance of the field oxide layer is best described using the basic Flash cell with dual gate transistors (see Figure 2). A Flash cell is basically a floating-gate MOS transistor or a transistor with a gate completely surrounded by dielectrics, the floating gate (FG), and is electrically governed by a capacitively coupled control gate (CG). Being electrically isolated, the FG acts as the storing electrode for the cell device. Charge injected in the FG is maintained there, allowing modulation of the "apparent" threshold voltage (i.e., seen from the CG) of the cell transistor [2]. In this device, the tunnel oxide used is silicon dioxide, which is deposited using the high density plasma process.

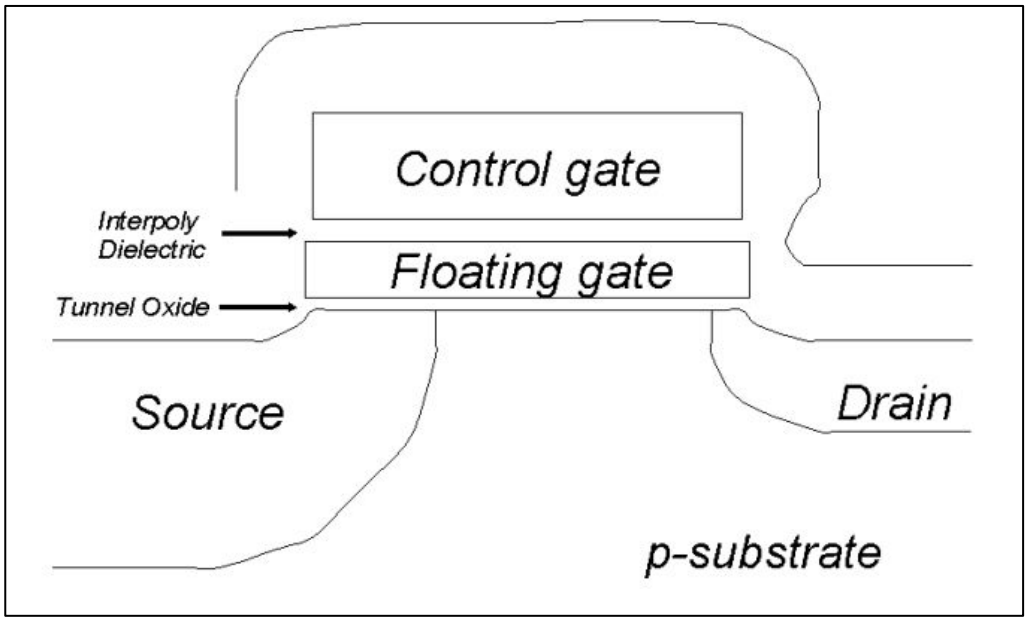

Figure 2. Schematic cross section of a Flash cell [2]. The floating-gate structure is common to all the nonvolatile memory cells based on the floating-gate MOS transistor [2].

As illustrated in Figure 3, when there are several holes or etch outs in the field oxide layer, the floating gate would be in direct contact with the substrate, source, drain or all of them together causing the Flash cell to malfunction.

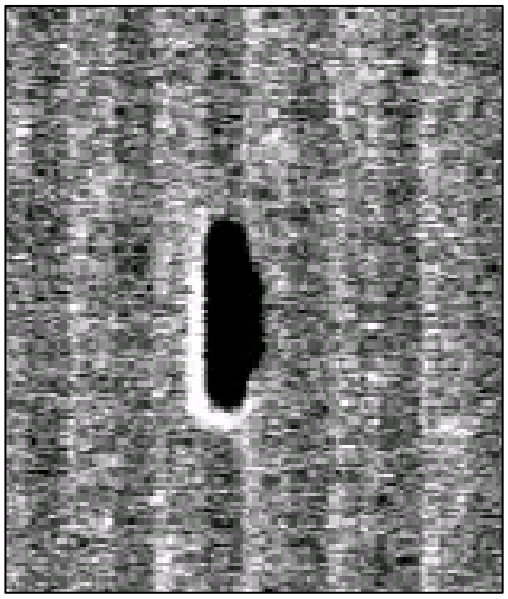

Figure 3. Scanning electron microscopy image of an Etch-out on a silicon device [3]

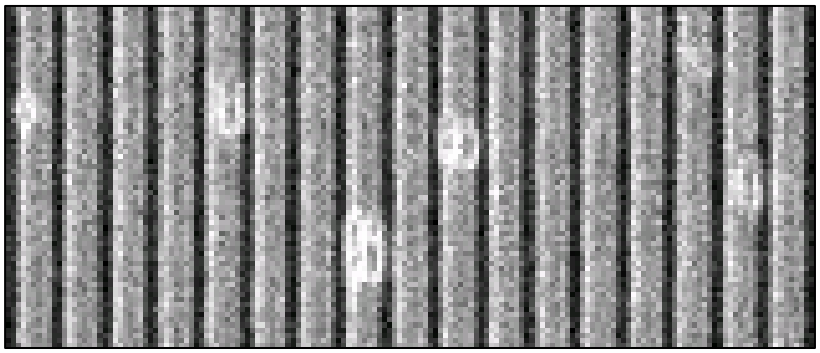

Figure 4. Scanning electron microscope image of several etch-outs on a field oxide layer [3]

Figure 4 illustrates typical etch-out. Etch-out usually contains a flat and a convex side. In Figure 5, a similar defect can also be seen. This is also known as a void, typically centered between two circuit structures. Therefore, it is likely that small structure sizes

would contain more etch-outs and larger ones would contain more voids as demonstrated through previous experiments. In essence, the larger structures have much smaller gaps to fill between them, hence resulting in a void illustrated in Figure 5.

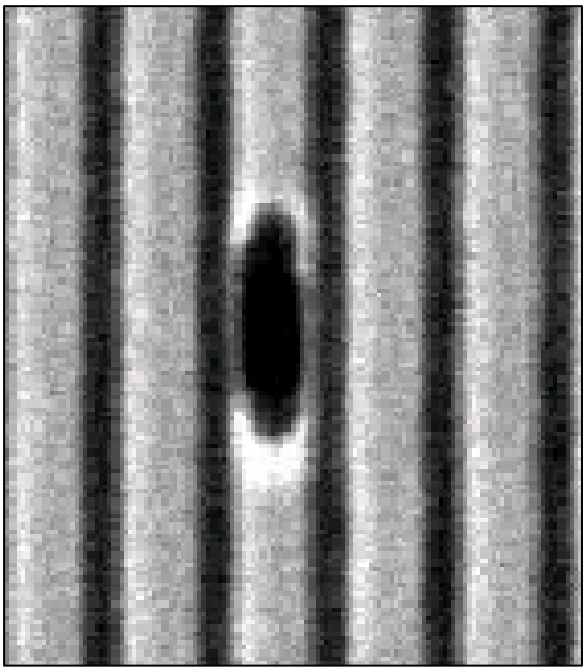

Figure 5. Scanning Electron Microscopy image showing a void. [3]

Voids, like those in Figure 5, were observed through various experiments on various product wafers as well as test wafer lots. Upon further analysis of each of these images, the high density plasma process was pinpointed as the source for such particular scrap wafers.

The trench isolations (in Flash cells) were also affected as illustrated in the Figure 4. Short circuiting occurred leaving the entire die with little or no memory function.

Reworks at later stages in attempt to address etch-out problem was unsuccessful leading to restrictions for exploring solutions at the process step.

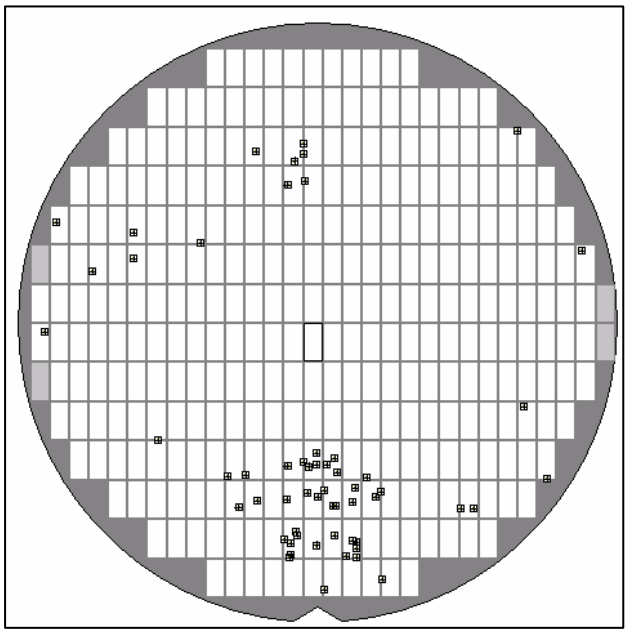

Figure 6. A silicon wafer from the process line with etch-outs. [3]

In Figure 6, a wafer (from a fabrication line of memory cells) with etch-outs due to the HDP (high deposition plasma) step is shown. Other lot wafers consisted of etch-outs that were located towards the center of the wafer. Normal inspection with a scanning electron microscope did not reveal shading (an indication of etch-out), so etch-outs could not be identified in the middle of the manufacturing process in the memory cell process. Etch-outs were first discovered at the probe step after completion of the entire process. This is unsatisfactory from a fabrication standpoint as numerous wafers were lost, resulting in wasted man power, equipment over use, depletion, and lower product yield.

Tools employed in this thesis were the same as those on the production line. The process chambers, loadlocks, and transfer chambers were examined before running any design of experiments (DOE). However, the experiments discussed in this thesis were performed on process chambers, which served as the most likely candidates for etch outs.

Due to the Non Disclosure Agreement with Micron Technology, description and the exact details of their process, the process recipe, the product details are not discussed. Therefore, the data presented is appropriately normalized.

The remainder of this thesis is focused on experiments, which were conducted to investigate the onset of etch-outs. This study also includes closer examination of the plasma process, specifically, the influence of sputtering and deposition processes. The thesis also includes results of HDP experiments, and related research regarding these fabrication challenges. The processes, mechanisms for sputtering and deposition, and hardware set up are discussed in the following chapters.

.

CHAPTER 2

BACKGROUND INFORMATION & PROCESS DETAILS

In this chapter, plasma processes and sputtering are discussed, beginning with the basics of the process and concepts behind deposition and high density plasma. This chapter also includes a section on Paschen's law, which has been useful for exploring correlations between chamber pressures and applied voltages employed at different steps for any process during any microelectronic fabrication.

A. High Density Plasma Process:

The high density plasma silicon dioxide process involves deposition and sputtering in various steps inside the process chamber. The overall thickness of silicon dioxide on the wafer is obtained in multiple deposition steps rather than one long step. The time duration for each step depends on the target thickness and parameters used for the process recipe. This section begins with the structure of silicon dioxide and then concludes with further details about the entire process and mechanisms involved during high density plasma process.

i. The Structure of Silicon Dioxide:

In microelectronic fabrication, SiO_2 is also referred to as fused silica. It is amorphous and thermodynamically unstable below 1710ºC. The structure contains two oxygen atoms and one single silicon atom in the center. There exist covalent bonds between oxygen and

silicon, and this satisfies the silicon valence shell. Now, if each oxygen atom is attached to two polyhedrons, the oxygen valence is also satisfied. This structure is called quartz, where oxygen atoms are located at the corners of a triangular polyhedron.

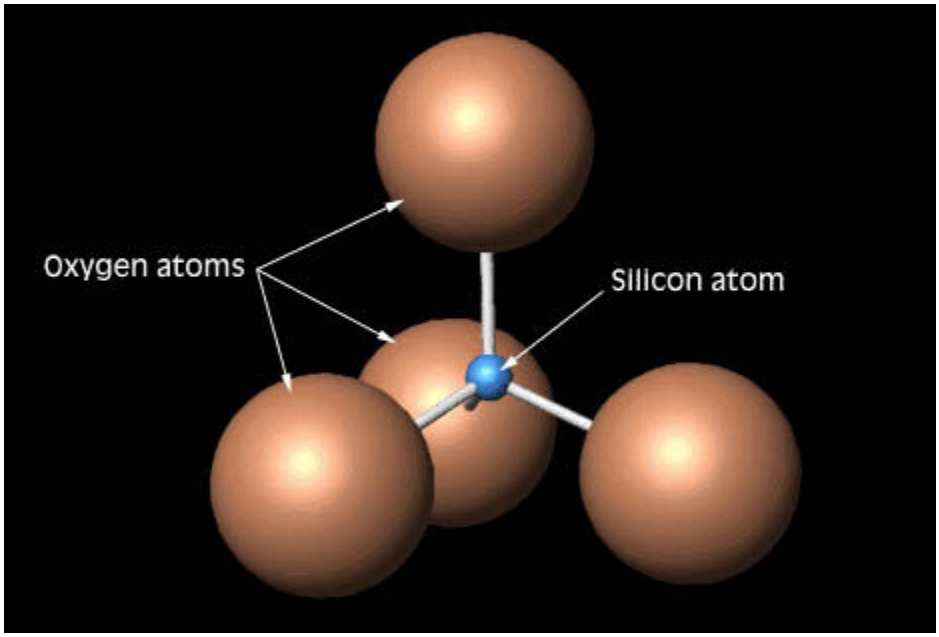

Figure 7. Structure of Quartz [4]

As shown in Figure 7, one silicon ion is covalently bonded to four oxygen ions. Notice that the silicon ion is significantly smaller than oxygen atoms. In fused silica, some oxygen atoms, called bridging oxygen, are bonded to two silicon atoms. Some oxygen atoms are non-bridging, bonding to silicon atoms. During the HDP process, thermally grown SiO_2 consists primarily of randomly oriented polyhedrons. The larger the fraction of bridging to non-bridging sites, the more cohesive and less prone to damage the oxide becomes. Unfortunately, not all oxides are identical. Dry oxides have a much larger ratio of bridging to non-bridging sites compared to wet oxides. Moreover, a variety of

impurities exist in thermal oxides, like water related complexes. If H_2O is present during oxide growth, one reaction that can occur is the reduction of a bridging oxygen site into two hydroxyls:

$$Si:O:Si + H_2 \rightarrow Si:O:H + H:O:Si$$

These hydrogen atoms are weakly bonded and can be removed under electrical stress or ionizing radiation, leaving a trap or potential charged state in oxide. Conveniently, other impurities can be intentionally incorporated into thermally deposited SiO_2 to change its physical properties. When impurities replace the silicon atom, they are called network formers, like boron and phosphorus, which tend to reduce bridging to non-bridging ratios. Such impurities are normally used in deposited oxides rather than in thermal oxides.

ii. The concept of Plasma:

In 1942, the American chemist Irving Langmuir investigated the electrical discharges in gases and in 1929, while experimenting together with another American scientist, Levy Tonks, used the term plasma to describe the oscillations of the electron cloud during the discharge. The cloud was similar to a jelly which reminded Langmuir of blood plasma. However, the term plasma in Langmuir's experiments is completely misleading. The plasma term in physics describes a gas of electrons and ions (atoms which have lost one or more electrons), while the plasma in blood is a clear yellowish fluid in a liquid form in which the blood cells are carried [5].

In physics, plasma is often described as the fourth state of matter after solid, liquid and gaseous states. Now, a gas is normally an electrical insulator, that is, electric currents cannot easily pass through it. By heating the gas to appropriate temperatures, the

insulator gas becomes a good electric conductor. The gas is transformed into α plasma, which consists of free electrons: the carriers of electric current. The electrons in atomic gas are buried safely; the ones in plasma are free to move around. In short, plasma will conduct electricity because the free electrons can easily be moved.

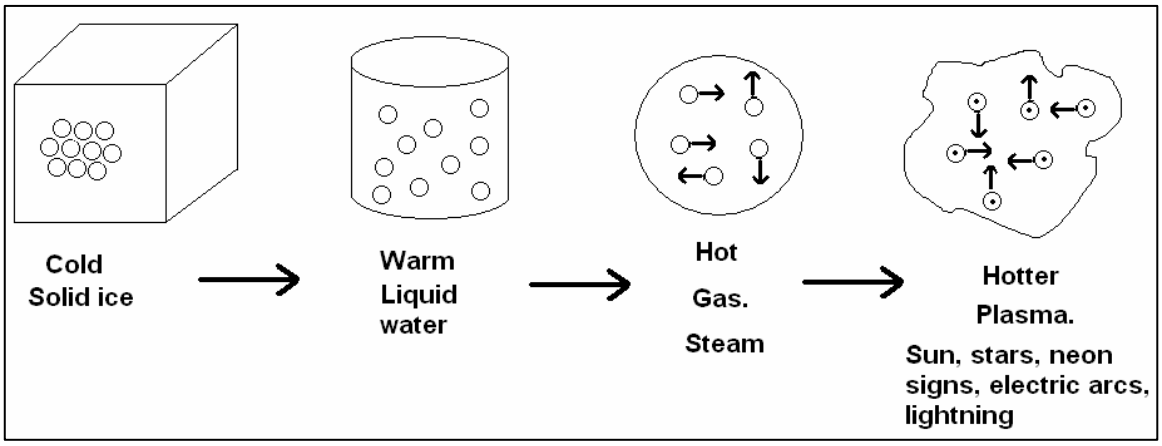

Figure 8. The four states of matter, and plasma, which is also referred to as fourth matter.

If molecules in the gas state acquire more energy, they will first dissociate into the atoms forming the molecule. The supply of atoms with more energy causes the electrons to leave the atoms and move freely inside any confined space. Plasma is formed as a result. Materials can be brought to a gaseous state by inserting the appropriate amount of energy. In a process chamber, the molecules or atoms move freely inside the vessel, colliding mainly with the walls of the vessel.

If energy in the system is further increased, the molecules break up into their atomic constituents and in the same fashion, with more energy supplied, the atoms will lose electrons. As soon as they lose electrons, a positive charge is acquired (positive ion).

Therefore, ions and electrons from any material can be produced by adding enough energy. [5].

iii. Radio Frequency (RF) discharges:

In an RF discharge, the power supplied interacts with the plasma almost exclusively by displacement current (the electrodes are not necessarily in contact with the plasma). The radio frequency power creates displacement currents inside the plasma and delivers energy to the plasma. The RF, in comparison with the DC method, can be advantageous since the material of the electrodes may introduce impurities into the plasma. The interaction between plasma and RF power can be inductive or capacitive. These methods are discussed below.

Induction transfers power to plasma in the same way as a transformer transfers the power from one line to another. A coil connected to the RF power supply is wrapped around a plasma quartz tube causing the energy to be transferred in an inductive way. This plasma is maintained in a steady state by the RF power supplied to the coil. The RF used is between frequencies of 10 kHz (kilohertz) and 30 kHz (kilohertz). The gas pressure in these devices is usually below one atmosphere, although in some applications atmospheric pressure can be used.

In capacitive coupled RF plasmas, two electrodes connected to the RF power source are used instead of the coils. This method operates between 1 to 100 MHz and the plasma is directly heated by RF electric fields.

A glow discharge can be produced at atmospheric pressure by using a high voltage RF at kHz frequencies. This plasma can exist in steady state at one atmospheric

pressure in air or other gases and does not require a vacuum system as in the case of DC plasma discharge [5].

iv. Material Modifications by Plasma:

Plasma modification of materials is used to improve the surface properties without changing their bulk properties. Plasma modification for various materials is carried out by ion implantation into the material. This method has become economically attractive in high tech centers and can be accomplished on metals and alloys, semiconductors, ceramics, insulators and polymers.

The refractory metals are best deposited by plasma using the sputtering or plasma assisted chemical vapor deposition (PACVD). Plasma is used in a reactor to initiate chemical reactions with an electric discharge in a gas. In any standard CVD process, high temperatures are used for the interactions between substrate and the vapor from the gas used during the process, but such high temperatures may cause damage to the substrate.

Through the use of PACVD, the ions are attracted from plasma toward the substrate at high temperatures. The substrate can be kept at lower temperatures as compared to CVD method. In a plasma polymerization method, similar to PACVD, the deposition is for organic materials like polymers. In PACVD, the deposition is for inorganic materials. A simple example is when tetrafluoroethylene gas is injected into plasma and a layer like Teflon gets deposited on a substrate. Plasma turns this gas into fragments and one of the following can happen:

1) Either they nucleate into a polymer film at the surface of the substrate.
2) Or polymerize into a chain of clusters.

Monomers, if introduced under suitable conditions into a plasma environment, can combine to create polymers. Polymers are nothing but repeated units of one or more compounds. Plasma processing can produce thin polymers films necessary for coating of other materials, multiple layers for magnetic recording tapes or disks, and plastic wrapping materials. The surface properties that can be modified by plasma assisted chemical vapor deposition are the following: hardness of the material; fatigue or extreme weariness from prolonged exertion or stress; toughness or the ability to withstand great strain without breaking or physical damage; adhesion or the ability to stay in a united form; friction or the resistance of a surface with another surface for relative motion; corrosion due to chemical actions; resistivity or the ability of opposing an electrical current to pass through; oxidation or the ability to combine with oxygen; dielectric properties (insulator materials capable of maintaining an electric field with minimum loss of power). Plasma can be used to extract ions in order to implant them into the materials to be modified. A strong electric field exists in plasma near the cathode (the cathode sheath).

B. The concept of Sputtering:

Sputtering is the primary alternative to evaporation for metal film deposition in microelectronics fabrication. It was discovered in 1852 [6] and further developed as a thin film deposition technique by Langmuir in the 1920s [7]. Sputtering has a better coverage than evaporation, induces far less radiation damage than electron beam evaporation, and is much better at producing layers of compound material and alloys.

Figure 9 represents a sputtering process chamber with electrostatic chuck, gas feed & power supply.

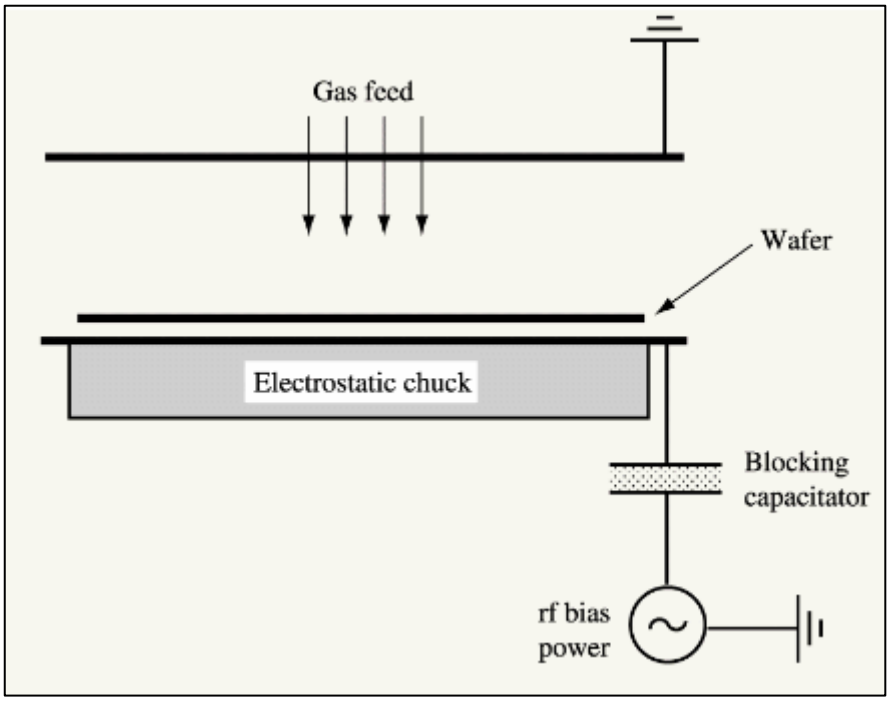

Figure 9. Schematic of a traditional parallel-plate (diode type) plasma reactor [7]

In sputtering applications, the chamber must be arranged so that high energy ions strike a target containing the material to be deposited. During sputtering, the target material, not the wafers, must be placed with maximum ion flux given to the electrode. For maximum deposition, the cathode and anode are closely spaced in the range of 10cm. The inert gas is supplied in the chamber and the process chamber, under vacuum, is around 0.1 Torr. For elemental metals, dc sputtering is usually favored due to large sputter rates. When depositing silicon dioxide (insulating materials), an RF plasma is commonly used [8].

If the target material is an alloy or compound, the stoichiometry of the deposited material may be slightly different than the target material. A material with a lower sputter yield will accumulate on the surface of the target until the composition of the deposited is approximately that of the bulk target [9]. (True only if the target temperature is kept sufficiently low to prevent solid state diffusion.) This makes sputtering very attractive for elements as well as for wide range of materials.

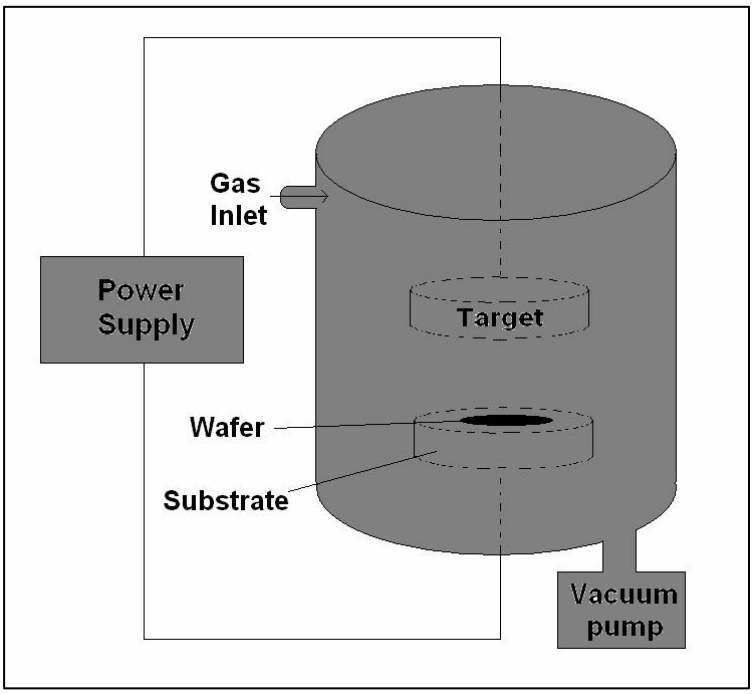

Figure 10. A simple chamber with parallel plate sputtering system

C. The Physics of Sputtering:

The Paschen's law is very important when investigating the correlations between the applied pressure and energy. It gives the required breakdown voltage for initiation of plasma across a gap containing a low-pressure gas:

$$V_{bd} \propto (P * L) \div (\log P * L + b)$$

Where V_{bd} is voltage needed for the breakdown, P is the chamber pressure, L is the electrode spacing, and b is the constant. Once the plasma is formed, ions are accelerated toward the negatively charged cathode. When they strike the surface, they release secondary electrons, which are accelerated away from the cathode to anode. If the energy transferred is less than the ionization potential of the gaseous species, the atom can be excited to an energetic state and then decays through optical transition, providing the characteristic glow. If the transfer of energy is high enough, then the atom will ionize and be accelerated toward the cathode. The bombardment of the cathode in this ion stream gives rise to the process of sputtering.

When an energetic ion strikes the surface of the material, there are several possible occurrences. Ions with very low energies may simply bounce off the surface. At energies of less than about 10eV, the ion may also absorb on the surface, giving up its energy to phonons (heat). At energies above about 10keV, the ion penetrates into the material many atomic layer spacings, depositing most of its energy deep into the substrate, where it changes the physical structure. These high energies are typical for ion implantation. Between these two extremes, both energy transfer mechanisms occur. Part of the ion energy is deposited in the form of heat and the remaining goes into substrate's physical rearrangement. At this energy, nuclear stopping at the surface is effective: most

of the energy transfer occurs within several atomic layers. During this time, substrate atoms and cluster of atoms will be ejected from the surface of the substrate. The atoms and atomic clusters ejected from the cathode escape with energies of 10 to 50 eV. This is about 100 times the energy of evaporated atoms. This additional energy provides sputtered atoms with additional surface mobility for improved step coverage relative to evaporation. At typical sputtering energies, about 95% of the ejected material is atomic and rest of them is diatomic molecules [10].

At high energies such as those used in implantation, chemical bonding processes can be largely ignored, and the target can be considered as simply a collection of atoms. At very low energies, no disruption of the target occurs and at sputtering energies, the physics of the material removal is quite complicated, involving the coupled effects of bond breaking and physical displacement. The figure below represents a model showing some processes that may occur when an ion is striking the surface. This model was developed by Wehner and Anderson [11, 12]. Ignoring chemical effects and treating the substrate atoms as hard spheres provides at least a qualitative picture of sputtering. An ion incident on the target surface may travel several atomic layers into the target until it strikes an atom

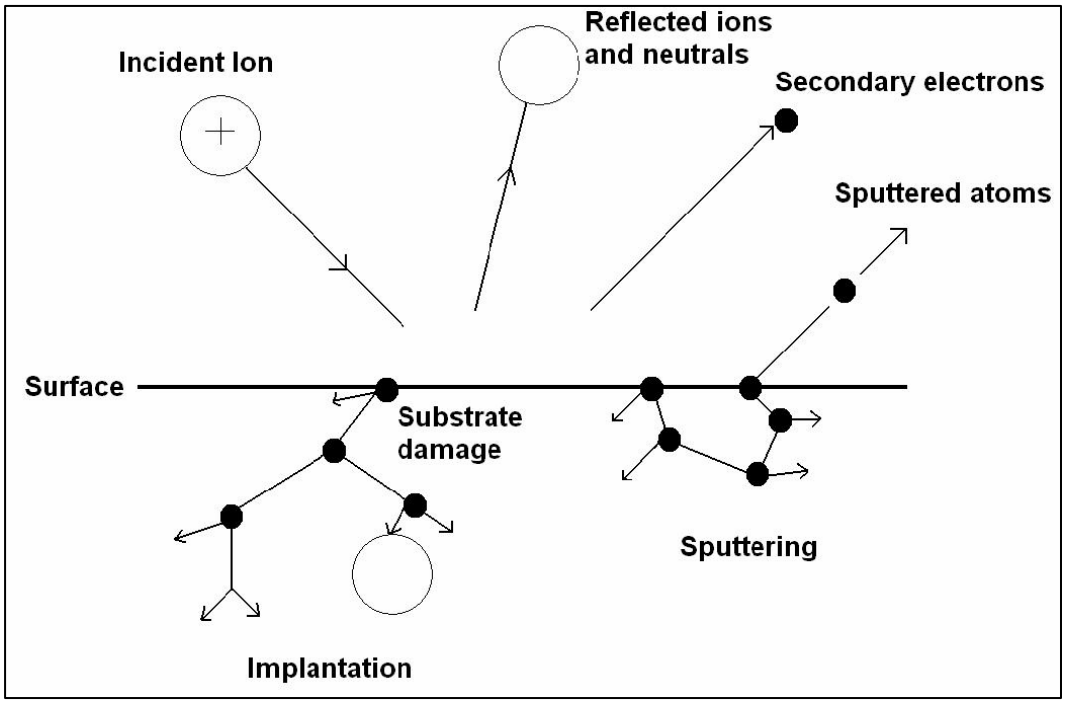

Figure 11. Possible outcomes for an ion accident on the surface of a wafer

D. Shallow trench isolation:

Semiconductor technology is steadily advancing, making the circuit elements and interconnections on wafers, or silicon substrates smaller and denser at every development step. In order to prevent unwanted interactions between these micro and nano sized circuit structures, insulator-filled gaps or trenches are provided between the circuit structures to physically and electrically isolate the elements and conductive lines. Now, the circuit densities further increase and hence the width of these gaps decreases causing the gap aspect ratios (AR) to increase, filling these narrower gaps becomes more difficult. Discontinuities in the insulation or gap filling material, unwanted etch-outs, voids, etc. come into play leading to disposal of the whole circuit or final product [13].

High deposition plasma process is used to fill the high aspect ratio gaps with silicon dioxide as the deposition layer. The deposition of silicon dioxide and other thin films such as silicon nitride is achieved by plasma enhanced chemical vapor deposition (also known as PECVD) technique at low temperatures [14, 15]. In the traditional PECVD process, the issue remains the radiation damage on the substrate, interface, and growing film surface due to bombardment of highly energetic charged particles that cannot be avoided. In addition, when silane and oxygen gases are source gases for the deposition of silicon oxide, generally speaking, Si–H and Si–OH bonds are introduced into the film. The incorporation of these bonds degrades the properties of PECVD silicon oxide chemically[16]. However, a typical HDP oxide deposition deployed in CVD has a gas mixture containing oxygen, silane, and inert gases, like argon, to achieve simultaneous deposition and etching and hence, the unwanted bonding of silane with hydrogen and with hydroxyl is also minimized by choosing the right gas configuration. An RF bias is applied to the wafer substrate in the process chamber. The ions of some molecules, especially argon gas, are formed by ionization in the plasma and accelerate toward the wafer surface as RF bias is applied to the substrate. When these heavy ions hit the surface, the material present on the wafer gets sputtered (etched or removed) due to this striking. Hence, dielectric material deposited on the wafer is sputter etched at the same time to keep the gaps open during the deposition process [13].

E. The Paschen's Law and Curve:

The Paschen's curve and Paschen's law aids in understanding the correlation between the applied pressure in the process chamber and the energy acting inside on the gas particles.

Primary ionization of gas occurs due to natural radioactivity or generated conditions of high temperature and pressure which is otherwise insulating. Ions and electrons hence produced are directed by external electric field. (Paschen's curve for air is provided in Figure 12.)

During the voltage increase, the current increases up to a certain value, called saturation current, where all the particles formed by external ionization take part in the conduction of current. If the voltage keeps increasing then electrons gain sufficient energy to able to ionize the gas molecules by collision (α-process). This current is not self-maintained because it depends on external ionization source or the applied electric field. The law essentially states that, at higher pressures (above a few torr) the breakdown characteristics of a gap are a function (generally not linear) of the product of the gas pressure and the gap length, usually written as V= f(pd), where p is the pressure and d is the gap distance.

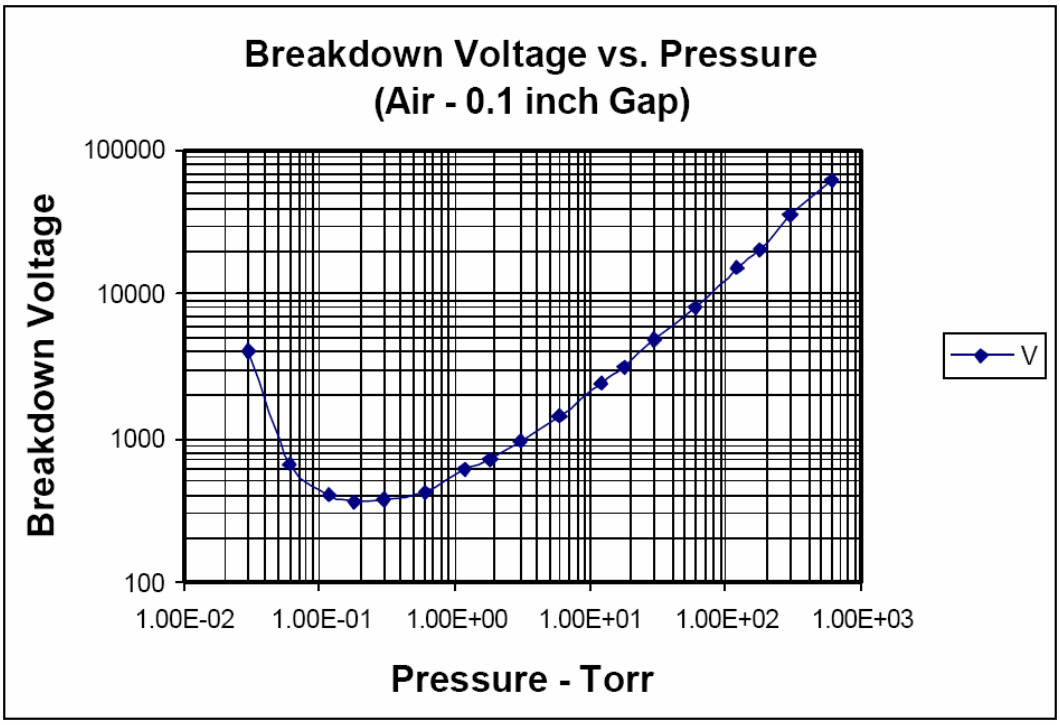

Figure 12. The Paschen's curve for air, two flat parallel copper electrodes for pressures between $3x10^{-2}$ torr and 760 torr [19].

Paschen's curve gives the dependence of the intensity of the breakdown voltage, $V_{p,}$ and the **p*d** product, where **p** is pressure, **d** is the gap between electrodes, γ-coefficient represents the efficiency of producing secondary electrons per ion hitting the electrode and it depends on the cathode material, the ion itself and its energy which is determined by the ratio E/N (E - electric field, N - gas particle number density). Since the positively and negatively charged particles have different masses the positive and negative charges move with different speed so that the space charges do not compensate one another completely [17].

The Paschen's curve hence defines the relation of chamber pressure and the energy which shows the same behavior for all kinds of gases. The breakdown voltage U,

between two parallel plane electrodes is a function of the product of distance **d** between the electrodes and gas pressure **p** [18].

The ions can, however, produce additional ionization by producing secondary electrons from the surface of the cathode (γ-process). When a number of secondary electrons become equal to the number of electrons that initiated the discharge, it becomes self-sustained and external ionization is not necessary for the discharge current to flow. The voltage at this moment is called a breakdown voltage and for the higher voltages, the current is self-maintained.

F. High density plasma oxide process for deposition of silicon dioxide:

As discussed earlier, the process involves various factors including RF bias applied on the substrate of wafer (RF power), oxygen gas, silane gas, an inert gas like argon or deuterium, a high chamber pressure, a range of high temperatures during various steps through the process recipe for acquiring the needed thickness of silicon dioxide over the wafer.

The power applied is LF (low frequency) power, HF (high frequency) power, and MF (medium frequency) power. LF and HF powers are the main regulatory factors for the total applied power. MF power is used for fine tuning purposes. In the diagrams representing the HDP process, the wafer substrate is referred to “a”, the circuit elements are known as “C1” and “C2”. The gap between the two circuit elements is named as “g”. Figure 13 shows the HDP process.

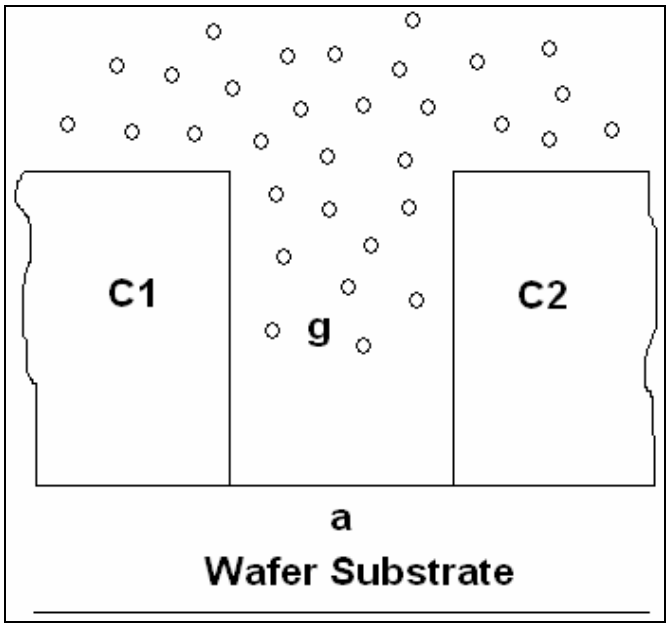

Figure 13. The HDP process for silicon dioxide where the ions start moving towards the wafer substrate due to the effect of RF biasing and starting striking the surface.

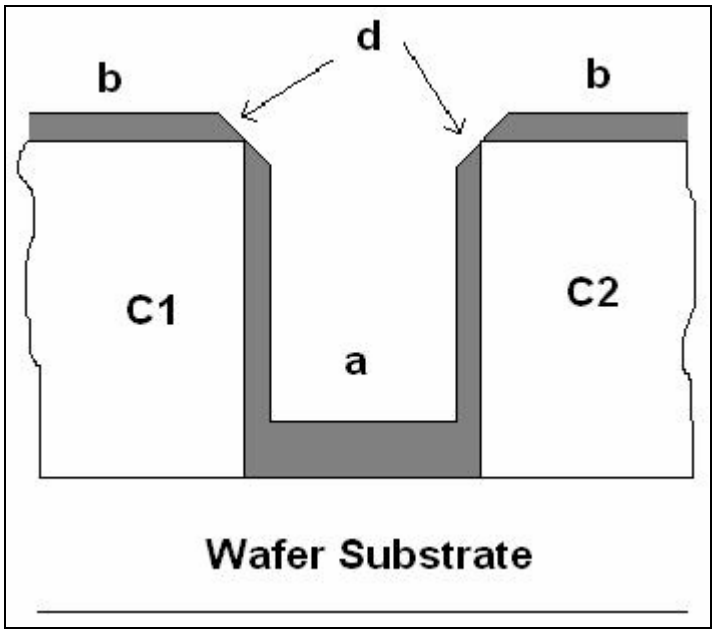

Figure 14. The figure above shows the deposition taking place as a thin layer in the gap and on the top of the circuit elements.

In the Figure 14, the deposition of oxide is lesser on the edges of the structures. This provides a slant shape to the deposition layer. The slant shape formed during the deposition process is due to the simultaneous sputtering – deposition. The sputtering or etching continues and their impact appears more in the corner areas. Therefore, the deposition rate on the corners is lesser than the deposition rate in gaps or on the top of the circuit elements.

As seen in Figures 13 & 14, these cases can vary according to various sputter to deposition ratios. It is unacceptable to support a high sputter to deposition ratio as it would create voids and etch-outs even when the deposition time is kept sufficiently high. If the process time is long, then deposition is uneven at various locations on the wafer, depending on the structures present on it. Hence, longer etching (wet or dry) step or

chemical material planarization (CMP) step are necessary facilitate even oxide layer deposition.

If the thickness is particularly high (around 5000Å), CMP step can not be used to remove it. It can only be used for making the rough surfaces smooth enough, while etching steps would be more suitable for removing the thick oxide and achieving the required thickness of the oxide layer.

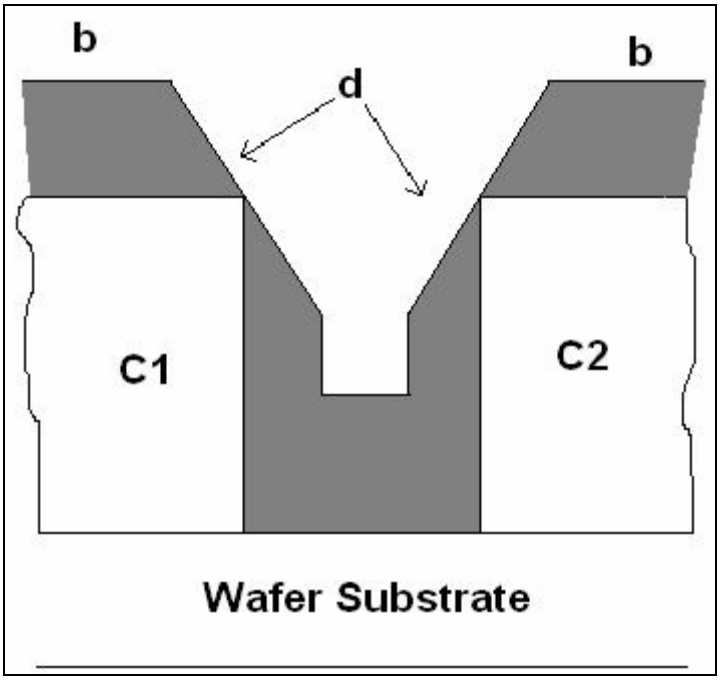

Figure 15. The figure shows the deposition layer getting thicker with deposition time. The height of the deposited layer increased everywhere, except for the corners.

As illustrated in Figure 15, during HDP, the gap gets filled and the peak height and its width depend on how wide the circuit element is. Now, if the peaks become tall, the

temperature, power and pressure of the process chamber would start impacting it along with sputtering – deposition mechanism. The temperature of the wafer can be between 400 to 700º C and hence, the peaks either bend or melt. The melting point of silicon dioxide is as high as 1650 (±75) °C, but due to excessive pressure along with high range of temperatures, the shape of the peak can be affected.

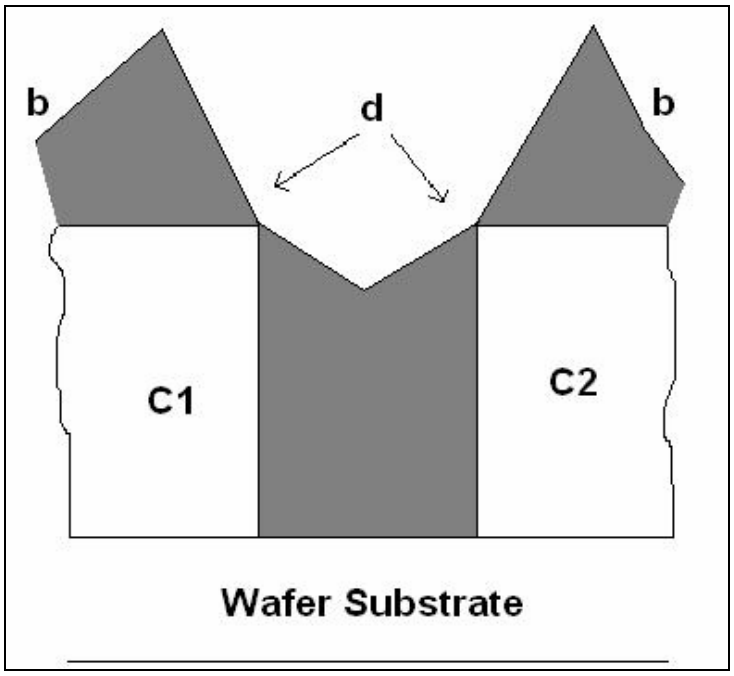

Figure 16. The figure shows the peak formation after a longer deposition time during simultaneous sputtering – deposition action on the wafer circuit elements.

When the peaks bend, the corners get covered and a loop forms. This is shown in Figure 18 where a small gap is created. Figure also shows how the entire layer of STI HDP oxide is deposited on the wafer with a great thickness, but the etch-outs remain present at

the corners. They are not filled during the deposition process and, even further the deposition started continues on the top surface.

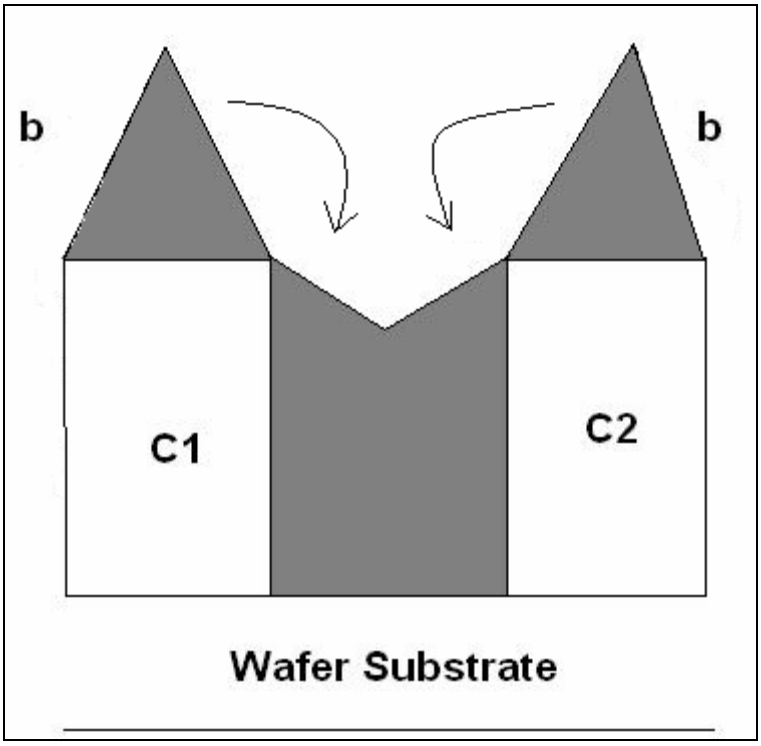

Figure 17. The figure above represents the peaks actually bending downwards toward either direction.

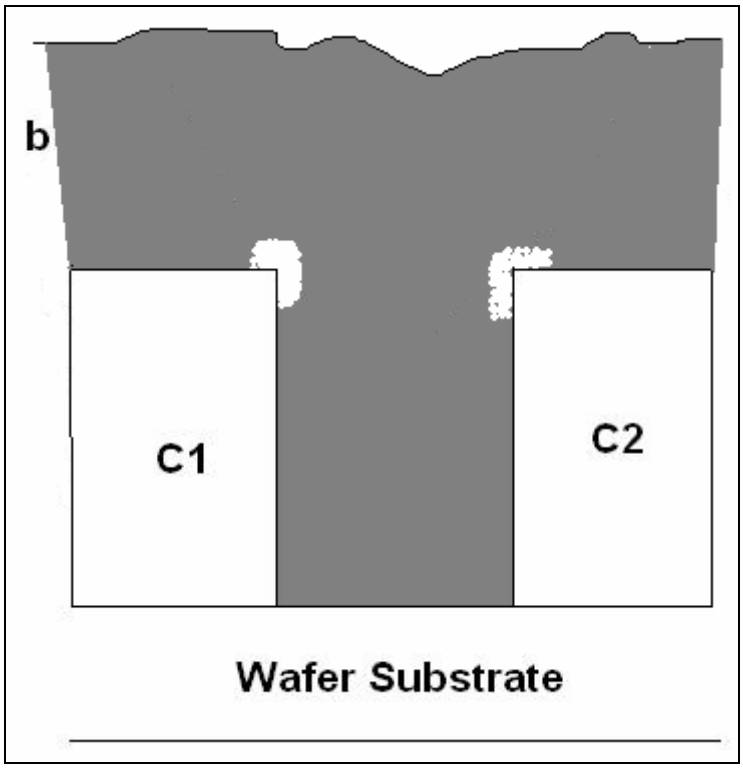

Figure 18. The figure in the next page shows the peaks formed and bending down towards the trenches, hence creating a hole or an etch-out.

Through the step by step procedures of HDP process, it is observed that any imbalance can create an excursion which can not be seen or detected in steps immediately following HDP. Circuits fail to perform at testing or probe steps and the whole product is scrapped. The results are disastrous as the entire process is wasted.

Alternative reasoning that describes etch-out is excessive sputtering at corners. This potentially creates huge spaces at ends of the structures, hence, resulting in etch-outs in later stages when the oxide layer is removed through etching process. Wet etching would enlarge the already huge gaps on the corners.

In the next chapters, the data collected (through a screening design) is introduced. This includes key parameters that affect the process' sputtering mechanism and the details of experiments which were conducted using ten test wafers. Background information, process details, and other basics introduced in this chapter aid in understanding the model created. The plasma, sputtering, and RF discharge mechanisms are similar and the physics involved behind Paschen's law are applied to the process recipes. A designed experiment provides clarity on etch-out recreation.

Chapter 3

A. The design of experiment (DOE) and the model:

In this chapter, the experiment performed is discussed and the analysis of data is presented. The original set of data and its model is not provided due to the Non Disclosure Agreement with Micron Technology. The data set is normalized along with the analysis. The two are in sync with the original model and data; hence the analysis and the reporting of these results are noteworthy.

DOE (design of experiment) is designed using JMP© (software by SAS) and the analysis and the modeling are also performed using this package. This statistical analysis tool produced prediction plots, interaction plots, bivariate analysis, and other fitting plots on the basis of summary data. The key factors for this experiment were selected on the basis of previous experiments and observations made when the process became imbalanced due to etch-outs.

The key factors used include low frequency power, high frequency power, and deuterium gas flow. The entire process recipe for this experiment was divided into two parts: one was the deposition step, and the other was sputtering step. Note that these steps have the names not according to the mechanisms involved during the steps, but due to the effect of steps overall. The deposition step, for example, has sputtering and deposition taking place at the same time on the test wafer, but the level of deposition is dominating during this step. Similarly, the sputtering step has the sputtering factor dominating the deposition mechanism but in both the steps, sputtering and deposition are taking place at

the same moment. One added difference between the two steps is that deuterium gas flow is not present in second step, which is the sputtering step. The deuterium gas flow is only involved during the deposition step and hence, the value of the gas flow was kept zero during the sputtering step for test wafers of DOE.

The screening design was used to explore these three parameters as it utilizes the minimum number of data points, but provides enough statistical significance for determining the correlation between the parameters. In this study, full factorial, with three factors, was employed that include ten total runs. The eight runs having varied parameters and two runs having the original recipe values. The numbers of center points taken in the experiment are set to 2.

No effect up to two-way interactions aliased with any other effects higher than two-way interactions was set by JMP for this kind of configuration. The deposition time for each step of the experiment was similar to the original process recipe and sputter to deposition rate was also kept the same as in original recipe. The measure of sputter – deposition rate is derived from total power (LF + HF + MF) applied during the step.

The total power didn't exceed 12 kW due to hardware limitations (the process tool used was Novellus Speed and some pictures are shown below). Although each generator is rated at 8000W, the system power is limited to this sum (eg: LF = 7000W, HF=5000W). Hence the power limitations for variations are while changing the values for each test recipe for each wafer.

Deposition-Etch-Deposition Optimization and the parameters to optimize for trench fill include: sputter to deposition ratio in the first step and of the second step, deposition of the first step versus deposition of second step that is the total thickness %,

etch amount (time of the step), etch type (rate and uniformity with respect to LF biasing, HF biasing, Argon gas flow and Helium gas flow), deposition of the liner for thickness, uniformity and HF biasing, film's stack thickness uniformity.

Factors were chosen to vary by 3% of their original value to achieve the experiment process recipes. The normalized values thus obtained are provided in Table 1. The values have been normalized with respect to the maximum value of the parameter obtained (that is the original value + 3% of the original value).

Table 1. The experiment factors with normalized values for parameters

LF Power	HF Power	D2 Flow
1	1	1
0.970874	0.970795	0.969828
0.941748	0.941752	0.94181

The algorithm used to create the recipes with maximum and minimum values of the factors is given by JMP and is provided in the Table 2 where 0 represents the original recipe values, which are unchanged, + represents the values incremented by 3% of the original value of the parameter and represents the values reduced by 3% of the original value of the parameter.

Table 2. The algorithm for design of experiment

++−
+++
+−−
−++
+−+

0
−−−
−−+
−+−
0

The order for three factors in the code above is LF power, HF power and Deuterium gas flow. The parameter for the experiments are provided in Table 3. The deposition step included the varied parameters and the sputtering step included the varied parameters except for the gas flow. The experiment included a pre deposition measurement to ensure that the wafers were new or to obtain a range of pre thickness. The deposition step was processed for 10 test runs with 10 different parameters' combinations in their recipe. Then metrology tools were used to obtain thickness, refractive index, sputter rate and deposition rate, stress and other data. The final step was sputtering over the same wafers, concluded by a final post measurement.

Table 3 The parameters for ten runs used for the experiment recipes

LF Power	HF Power	D2 Flow	Figure Numbers
1	1	0.94	32
1	1	1	33
1	0.94	0.94	30
0.94	1	1	28
1	0.94	1	31
0.97	0.97	0.97	29
0.94	0.94	0.94	25

0.94	0.94	1	26
0.94	1	0.94	27
0.97	0.97	0.97	29

The term sputter to deposition ratio was calculated by the following equation:

Delta = D – S = Δ **[Equation 1]**

where D is deposition rate of the deposition step and S is sputtering rate of the sputtering step.

Sputtering to Deposition rate = S/D = Δ/(Δ + D) **[Equation 2]**

The total number of data points on every wafer was 49. Figure 19 is a wafer-map representing the points and the locations on the wafer itself. The wafer-map and fitting has been obtained from JMP using x and y coordinates for the data.

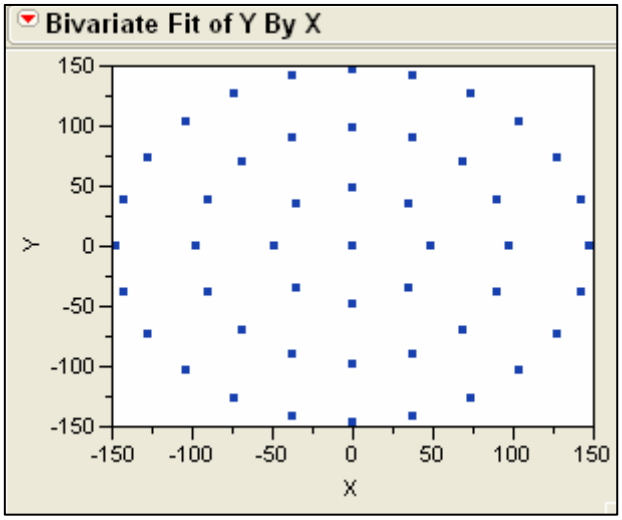

Figure 19. The wafer map representing the various points of measurements on a single wafer for metrology tool.

The metrology tools not only measure the deposition and sputtering rates, but they also measure the goodness of fit (GOF) for deposition and sputtering rates. The data for goodness of fit for deposition & sputtering rates are provided by the metrology tool on a 0 to 1 scale. The position of the data point on the wafer is given by its x (X) and y (Y) coordinates. Radius (R) is also calculated according to the given coordinates. The Zone is defined as the area of measurement, for a better understanding and it is divided into 4 different zones for a given wafer irrespective of the wafer size. The zones are the following: 1. Inner Zone(I), 2. Middle Zone(M), 3. Outer Zone(O), 4. Center(C). The center zone is only having one data point for the measurement as X = Y = R =0. Other points of measurements follow a circle in every zone. The inner zone has 8 points, middle zone has 16 points, and the outer zone has 24 points. Thus, 49 data points are collected from every single wafer.

Various analysis charts and model images follow. The charts provided have the details generated by JMP for various mathematical analyses. The data sheets are also included at the end of the chapter. Analysis includes bivariate fitting charts, variability charts, standard deviation charts, interaction profilers and prediction plots and more estimates. The details for each of them are included as a screenshot with every chart itself.

Table 4. Various responses of the experiment

N-Dep	Normalized Deposition rate of Deposition step
N-DpRI	Normalized Deposition step Refractive index

N-Du	Normalized Deuterium gas flow as a factor
N-LF	Normalized low frequency power as a factor
N-HF	Normalized high frequency power as a factor
N-Sput	Normalized sputtering rate of the sputtering rate
N-Delta	Normalized delta (calculated as mentioned before)

The variability gauge charts for N-Dep and N-DpRI with their standard deviations are given below (Figures 20 and 21).

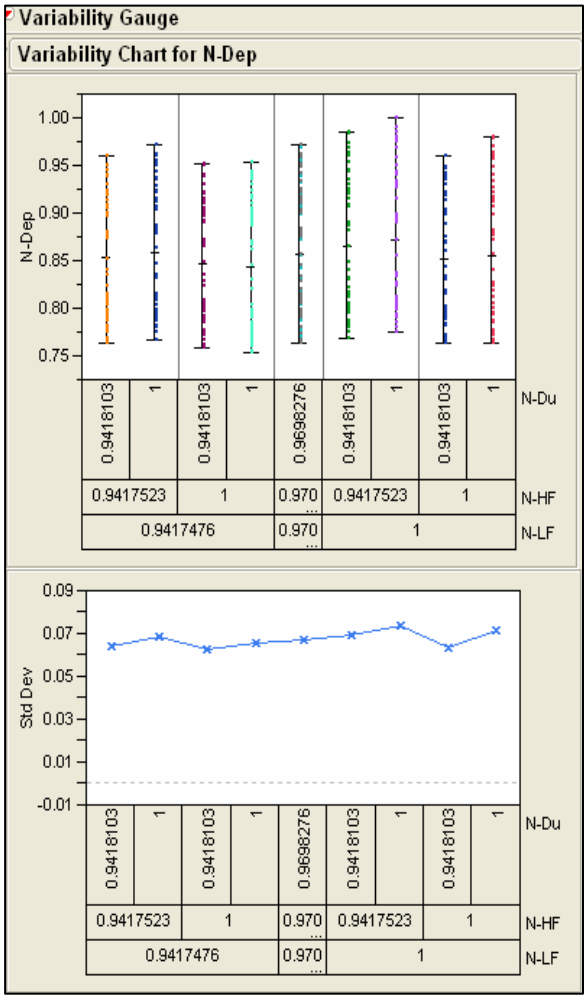

Figure 20. Variability chart of N-Dep

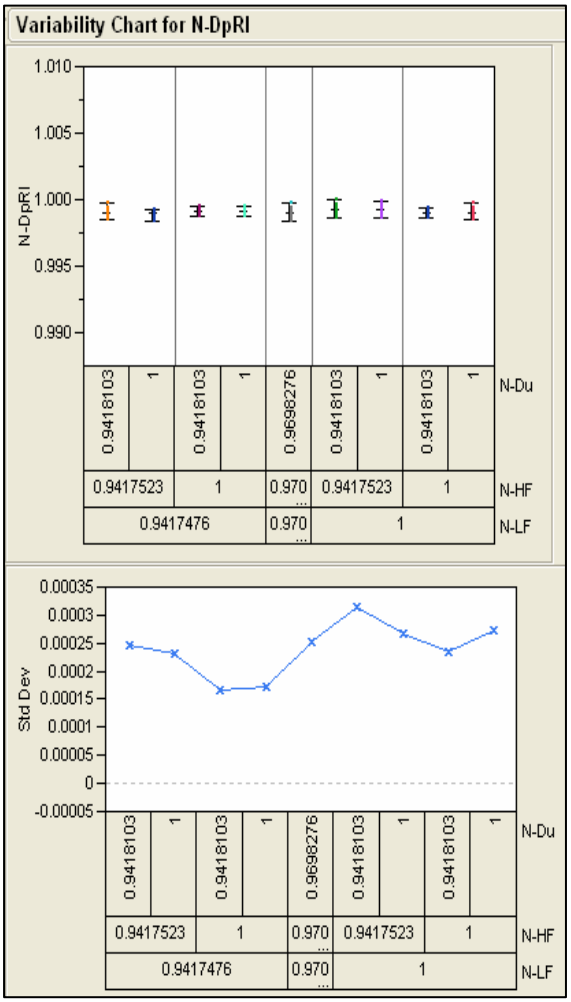

Figure 21. Variability chart of N-DpRI

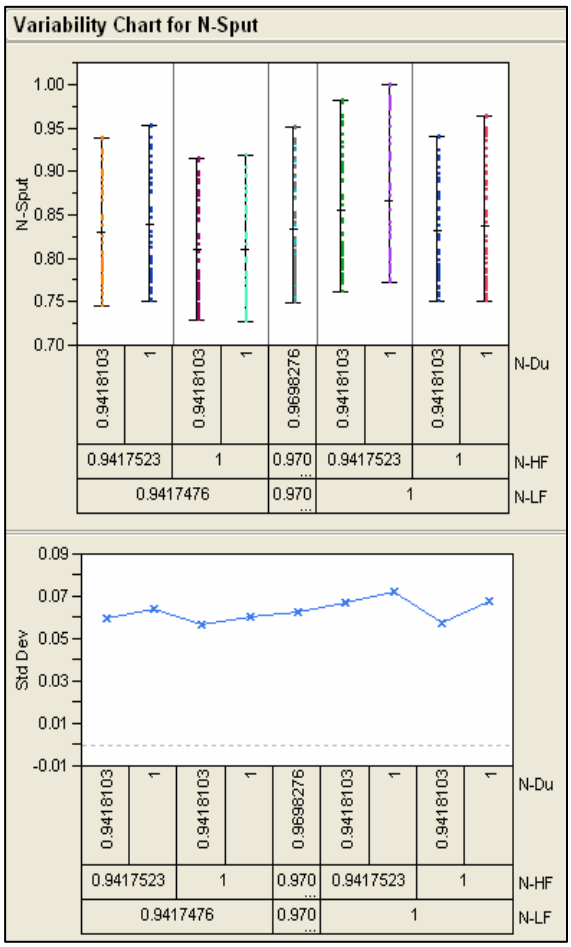

Figure 22. The variability gauge charts for N-Spu with the standard deviation.

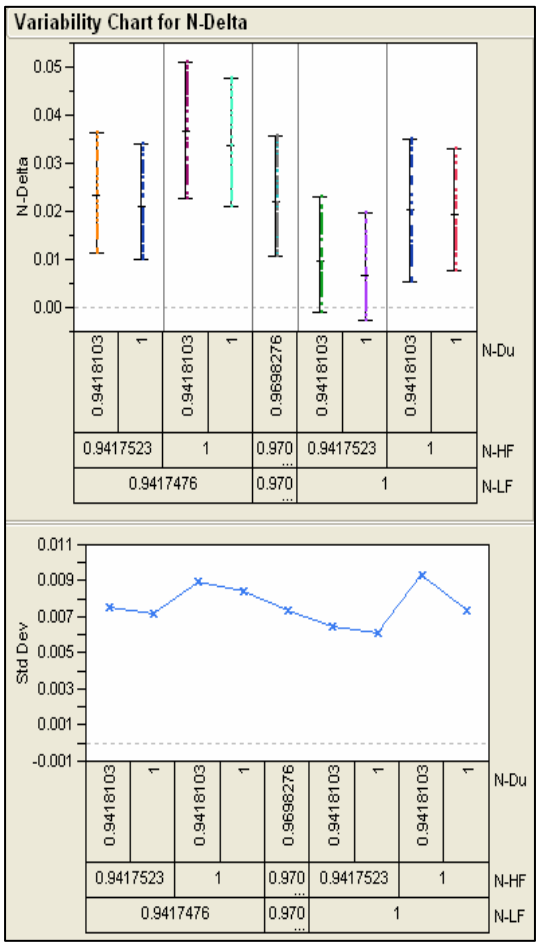

Figure 23. The variability gauge charts for N-Delta with the standard deviation.

B. Analysis:

As we can see, the various sets of data in Figures 22 & 23 are coordinated in different sections with respect to the source wafer of the data. For example, the data set or the points of measurements from wafer 1 or slot 1 in the experiment is shown in the charts with respect to their recipe parameters and so on. This makes the analysis much easier while drawing the conclusions. The charts made with the help of such sections and

various zones for each wafer also give a very good idea about the differences in impact at different points on the wafer depending on the distance from the center.

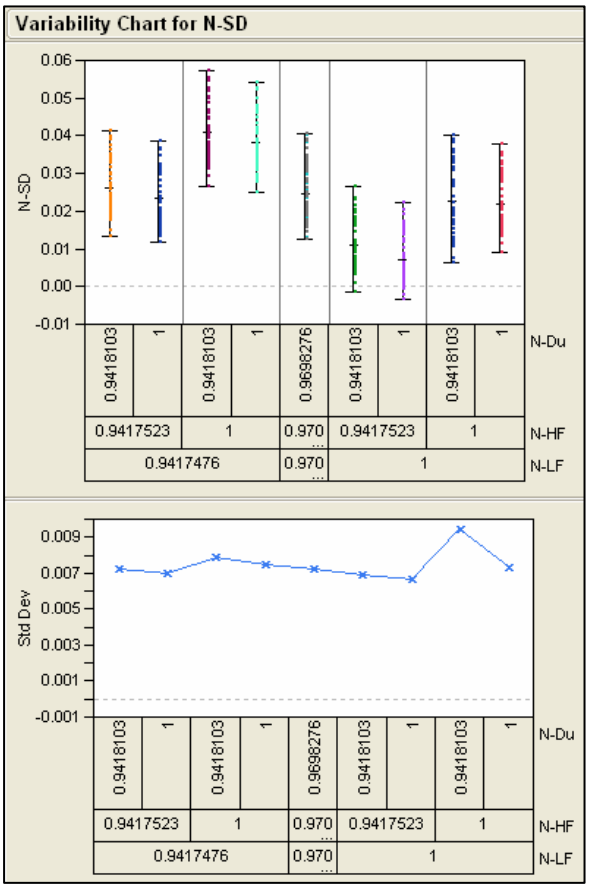

Figure 24. Variability chart of N-SD

The various standard deviation charts below in Figures 25 & 26 each variability charts basically represent fewer number of points from each wafer and hence we can see a total of 9 crosses (points) on the chart with the details of the values of the factors corresponding to the specific point.

Hence we can clearly see that refractive index and the standard deviation both get heavily affected within a really close range of values. The impact of refractive indices can be crucial for finding out the etch-outs as well.

What follows are bivariate charts for various responses with specific data points and sections as shown in the Figures 25, 26, 27 & 28. The bivariate charts have been curve fitted as well for a better analysis with x-axis as radius.

Figures 25, 26, 27 & 28 include variability analysis of the responses. Bivariate charts analyze the data with radius of the wafer as a factor. Bivariate charts highlight the differences across various zones.

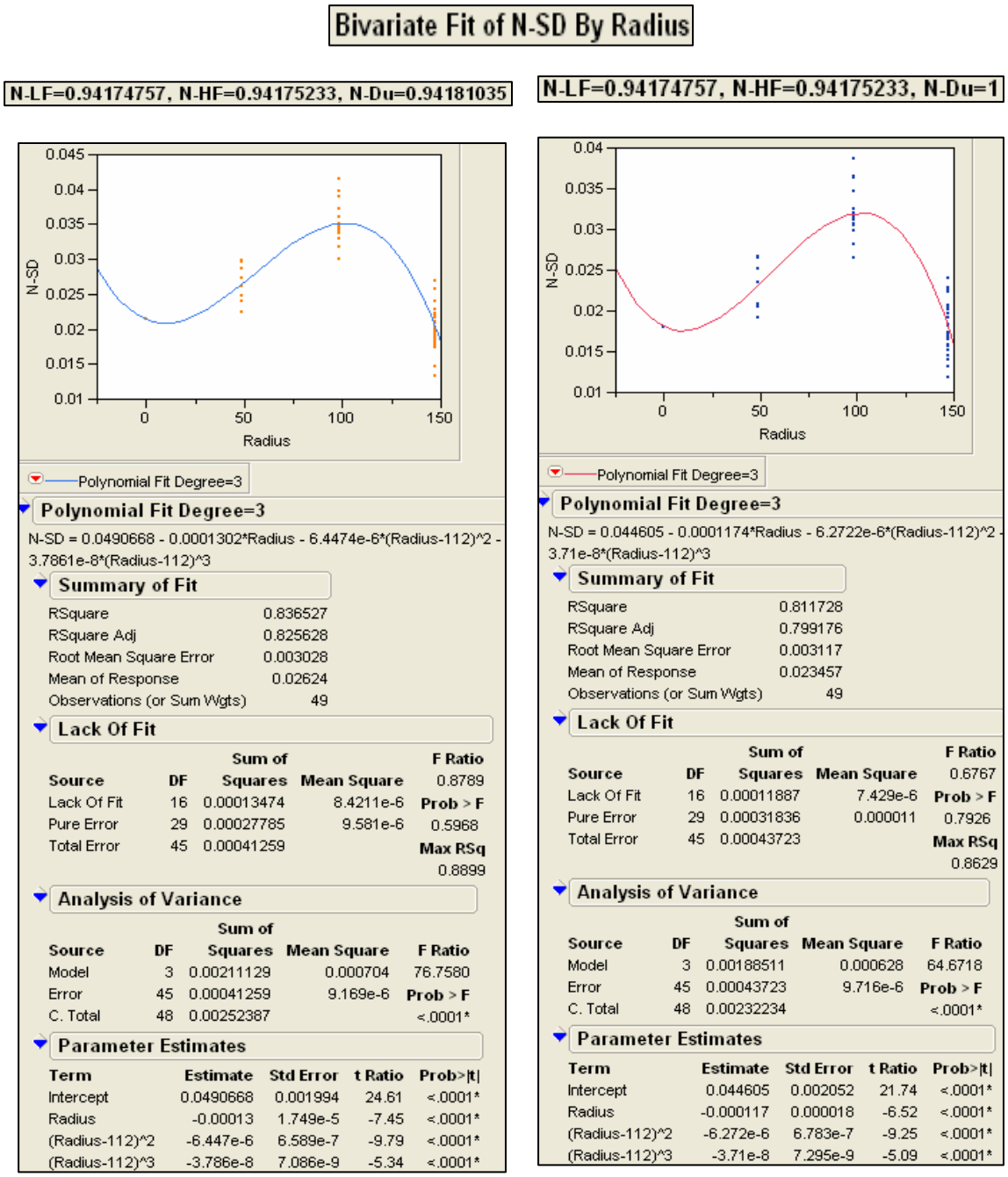

Figure 25. & Figure 26. Bivariate fitting of Sputter to deposition ratio by radius of point of measurement on the wafer.

N-LF=0.94174757, N-HF=1, N-Du=0.94181035

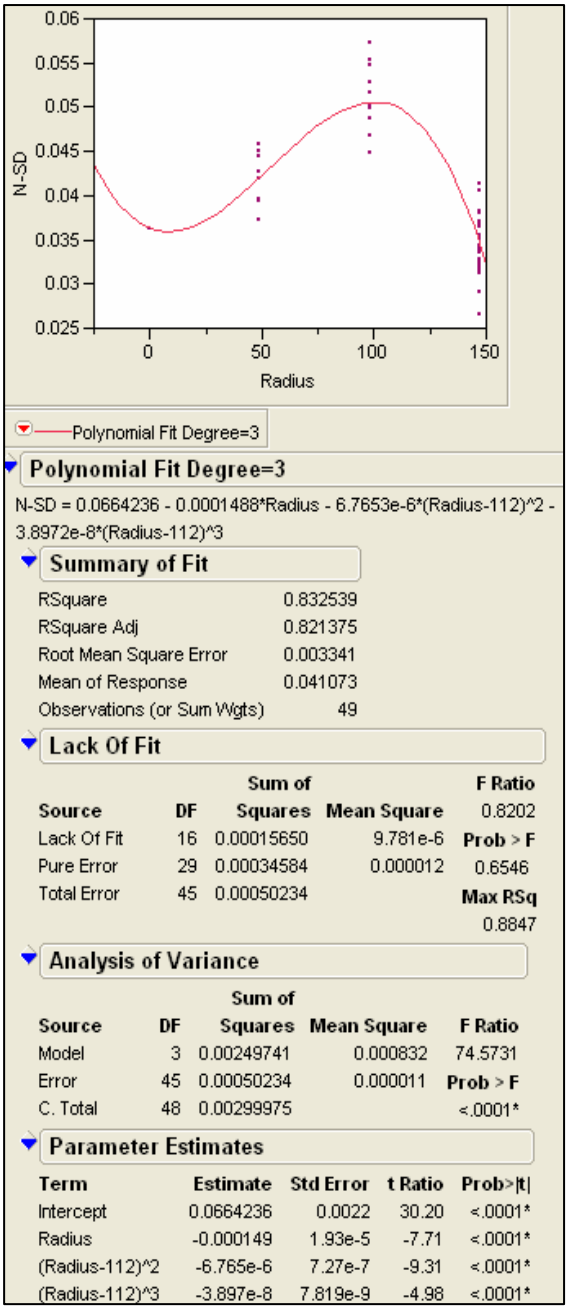

N-LF=0.94174757, N-HF=1, N-Du=1

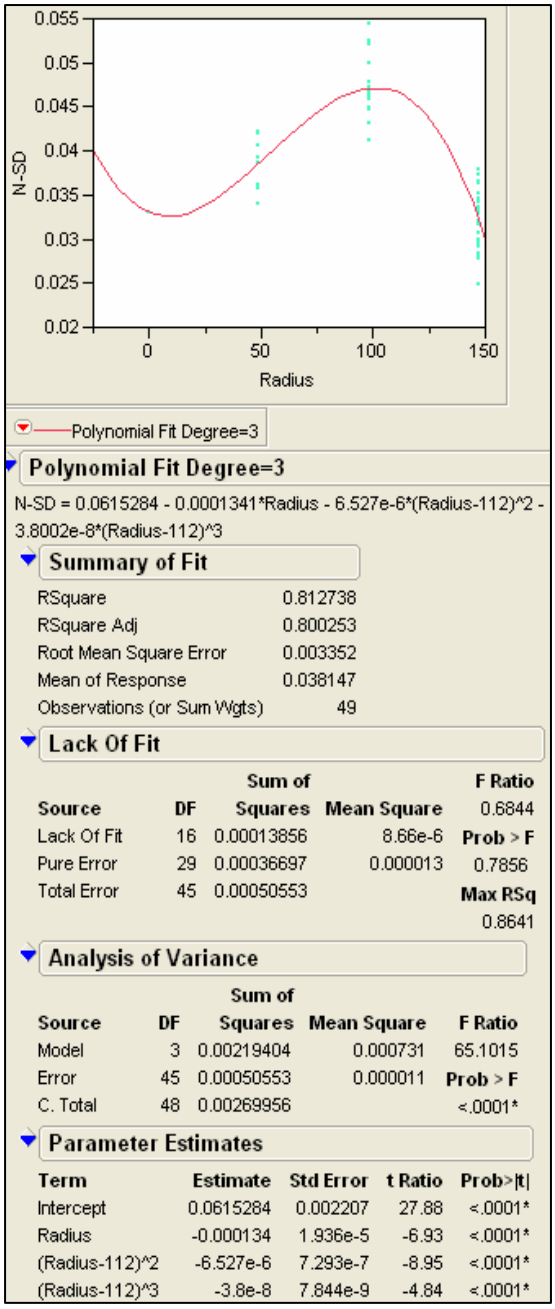

Figure 27. & Figure 28. Bivariate fitting of Sputter to deposition ratio by radius of point of measurement on the wafer.

N-LF=0.97087378, N-HF=0.97079458, N-Du=0.96982759

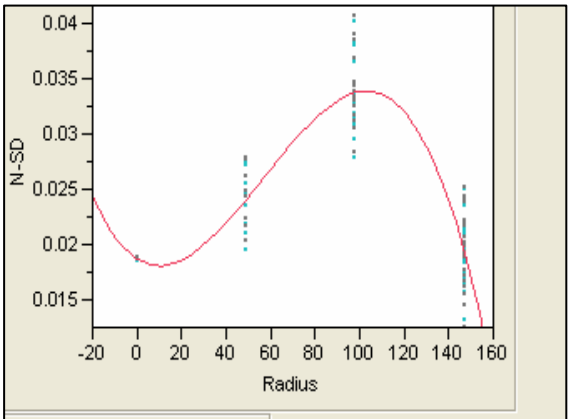

Polynomial Fit Degree=3

Polynomial Fit Degree=3

N-SD = 0.0464491 - 0.0001171*Radius - 6.7303e-6*(Radius-112)^2 - 4.0345e-8*(Radius-112)^3

Summary of Fit

RSquare	0.81775
RSquare Adj	0.811934
Root Mean Square Error	0.003128
Mean of Response	0.024778
Observations (or Sum Wgts)	98

Lack Of Fit

Source	DF	Sum of Squares	Mean Square	F Ratio
Lack Of Fit	16	0.00022891	0.000014	1.6158
Pure Error	78	0.00069063	8.854e-6	Prob > F
Total Error	94	0.00091954		0.0842
				Max RSq
				0.8631

Analysis of Variance

Source	DF	Sum of Squares	Mean Square	F Ratio
Model	3	0.00412597	0.001375	140.5918
Error	94	0.00091954	9.782e-6	Prob > F
C. Total	97	0.00504551		<.0001*

Parameter Estimates

Term	Estimate	Std Error	t Ratio	Prob>|t|
Intercept	0.0464491	0.001456	31.90	<.0001*
Radius	-0.000117	1.278e-5	-9.16	<.0001*
(Radius-112)^2	-6.73e-6	4.812e-7	-13.99	<.0001*
(Radius-112)^3	-4.034e-8	5.176e-9	-7.79	<.0001*

N-LF=1, N-HF=0.94175233, N-Du=0.94181035

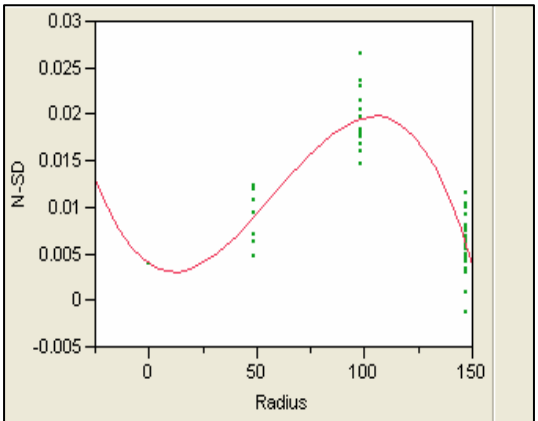

Polynomial Fit Degree=3

Polynomial Fit Degree=3

N-SD = 0.0302067 - 9.5728e-5*Radius - 6.8054e-6*(Radius-112)^2 - 4.2039e-8*(Radius-112)^3

Summary of Fit

RSquare	0.822679
RSquare Adj	0.810858
Root Mean Square Error	0.002991
Mean of Response	0.010891
Observations (or Sum Wgts)	49

Lack Of Fit

Source	DF	Sum of Squares	Mean Square	F Ratio
Lack Of Fit	16	0.00013043	8.1518e-6	0.8688
Pure Error	29	0.00027211	9.383e-6	Prob > F
Total Error	45	0.00040254		0.6067
				Max RSq
				0.8801

Analysis of Variance

Source	DF	Sum of Squares	Mean Square	F Ratio
Model	3	0.00186757	0.000623	69.5924
Error	45	0.00040254	8.945e-6	Prob > F
C. Total	48	0.00227010		<.0001*

Parameter Estimates

Term	Estimate	Std Error	t Ratio	Prob>|t|
Intercept	0.0302067	0.001969	15.34	<.0001*
Radius	-9.573e-5	1.728e-5	-5.54	<.0001*
(Radius-112)^2	-6.805e-6	6.508e-7	-10.46	<.0001*
(Radius-112)^3	-4.204e-8	7e-9	-6.01	<.0001*

Figure 29. & Figure 30. Bivariate fitting of Sputter to deposition ratio by radius of point of measurement on the wafer.

N-LF=1, N-HF=0.94175233, N-Du=1

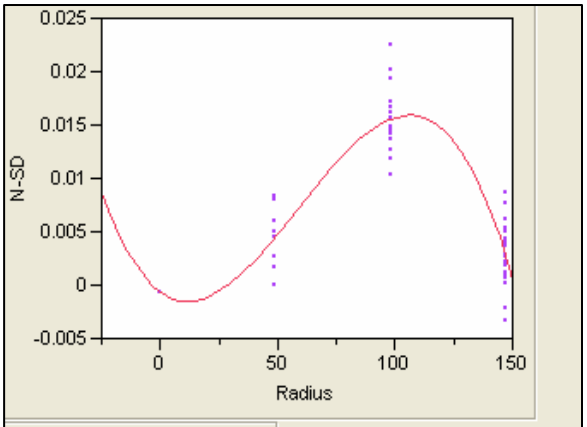

Polynomial Fit Degree=3

Polynomial Fit Degree=3

N-SD = 0.0246993 - 0.0000804*Radius - 6.7541e-6*(Radius-112)^2 - 4.2251e-8*(Radius-112)^3

Summary of Fit

RSquare	0.812972
RSquare Adj	0.800504
Root Mean Square Error	0.002963
Mean of Response	0.00719
Observations (or Sum Wgts)	49

Lack Of Fit

Source	DF	Sum of Squares	Mean Square	F Ratio
Lack Of Fit	16	0.00011100	6.9376e-6	0.7082
Pure Error	29	0.00028409	9.796e-6	Prob > F
Total Error	45	0.00039509		0.7635
				Max RSq
				0.8655

Analysis of Variance

Source	DF	Sum of Squares	Mean Square	F Ratio
Model	3	0.00171737	0.000572	65.2021
Error	45	0.00039509	8.78e-6	Prob > F
C. Total	48	0.00211246		<.0001*

Parameter Estimates

Term	Estimate	Std Error	t Ratio	Prob>|t|
Intercept	0.0246993	0.001951	12.66	<.0001*
Radius	-8.041e-5	1.712e-5	-4.70	<.0001*
(Radius-112)^2	-6.754e-6	6.448e-7	-10.48	<.0001*
(Radius-112)^3	-4.225e-8	6.935e-9	-6.09	<.0001*

N-LF=1, N-HF=1, N-Du=0.94181035

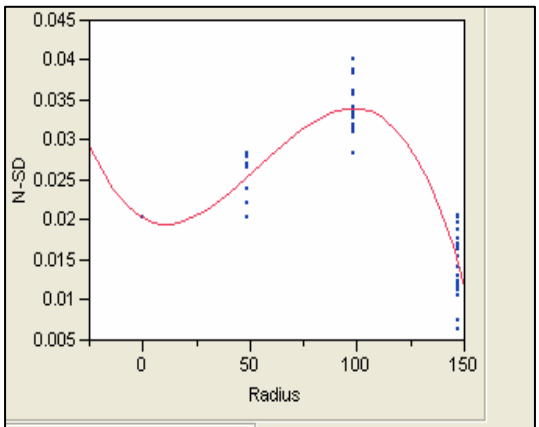

Polynomial Fit Degree=3

Polynomial Fit Degree=3

N-SD = 0.0544021 - 0.0001936*Radius - 7.7542e-6*(Radius-112)^2 - 4.4934e-8*(Radius-112)^3

Summary of Fit

RSquare	0.86922
RSquare Adj	0.860501
Root Mean Square Error	0.003529
Mean of Response	0.022779
Observations (or Sum Wgts)	49

Lack Of Fit

Source	DF	Sum of Squares	Mean Square	F Ratio
Lack Of Fit	16	0.00018935	0.000012	0.9249
Pure Error	29	0.00037107	0.000013	Prob > F
Total Error	45	0.00056042		0.5525
				Max RSq
				0.9134

Analysis of Variance

Source	DF	Sum of Squares	Mean Square	F Ratio
Model	3	0.00372481	0.001242	99.6964
Error	45	0.00056042	0.000012	Prob > F
C. Total	48	0.00428523		<.0001*

Parameter Estimates

Term	Estimate	Std Error	t Ratio	Prob>|t|
Intercept	0.0544021	0.002323	23.42	<.0001*
Radius	-0.000194	2.038e-5	-9.50	<.0001*
(Radius-112)^2	-7.754e-6	7.679e-7	-10.10	<.0001*
(Radius-112)^3	-4.493e-8	8.259e-9	-5.44	<.0001*

Figure 31. & Figure 32. Bivariate fitting of Sputter to deposition ratio by radius of point of measurement on the wafer

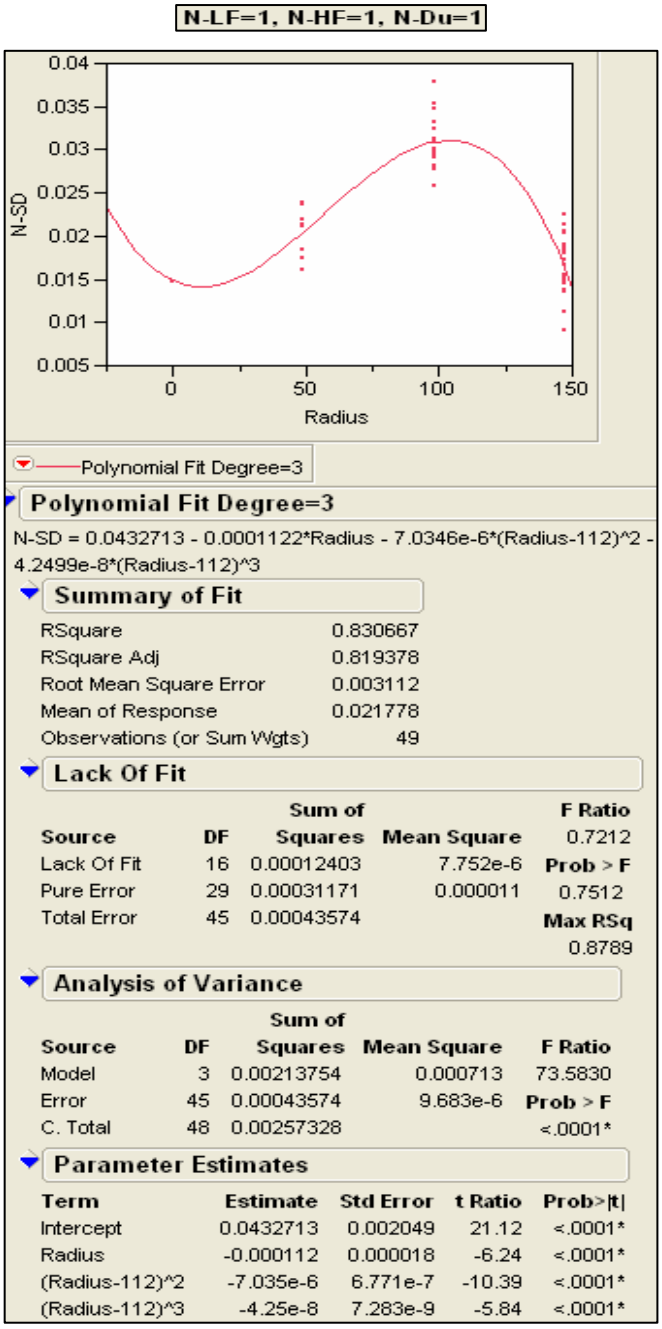

Figure 33. Bivariate fitting of Sputter to deposition by radius

As seen in all the figures 25 to 33, the middle zone is highly affected and sputter to deposition rate varies greatly all across the wafer. Hence the response derived from the

original responses would give a much better picture regarding the impact on sputter-to-deposition ratio with respect to all factors.

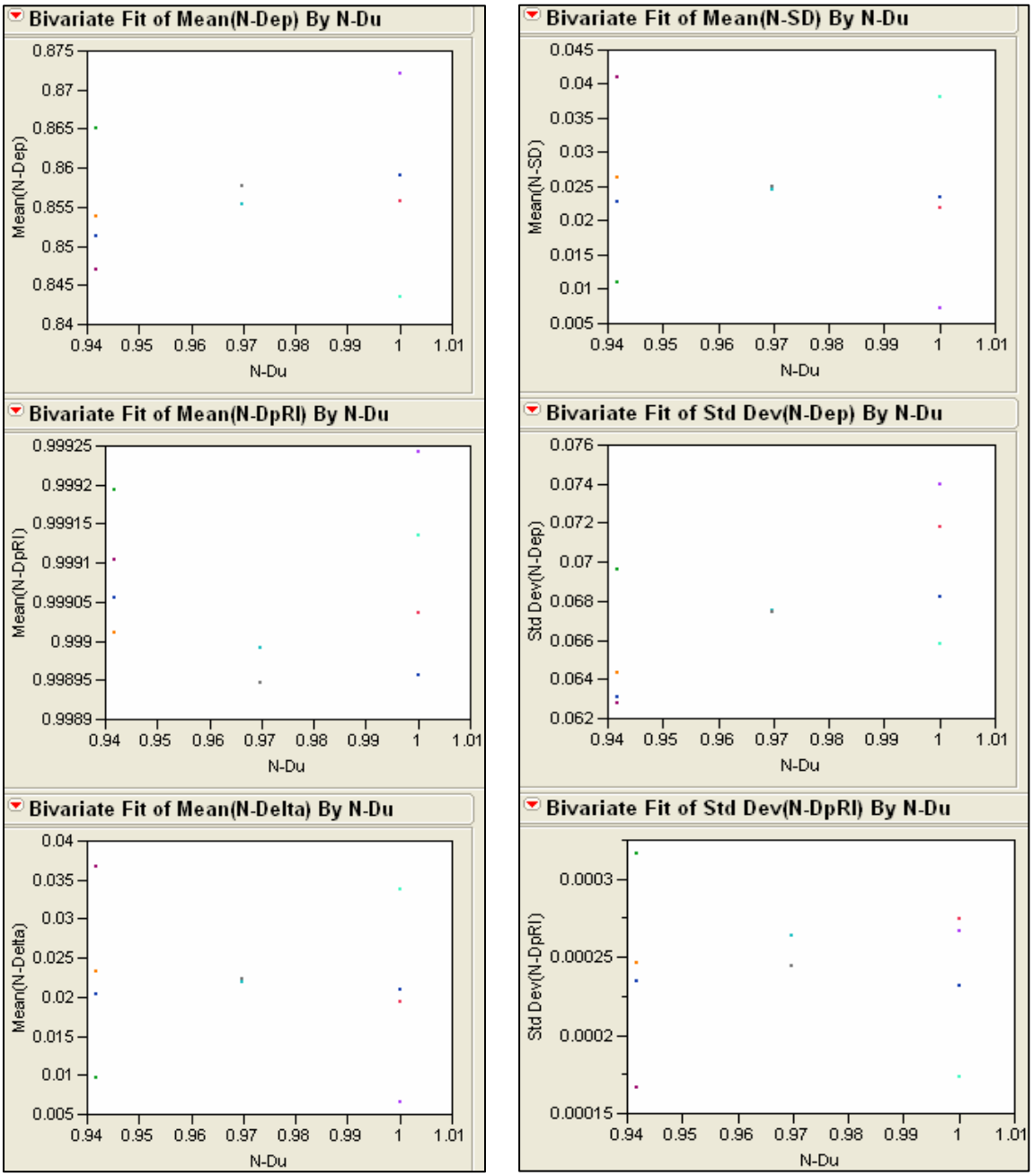

Figure 34. & Figure 35. Bivariate fitting by Du gas flow for various responses

Figures 34 & 35 and 36, are shown with x axis as deuterium gas flow. Deuterium flow is not used in the other microelectronic fabrication process for DRAM and these product did not reveal etch-outs. So Deuterium gas flow was an important factor to be monitored. However little correlation can be observed in the bivariate analysis and the points do not seem to follow any pattern whatsoever.

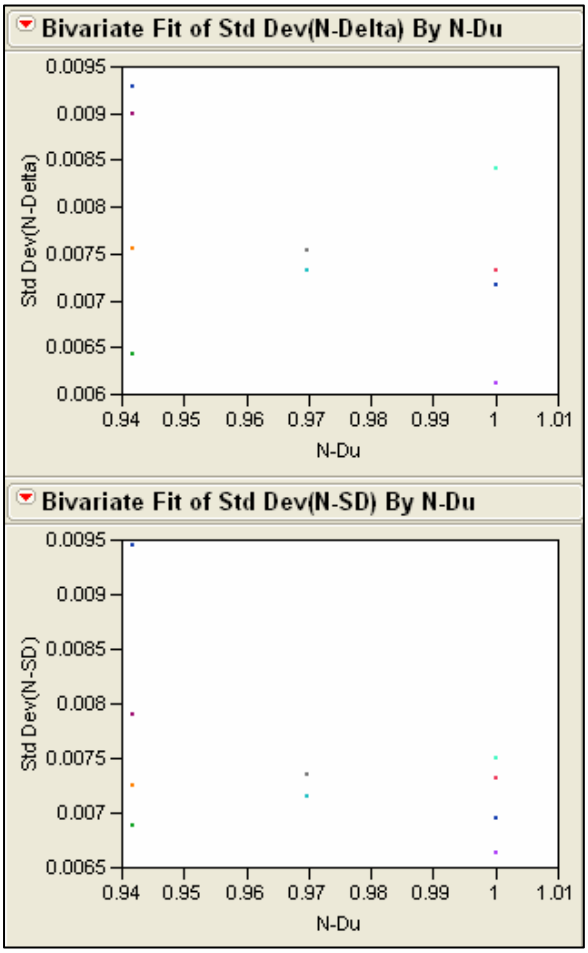

Figure 36. Bivariate fitting by Deuterium

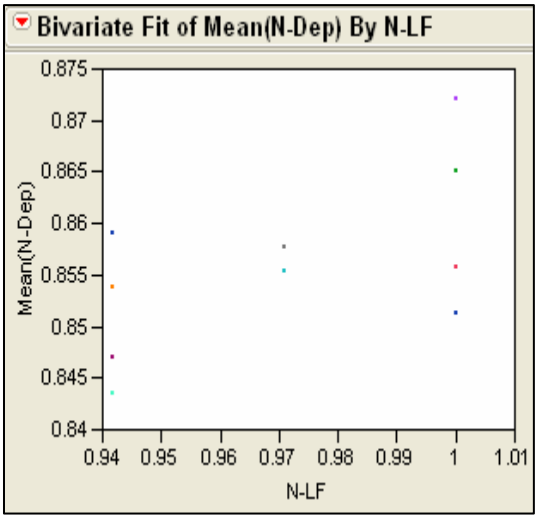

Figure 37. Bivariate fitting by LF power for Deposition rate

Figure 37 given is with LF power as the x variable and the other similar charts are given on the next pages.

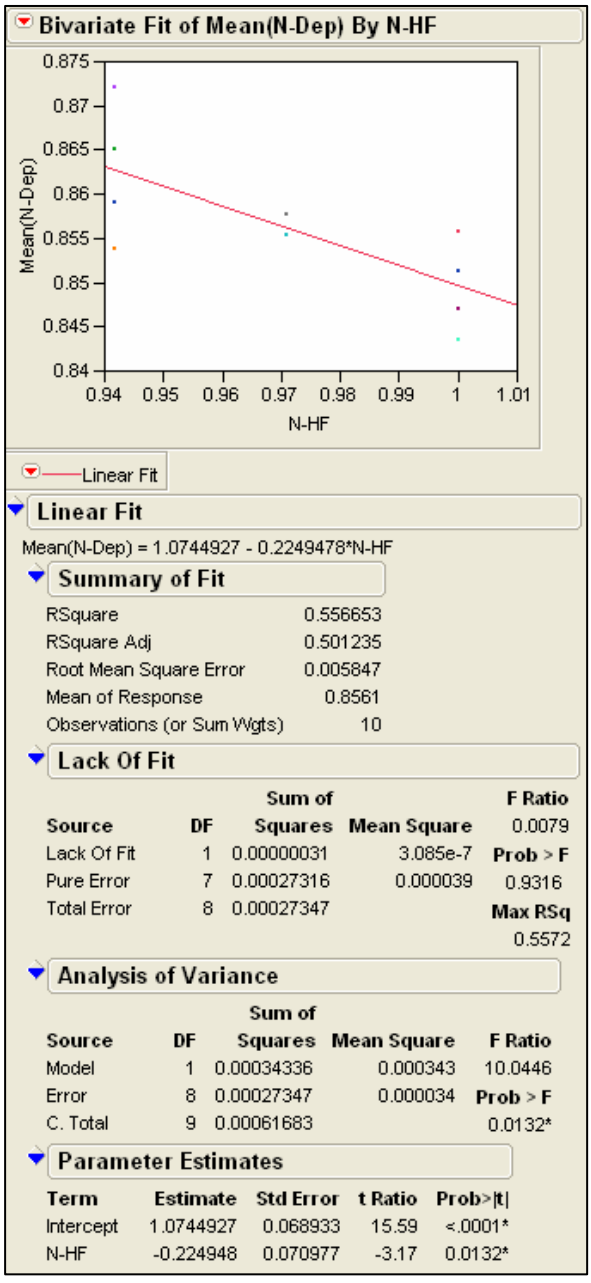

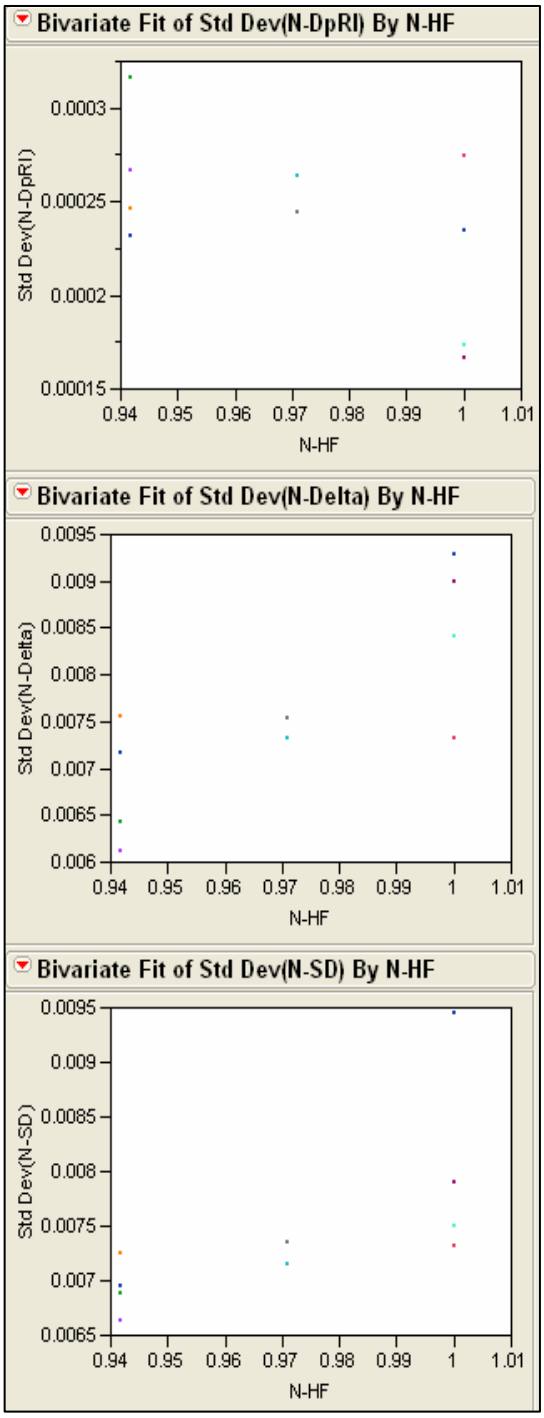

Figure 38. & Figure 39. Bivariate fitting by HF power

Figures 38, 39 & 40 have HF power as the x axis, and we can see a linear fit for deposition rate.

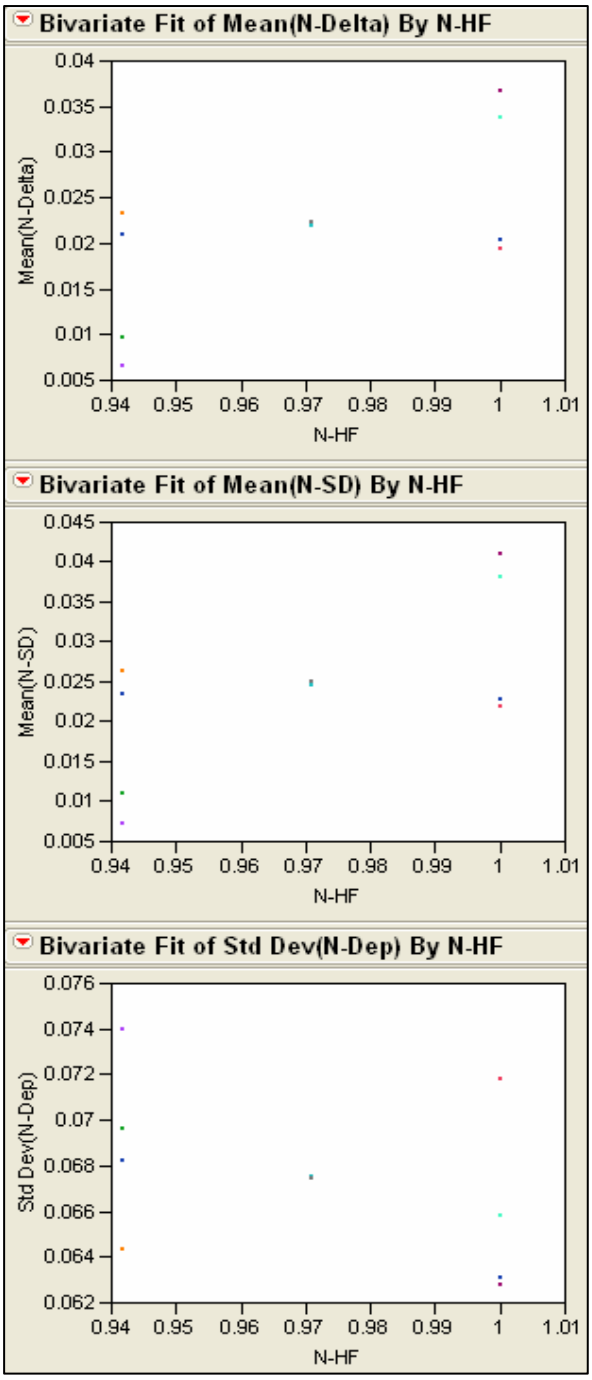

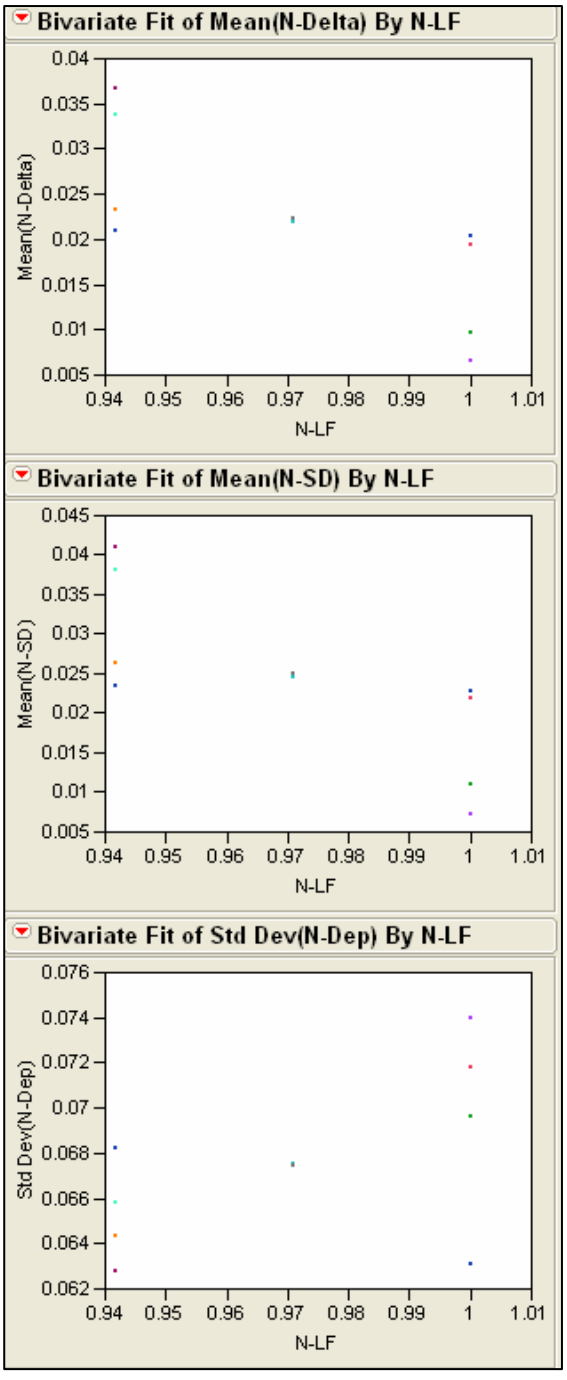

Figure 40. Bivariate fitting by HF Power **Figure 41. Bivariate fitting by LF Power**

Figures 40 & 41 are shown with other factors. There lacks a correlation, as is seen in the charts. Analysis of variance is also a part of analysis in Figure 43 where two linear fits are involved.

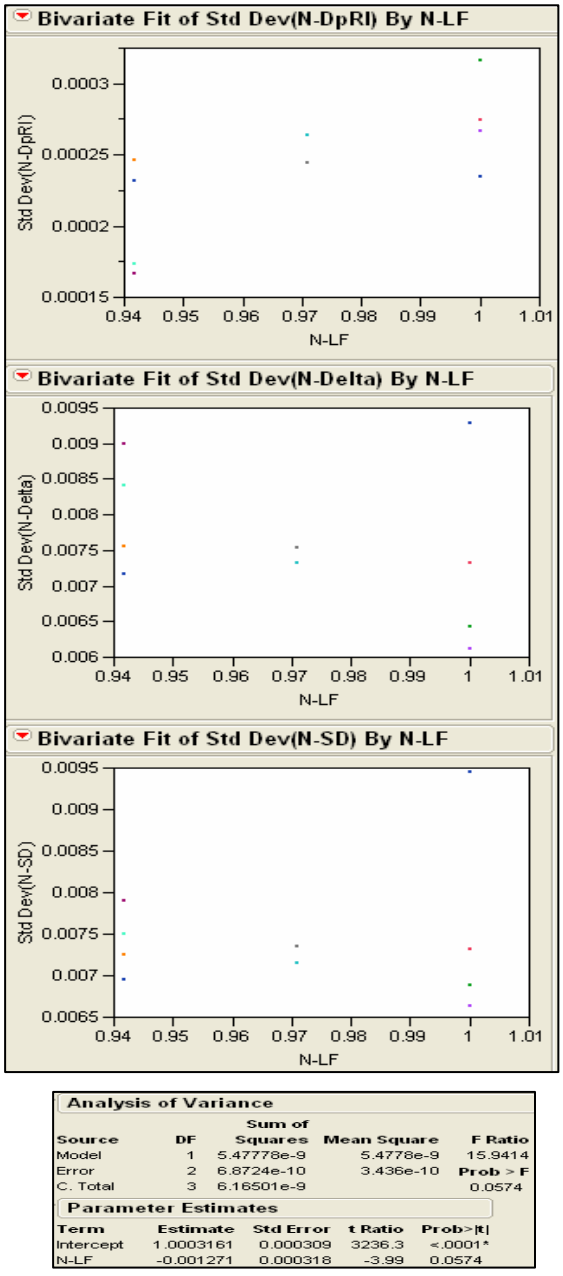

Analysis of Variance

Source	DF	Sum of Squares	Mean Square	F Ratio
Model	1	5.47778e-9	5.4778e-9	15.9414
Error	2	6.8724e-10	3.436e-10	Prob > F
C. Total	3	6.16501e-9		0.0574

Parameter Estimates

Term	Estimate	Std Error	t Ratio	Prob>|t|
Intercept	1.0003161	0.000309	3236.3	<.0001*
N-LF	-0.001271	0.000318	-3.99	0.0574

Figure 42. Bivariate fitting by LF power for standard deviation of three responses

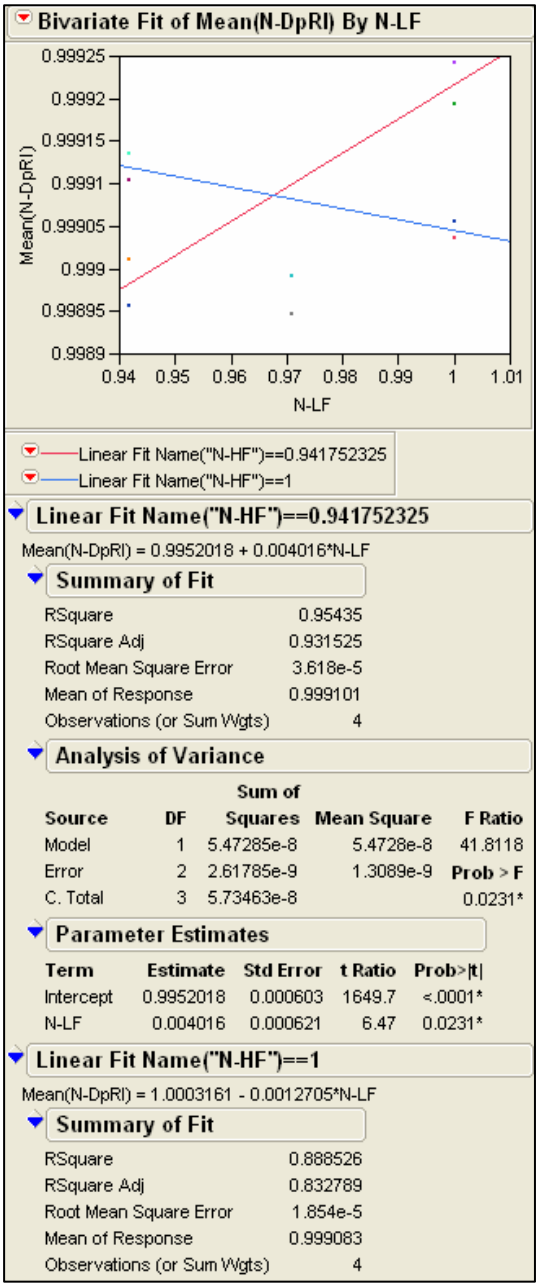

Figure 43. Bivariate fitting of mean of refractive indices by LF

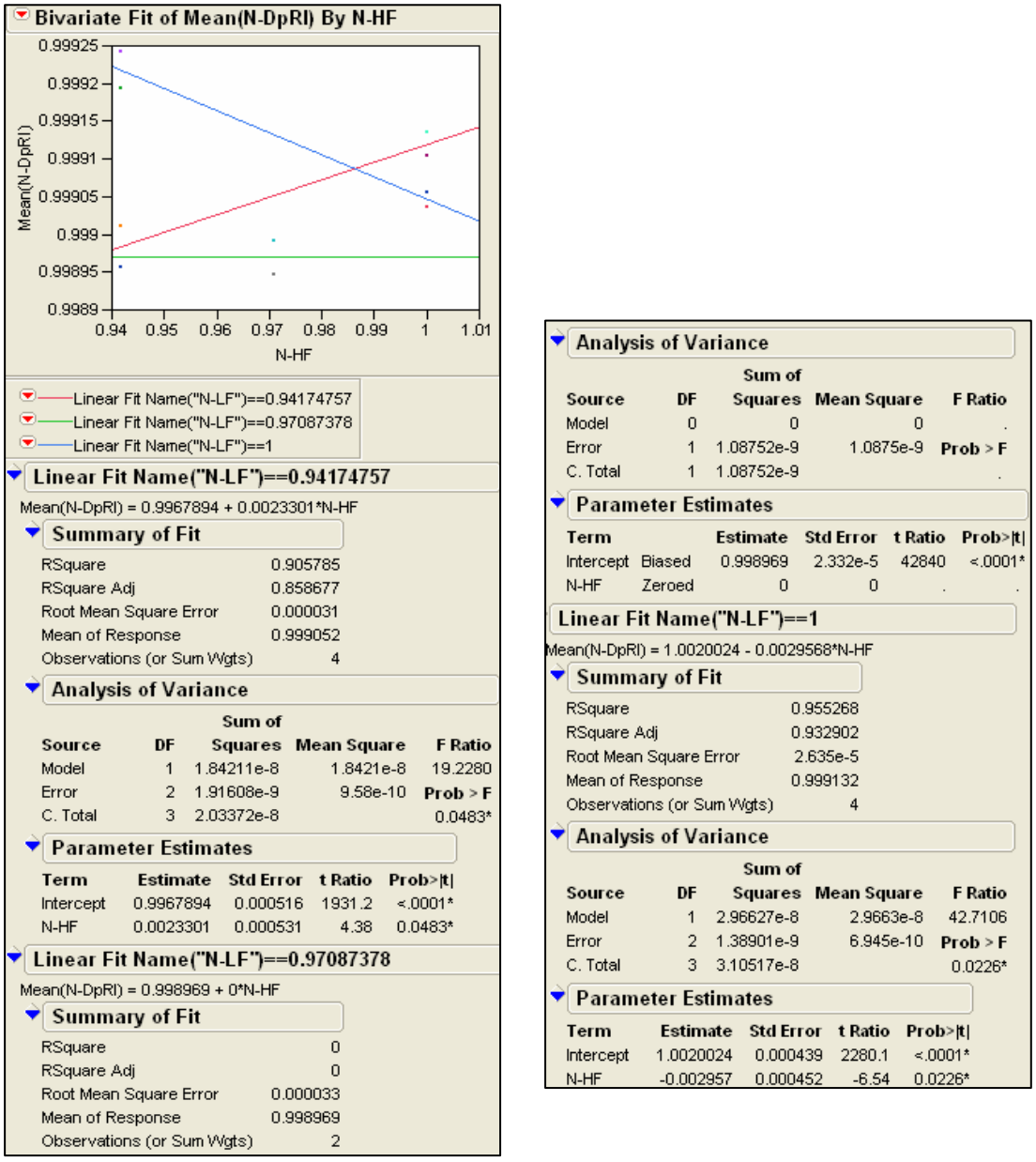

Figure 44. Bivariate fitting showing three linear fits for various levels of HF power as the factor and the response shown is refractive indices and as it can be seen, all the three different values give a complete different line fit. The analysis for fitting and the variance is given in the chart details.

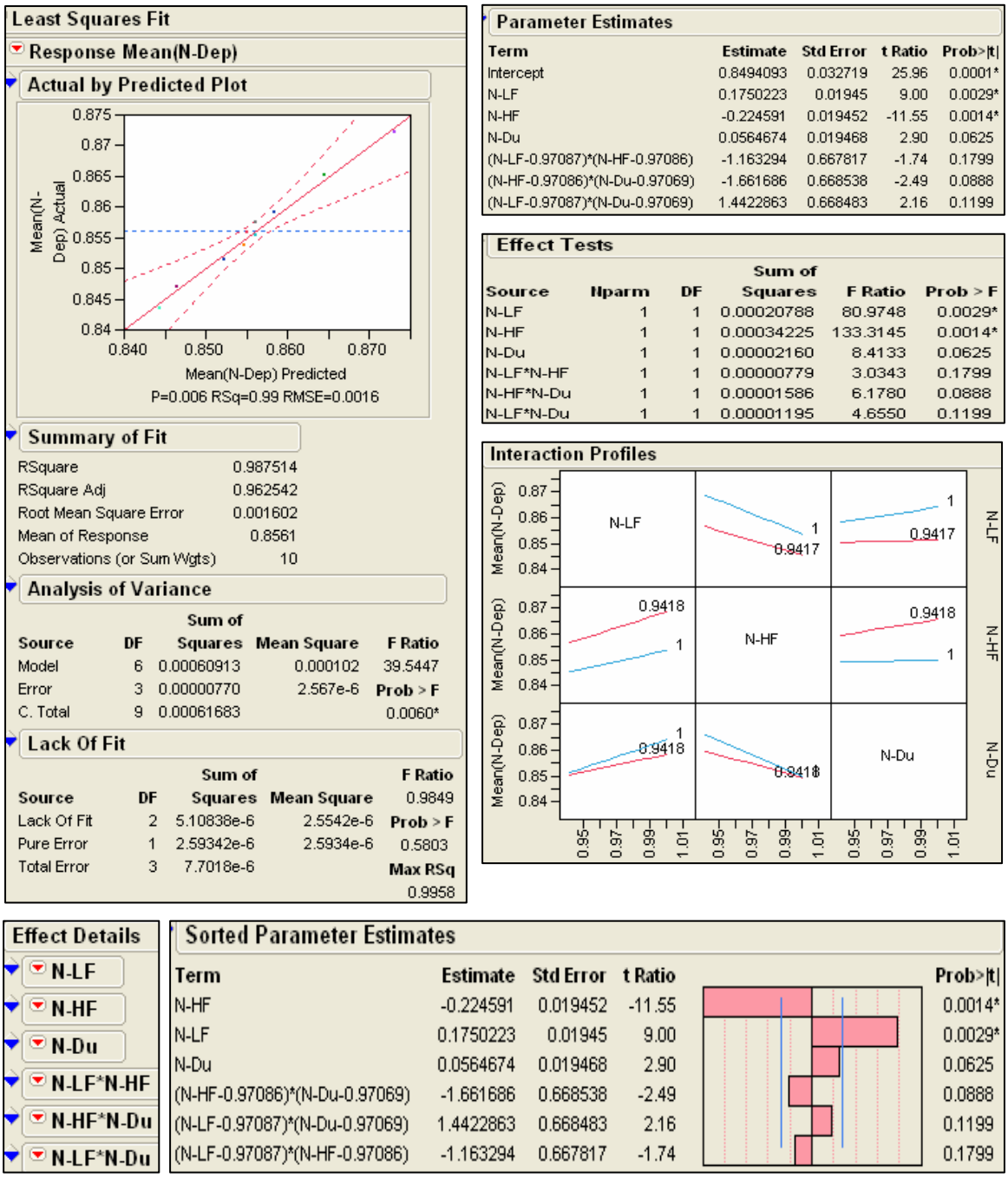

Figure 45. Actual v/s predicted plot for deposition rate on the basis of interaction profiles

Figure 45 is the predicted plot for the deposition rate. As we can see, the limits are having a close range meaning that the certainty of the estimation or the prediction increases to a very high value. The interaction profiles in Figure 45 show the interaction fittings between LF power, HF power, and Deuterium gas flow with the deposition rate. The scaled estimates are given for deposition rates. The scaled estimates and the sorted parameter estimates given by JMP can be chosen to obtain results with intercepts. The details are also mentioned in the prediction plot. The scaled estimates report displays a bar chart of the individual effects embedded in a table of parameter estimates. The last column of the table (probability) includes the p-values for each effect. None of the factor effects are significant, but the intercept estimate is large enough to be interesting.

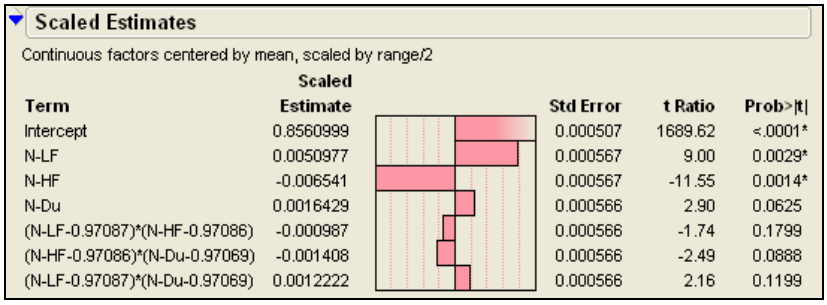

Term	Scaled Estimate	Std Error	t Ratio	Prob>|t|
Intercept	0.8560999	0.000507	1689.62	<.0001*
N-LF	0.0050977	0.000567	9.00	0.0029*
N-HF	-0.006541	0.000567	-11.55	0.0014*
N-Du	0.0016429	0.000566	2.90	0.0625
(N-LF-0.97087)*(N-HF-0.97086)	-0.000987	0.000566	-1.74	0.1799
(N-HF-0.97086)*(N-Du-0.97069)	-0.001408	0.000566	-2.49	0.0888
(N-LF-0.97087)*(N-Du-0.97069)	0.0012222	0.000566	2.16	0.1199

Figure 46. Scaled estimates for deposition rate prediction plots.

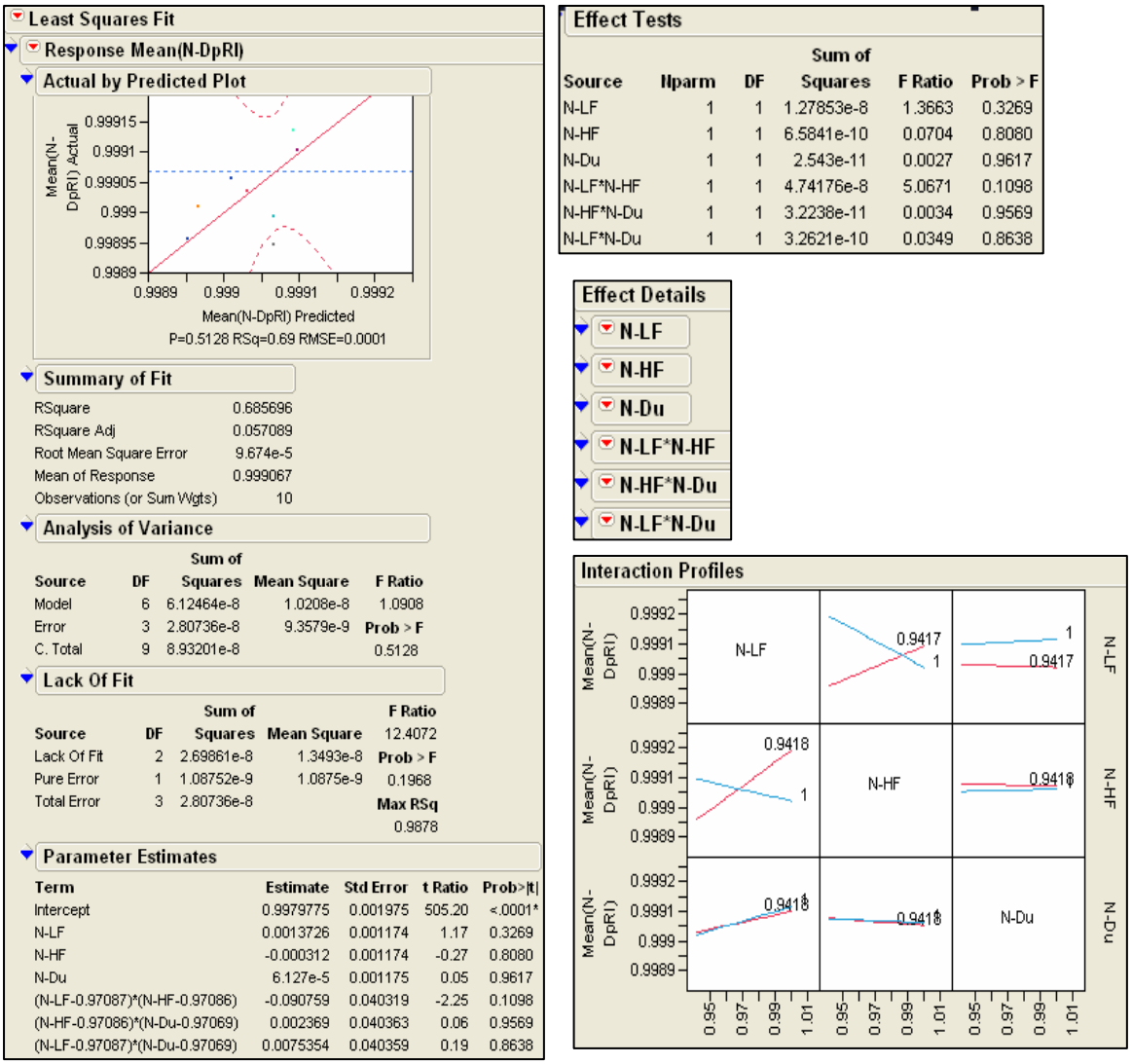

Figure 46. Actual versus predicted plot for Refractive indices

Figure 47 represents refractive indices (RI). It lacks an acceptable prediction as the error margin is high and the curves are far apart, which means that probability for errors is more than their failure. The interaction profiles suggest the correlation between RI and LF power, HF power, Deuterium gas flow. As we can see in the profiles for interactions, the HF power and RI have a very good correlation as so does LF power. The gas flow does not seem to have a significant effect.

Scaled Estimates

Continuous factors centered by mean, scaled by range/2

Term	Scaled Estimate	Std Error	t Ratio	Prob>|t|
Intercept	0.9990671	3.059e-5	32659.23	<.0001*
N-LF	3.9978e-5	3.42e-5	1.17	0.3269
N-HF	-9.072e-6	3.42e-5	-0.27	0.8080
N-Du	1.7826e-6	3.42e-5	0.05	0.9617
(N-LF-0.97087)*(N-HF-0.97086)	-0.000077	3.42e-5	-2.25	0.1098
(N-HF-0.97086)*(N-Du-0.97069)	2.0074e-6	3.42e-5	0.06	0.9569
(N-LF-0.97087)*(N-Du-0.97069)	6.3857e-6	3.42e-5	0.19	0.8638

Figure 47, Scaled estimates for refractive indices prediction plot

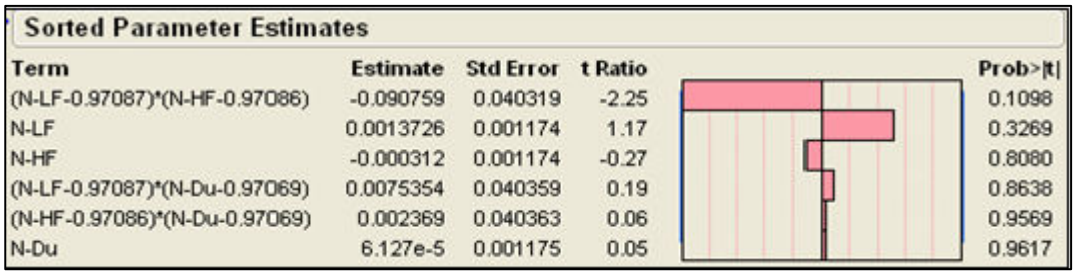

Sorted Parameter Estimates

Term	Estimate	Std Error	t Ratio	Prob>|t|
(N-LF-0.97087)*(N-HF-0.97086)	-0.090759	0.040319	-2.25	0.1098
N-LF	0.0013726	0.001174	1.17	0.3269
N-HF	-0.000312	0.001174	-0.27	0.8080
(N-LF-0.97087)*(N-Du-0.97069)	0.0075354	0.040359	0.19	0.8638
(N-HF-0.97086)*(N-Du-0.97069)	0.002369	0.040363	0.06	0.9569
N-Du	6.127e-5	0.001175	0.05	0.9617

Figure 48. Sorted parameter estimates for refractive indices prediction plot

The sorted estimates and the scaled estimates include factors, estimated errors, and the probability. These two estimates' sets represent the analysis of RI in Figure 47. The terms on the two tables in Figure 48 & 49 are also provided. The intercept is also given on the scaled estimates.

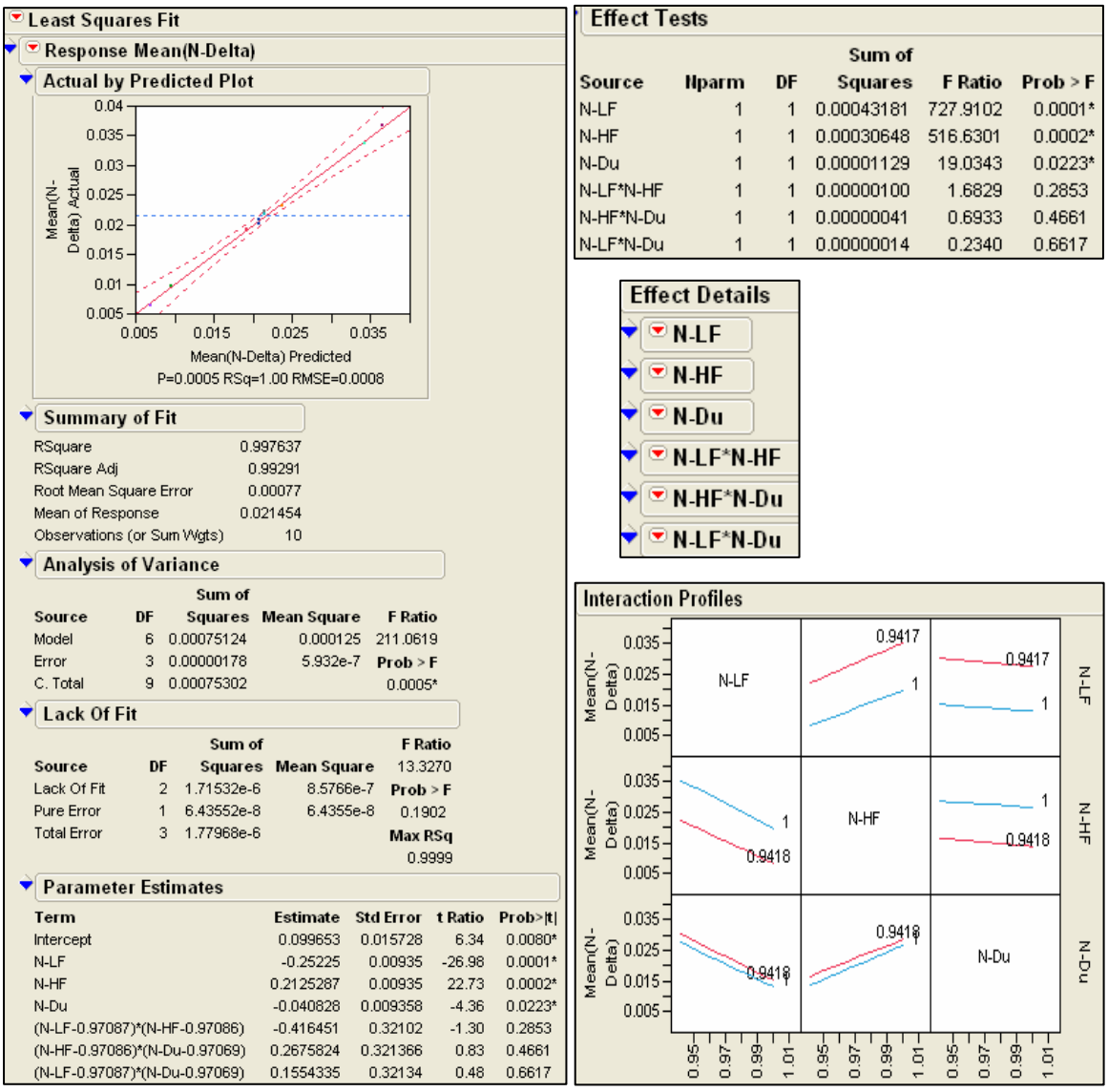

Figure 49. Actual versus prediction plot for delta

Figure 50 represents the analysis for Delta, just like the previous analysis prediction. We can see that Delta has a close correlation with HF power and LF power (the straight lines almost parallel to each other) and same with Deuterium gas flow, but not much of a difference in magnitude change.

Sorted Parameter Estimates

Term	Estimate	Std Error	t Ratio	Prob>|t|
N-LF	-0.25225	0.00935	-26.98	0.0001*
N-HF	0.2125287	0.00935	22.73	0.0002*
N-Du	-0.040828	0.009358	-4.36	0.0223*
(N-LF-0.97087)*(N-HF-0.97086)	-0.416451	0.32102	-1.30	0.2853
(N-HF-0.97086)*(N-Du-0.97069)	0.2675824	0.321366	0.83	0.4661
(N-LF-0.97087)*(N-Du-0.97069)	0.1554335	0.32134	0.48	0.6617

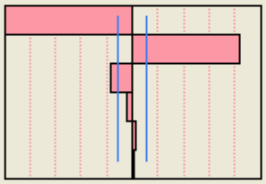

Figure 50. Sorted estimated parameters of prediction plot for Delta

Scaled Estimates

Continuous factors centered by mean, scaled by range/2

Term	Scaled Estimate	Std Error	t Ratio	Prob>|t|
Intercept	0.0214541	0.000244	88.08	<.0001*
N-LF	-0.007347	0.000272	-26.98	0.0001*
N-HF	0.0061897	0.000272	22.73	0.0002*
N-Du	-0.001188	0.000272	-4.36	0.0223*
(N-LF-0.97087)*(N-HF-0.97086)	-0.000353	0.000272	-1.30	0.2853
(N-HF-0.97086)*(N-Du-0.97069)	0.0002267	0.000272	0.83	0.4661
(N-LF-0.97087)*(N-Du-0.97069)	0.0001317	0.000272	0.48	0.6617

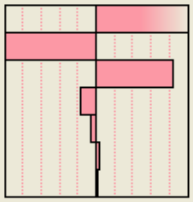

Figure 51. Scaled estimates of prediction plot for Delta

Figure 53 shows the analysis for sputter to deposition rate and the estimates, the interaction profiles, effects and other charts have been pasted on this page.

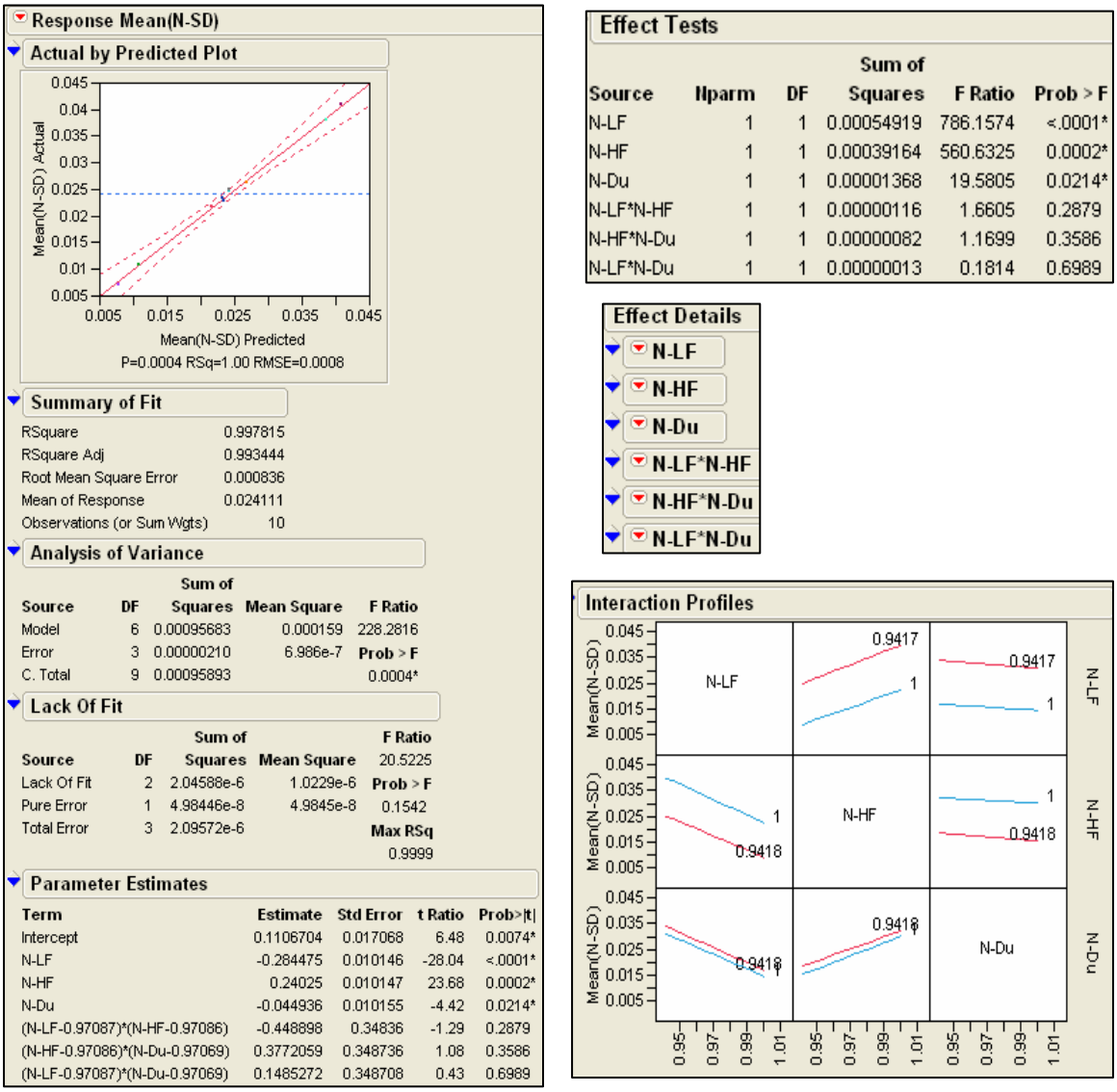

Figure 52. Actual versus prediction plot for sputter to deposition ratio with its analysis

Scaled Estimates

Continuous factors centered by mean, scaled by range/2

Term	Scaled Estimate	Std Error	t Ratio	Prob>|t|
Intercept	0.024111	0.000264	91.22	<.0001*
N-LF	-0.008286	0.000296	-28.04	<.0001*
N-HF	0.006997	0.000296	23.68	0.0002*
N-Du	-0.001307	0.000295	-4.42	0.0214*
(N-LF-0.97087)*(N-HF-0.97086)	-0.000381	0.000296	-1.29	0.2879
(N-HF-0.97086)*(N-Du-0.97069)	0.0003196	0.000296	1.08	0.3586
(N-LF-0.97087)*(N-Du-0.97069)	0.0001259	0.000296	0.43	0.6989

Figure 53. Scaled estimates for prediction plot of sputter to deposition ratio

Sorted Parameter Estimates

Term	Estimate	Std Error	t Ratio	Prob>|t|
N-LF	-0.284475	0.010146	-28.04	<.0001*
N-HF	0.24025	0.010147	23.68	0.0002*
N-Du	-0.044936	0.010155	-4.42	0.0214*
(N-LF-0.97087)*(N-HF-0.97086)	-0.448898	0.34836	-1.29	0.2879
(N-HF-0.97086)*(N-Du-0.97069)	0.3772059	0.348736	1.08	0.3586
(N-LF-0.97087)*(N-Du-0.97069)	0.1485272	0.348708	0.43	0.6989

Figure 54. Sorted parameter estimates for prediction plot of sputter to deposition ratio

Figure 53 represents the analysis for sputter to deposition. As we can see, sputter to deposition rate has a great correlation with the two powers and the Deuterium gas flow as well. However, similar to the previous Delta analysis, we can see that Deuterium gas flow does not impact the magnitude greatly at two different values. LF power and HF power have a huge impact on the sputter to deposition rate. This is clear in the first row and first column of the interaction profiles in Figure 53.

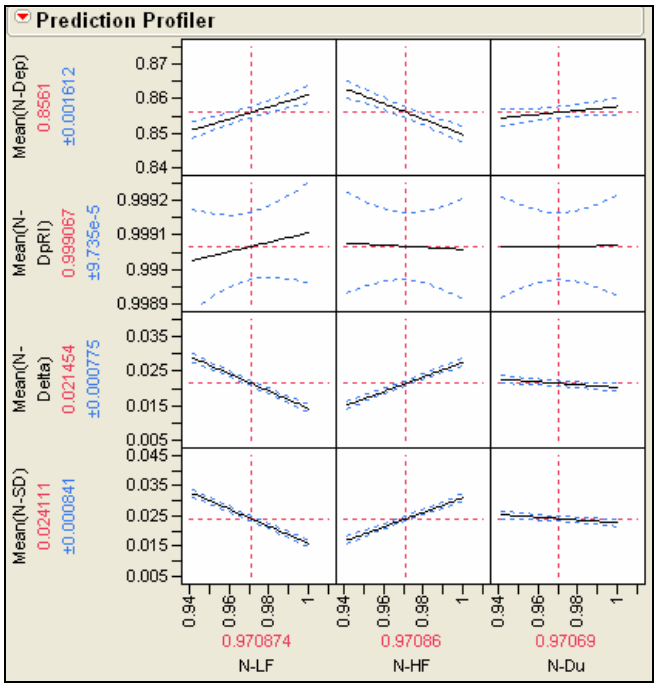

Figure 55. Prediction Profiler

Figure 56 represents the prediction profiler, which was made on the basis of all the other prediction analysis on the four responses and the three main factors. The prediction profiler clearly gives an idea regarding the dependency of the three continuous input changes with the four defined responses and the margin of error as well. As shown from the earlier analysis charts and with the prediction profiler, it can be stated that the deposition rate by HF and LF power is different and counter acting. All four responses show different relationships between the two power factors, which leads one to believe that frequency of the power used is important in this model. The frequency of the biasing or power applied during the process is crucial in determining its impact on the deposition rate and the sputtering rate.

So, from this entire modeling and DOE section, it is apparent how the frequency of the two powers applied impact the process and the responses. The assumptions about "the higher power leads to higher rate of etching" and similar cases may be confusing in many ways. The model clearly represents the effects of two different frequency powers in a significant way.

The rest of the chapter includes data sheets and pictures taken from the hardware set up (processing tool & chamber), used for this model. The data has been normalized with respect to their maximum values and then attached is the summary data obtained from JMP. The summary data is a set of 10 data points, each one taken from all the ten wafers. In the next chapters, the impact of such analysis and the conclusions along with suitable references and resources are discussed.

C.

Table 5. Data sheets for the normalized data:

Slot ID	N-Dep	N-DpRI	N-Sput	DpGOF	SpGOF	X	Y	Radius	N-Delta	N-SD	Zone	N-LF	N-HF	N-Du
1	0.935501	0.999179	0.916153	0.991	0.9926	0	0	0	0.019348	0.020263	C	1	1	0.94181
1	0.949119	0.999179	0.923003	0.991	0.9926	-0.0001	49	49	0.026117	0.02678	I	1	1	0.94181
1	0.941138	0.998974	0.91539	0.9907	0.9924	-34.6483	34.648	48.99988	0.025748	0.02663	I	1	1	0.94181
1	0.930624	0.999043	0.903562	0.9909	0.9925	-49	-0.0001	49	0.027062	0.028258	I	1	1	0.94181
1	0.922488	.	0.895999	0.991	0.9925	-34.648	-34.6483	48.99988	0.026489	0.027914	I	1	1	0.94181
1	0.938461	0.999043	0.91251	0.9909	0.9926	0.0001	-49	49	0.025951	0.026909	I	1	1	0.94181
1	0.947196	0.999111	0.923928	0.9909	0.9925	34.6483	-34.648	48.99988	0.023268	0.023976	I	1	1	0.94181
1	0.960389	0.999316	0.940464	0.9909	0.9924	49	0.0001	49	0.019925	0.020326	I	1	1	0.94181
1	0.960158	0.999248	0.938353	0.9908	0.9925	34.648	34.6483	48.99988	0.021805	0.022206	I	1	1	0.94181
1	0.918021	0.999179	0.888137	0.9911	0.9925	-0.0003	98	98	0.029884	0.031526	M	1	1	0.94181
1	0.902113	0.998974	0.87082	0.9912	0.9924	-37.5034	90.5401	98.00008	0.031293	0.033526	M	1	1	0.94181
1	0.904001	0.999111	0.873368	0.9912	0.9924	-69.2967	69.2962	97.99998	0.030633	0.032776	M	1	1	0.94181
1	0.898082	0.999043	0.867044	0.9914	0.9926	-90.5404	37.5026	98.00005	0.031038	0.033406	M	1	1	0.94181
1	0.860136	0.999111	0.825886	0.9918	0.9924	-98	-0.0004	98	0.034251	0.038295	M	1	1	0.94181
1	0.869797	0.999111	0.837223	0.9916	0.9923	-90.5401	-37.5034	98.00008	0.032574	0.036098	M	1	1	0.94181
1	0.842911	0.999043	0.808874	0.9918	0.9922	-69.2962	-69.2967	97.99998	0.034037	0.038813	M	1	1	0.94181
1	0.832647	0.998974	0.797801	0.9919	0.9923	-37.5026	-90.5404	98.00005	0.034846	0.040168	M	1	1	0.94181
1	0.874234	0.999111	0.844239	0.9916	0.9924	0.0004	-98	98	0.029995	0.033172	M	1	1	0.94181
1	0.867677	0.999111	0.836983	0.9918	0.9924	37.5034	-90.5401	98.00008	0.030694	0.034167	M	1	1	0.94181
1	0.875472	0.999179	0.845793	0.9916	0.9924	69.2968	-69.2962	98.00005	0.029678	0.032788	M	1	1	0.94181
1	0.913935	0.999316	0.887367	0.9914	0.9926	90.5404	-37.5026	98.00005	0.026568	0.028249	M	1	1	0.94181
1	0.887878	0.999179	0.85746	0.9915	0.9925	98	0.0004	98	0.030418	0.033125	M	1	1	0.94181
1	0.904032	0.999316	0.874353	0.9913	0.9925	90.5401	37.5034	98.00008	0.029679	0.031786	M	1	1	0.94181
1	0.920659	0.999111	0.891234	0.991	0.9925	69.2961	69.2968	97.99998	0.029425	0.030971	M	1	1	0.94181
1	0.888783	0.999179	0.855929	0.9914	0.9925	37.5026	90.5404	98.00005	0.032854	0.035648	M	1	1	0.94181
1	0.831451	0.998837	0.821333	0.9918	0.9922	-0.0006	147	147	0.010119	0.012023	O	1	1	0.94181
1	0.799515	0.998632	0.785752	0.9917	0.992	-38.047	141.991	147.0001	0.013763	0.016923	O	1	1	0.94181
1	0.79506	0.998701	0.779897	0.9916	0.9918	-73.5004	127.3055	147	0.015163	0.018715	O	1	1	0.94181
1	0.801927	0.998632	0.790536	0.9914	0.9916	-103.945	103.9443	146.9999	0.011392	0.014007	O	1	1	0.94181

Slot ID	N-Dep	N-DpRI	N-Sput	DpGOF	SpGOF	X	Y	Radius	N-Delta	N-SD	Zone	N-LF	N-HF	N-Du
1	0.830311	0.998632	0.825101	0.9913	0.9918	-127.306	73.4996	147	0.00521	0.006236	O	1	1	0.94181
1	0.788686	0.998564	0.779687	0.9914	0.9917	-141.991	38.0458	147	0.008999	0.011281	O	1	1	0.94181
1	0.771545	0.998701	0.757728	0.9919	0.9923	-147	-0.0006	147	0.013817	0.017594	O	1	1	0.94181
1	0.768252	0.998701	0.755467	0.992	0.9924	-141.991	-38.047	147.0001	0.012784	0.016369	O	1	1	0.94181
1	0.797274	0.998701	0.791353	0.9914	0.9917	-127.305	-73.5004	146.9999	0.005921	0.007372	O	1	1	0.94181
1	0.765691	0.998701	0.756205	0.9909	0.9917	-103.944	-103.945	147.0001	0.009486	0.012237	O	1	1	0.94181
1	0.763413	0.998837	0.750627	0.9911	0.9918	-73.4994	-127.306	146.9999	0.012786	0.016472	O	1	1	0.94181
1	0.770758	0.998837	0.758732	0.9917	0.9921	-38.0458	-141.991	147	0.012027	0.015364	O	1	1	0.94181
1	0.792889	0.999248	0.783285	0.9925	0.9925	0.0006	-147	147	0.009605	0.011969	O	1	1	0.94181
1	0.796313	0.999111	0.786859	0.992	0.9922	38.047	-141.991	147.0001	0.009454	0.011733	O	1	1	0.94181
1	0.815992	0.999385	0.805224	0.9924	0.9925	73.5006	-127.305	147	0.010768	0.013025	O	1	1	0.94181
1	0.814413	0.999316	0.804686	0.9924	0.9925	103.9452	-103.944	147.0001	0.009727	0.011803	O	1	1	0.94181
1	0.814864	0.999385	0.80615	0.9927	0.9927	127.3061	-73.4994	147	0.008713	0.010579	O	1	1	0.94181
1	0.788053	0.999385	0.775735	0.9926	0.9927	141.9913	-38.0458	147	0.012318	0.01539	O	1	1	0.94181
1	0.782609	0.999179	0.766438	0.9924	0.9927	147	0.0006	147	0.016171	0.020245	O	1	1	0.94181
1	0.781101	0.999248	0.76541	0.9924	0.9926	141.991	38.047	147.0001	0.015691	0.019693	O	1	1	0.94181
1	0.818194	0.999248	0.808049	0.9925	0.9927	127.3054	73.5006	147	0.010145	0.012247	O	1	1	0.94181
1	0.798321	0.999179	0.784733	0.9922	0.9923	103.9443	103.9452	147.0001	0.013588	0.016736	O	1	1	0.94181
1	0.79416	0.998974	0.77743	0.9919	0.9921	73.4994	127.3061	147	0.016731	0.020632	O	1	1	0.94181
1	0.789879	0.999385	0.773963	0.9921	0.9922	38.0458	141.9913	147	0.015917	0.019753	O	1	1	0.94181
2	0.958952	0.999111	0.944608	0.9904	0.9922	0	0	0	0.014344	0.014738	C	1	1	1
2	0.970255	0.999111	0.949378	0.9904	0.9923	-0.0001	49	49	0.020877	0.021064	I	1	1	1
2	0.960883	0.998837	0.939282	0.9902	0.9921	-34.6483	34.648	48.99988	0.021601	0.021986	I	1	1	1
2	0.948609	0.998906	0.925473	0.9904	0.9923	-49	-0.0001	49	0.023136	0.023809	I	1	1	1
2	0.940354	0.999795	0.917524	0.9906	0.9923	-34.648	-34.6483	48.99988	0.022829	0.023702	I	1	1	1
2	0.956092	0.999043	0.935274	0.9903	0.9922	0.0001	-49	49	0.020818	0.02131	I	1	1	1
2	0.964162	0.999179	0.946037	0.9904	0.9922	34.6483	-34.648	48.99988	0.018125	0.018452	I	1	1	1
2	0.979687	0.999179	0.963657	0.9903	0.992	49	0.0001	49	0.01603	0.016099	I	1	1	1
2	0.979038	0.999248	0.961667	0.9903	0.9921	34.648	34.6483	48.99988	0.017371	0.017433	I	1	1	1

Slot ID	N-Dep	N-DpRl	N-Sput	DpGOF	SpGOF	X	Y	Radius	N-Delta	N-SD	Zone	N-LF	N-HF	N-Du
2	0.92617	0.999111	0.89926	0.9909	0.9924	-0.0003	98	98	0.02691	0.028234	M	1	1	1
2	0.916725	0.999043	0.888638	0.991	0.9924	-37.5034	90.5401	98.00008	0.028088	0.029728	M	1	1	1
2	0.912295	0.999043	0.884705	0.9907	0.9922	-69.2967	69.2962	97.99998	0.02759	0.029355	M	1	1	1
2	0.912691	0.999043	0.885401	0.991	0.9924	-90.5404	37.5026	98.00005	0.02729	0.029033	M	1	1	1
2	0.872481	0.998974	0.840983	0.9913	0.9922	-98	-0.0004	98	0.031498	0.034844	M	1	1	1
2	0.878374	0.999043	0.848241	0.9913	0.9923	-90.5401	-37.5034	98.00008	0.030133	0.033167	M	1	1	1
2	0.856055	0.998974	0.824652	0.9913	0.992	-69.2962	-69.2967	97.99998	0.031403	0.035385	M	1	1	1
2	0.839656	0.998906	0.806635	0.9917	0.9921	-37.5026	-90.5404	98.00005	0.033021	0.037839	M	1	1	1
2	0.879853	0.999043	0.851614	0.9913	0.9923	0.0004	-98	98	0.028239	0.031097	M	1	1	1
2	0.876585	0.998974	0.848289	0.9914	0.9922	37.5034	-90.5401	98.00008	0.028297	0.031271	M	1	1	1
2	0.880899	0.999043	0.852825	0.9913	0.9922	69.2968	-69.2962	98.00005	0.028074	0.030886	M	1	1	1
2	0.921362	0.999248	0.897043	0.991	0.9924	90.5404	-37.5026	98.00005	0.024319	0.025716	M	1	1	1
2	0.898088	0.999179	0.870193	0.9913	0.9924	98	0.0004	98	0.027894	0.030124	M	1	1	1
2	0.907092	0.999385	0.879564	0.9912	0.9924	90.5401	37.5034	98.00008	0.027528	0.029454	M	1	1	1
2	0.932609	0.999111	0.905969	0.9907	0.9924	69.2961	69.2968	97.99998	0.02664	0.027772	M	1	1	1
2	0.897662	0.999179	0.867632	0.9913	0.9924	37.5026	90.5404	98.00005	0.030029	0.03237	M	1	1	1
2	0.823134	0.998769	0.810428	0.9917	0.992	-0.0006	147	147	0.012706	0.015201	O	1	1	1
2	0.793866	0.998769	0.778534	0.9918	0.9921	-38.047	141.991	147.0001	0.015332	0.018947	O	1	1	1
2	0.792511	0.998701	0.777354	0.9915	0.9916	-73.5004	127.3055	147	0.015157	0.018766	O	1	1	1
2	0.799407	0.998496	0.786897	0.9913	0.9915	-103.945	103.9443	146.9999	0.01251	0.015408	O	1	1	1
2	0.826203	0.998564	0.818695	0.9911	0.9914	-127.306	73.4996	147	0.007508	0.009006	O	1	1	1
2	0.787475	0.998564	0.776722	0.9912	0.9914	-141.991	38.0458	147	0.010753	0.013471	O	1	1	1
2	0.777445	0.998564	0.763766	0.9911	0.9916	-147	-0.0006	147	0.013679	0.017291	O	1	1	1
2	0.771551	0.998701	0.758423	0.9911	0.9917	-141.991	-38.047	147.0001	0.013129	0.016731	O	1	1	1
2	0.792537	0.998564	0.783546	0.9913	0.9915	-127.305	-73.5004	146.9999	0.008991	0.011217	O	1	1	1
2	0.76289	0.998564	0.750918	0.9907	0.9914	-103.944	-103.945	147.0001	0.011972	0.015451	O	1	1	1
2	0.763967	0.998769	0.749928	0.9908	0.9914	-73.4994	-127.306	146.9999	0.014039	0.018045	O	1	1	1
2	0.767483	0.998906	0.754072	0.9915	0.992	-38.0458	-141.991	147	0.013411	0.017174	O	1	1	1
2	0.786024	0.999111	0.773589	0.9922	0.9923	0.0006	-147	147	0.012434	0.015573	O	1	1	1

Slot ID	N-Dep	N-DpRl	N-Sput	DpGOF	SpGOF	X	Y	Radius	N-Delta	N-SD	Zone	N-LF	N-HF	N-Du
2	0.81762	0.999316	0.805425	0.9921	0.9922	73.5006	-127.305	147	0.012195	0.014697	O	1	1	1
2	0.811613	0.999316	0.799703	0.9924	0.9924	103.9452	-103.944	147.0001	0.01191	0.014463	O	1	1	1
2	0.805476	0.999385	0.794378	0.9925	0.9925	127.3061	-73.4994	147	0.011098	0.013591	O	1	1	1
2	0.785754	0.999316	0.773371	0.9925	0.9925	141.9913	-38.0458	147	0.012383	0.015515	O	1	1	1
2	0.774369	0.999248	0.758148	0.9925	0.9926	147	0.0006	147	0.016221	0.020518	O	1	1	1
2	0.772957	0.999316	0.756839	0.9925	0.9926	141.991	38.047	147.0001	0.016119	0.020427	O	1	1	1
2	0.805372	0.999316	0.793286	0.9926	0.9925	127.3054	73.5006	147	0.012086	0.014785	O	1	1	1
2	0.78483	0.999316	0.770158	0.9924	0.9924	103.9443	103.9452	147.0001	0.014672	0.018351	O	1	1	1
2	0.78548	0.999111	0.767467	0.9922	0.9922	73.4994	127.3061	147	0.018012	0.022418	O	1	1	1
2	0.784172	0.999385	0.767002	0.9919	0.9921	38.0458	141.9913	147	0.01717	0.021426	O	1	1	1
3	0.960488	0.999248	0.956726	0.9916	0.9927	0	0	0	0.003762	0.003902	C	1	0.941752	0.94181
3	0.9738	0.999248	0.964508	0.9916	0.9928	-0.0001	49	49	0.009292	0.009451	I	1	0.941752	0.94181
3	0.964019	0.999111	0.953484	0.9915	0.9927	-34.6483	34.648	48.99988	0.010535	0.01081	I	1	0.941752	0.94181
3	0.954085	0.999111	0.942197	0.9915	0.9927	-49	-0.0001	49	0.011888	0.012307	I	1	0.941752	0.94181
3	0.944548	1	0.933087	0.9918	0.9929	-34.648	-34.6483	48.99988	0.011461	0.011988	I	1	0.941752	0.94181
3	0.96144	0.999248	0.952389	0.9916	0.9927	0.0001	-49	49	0.009051	0.009326	I	1	0.941752	0.94181
3	0.969121	0.999385	0.96217	0.9916	0.9927	34.6483	-34.648	48.99988	0.006951	0.007122	I	1	0.941752	0.94181
3	0.985799	0.999385	0.981063	0.9916	0.9926	49	0.0001	49	0.004736	0.004781	I	1	0.941752	0.94181
3	0.984139	0.999385	0.977849	0.9916	0.9926	34.648	34.6483	48.99988	0.006291	0.006351	I	1	0.941752	0.94181
3	0.935182	0.999385	0.919264	0.9918	0.9929	-0.0003	98	98	0.015918	0.016736	M	1	0.941752	0.94181
3	0.925503	0.999248	0.908569	0.9918	0.9929	-37.5034	90.5401	98.00008	0.016934	0.017968	M	1	0.941752	0.94181
3	0.920002	0.999316	0.902803	0.9919	0.9929	-69.2967	69.2962	97.99998	0.017198	0.018351	M	1	0.941752	0.94181
3	0.922601	0.999179	0.906067	0.9919	0.9929	-90.5404	37.5026	98.00005	0.016534	0.017605	M	1	0.941752	0.94181
3	0.882258	0.999179	0.861507	0.9921	0.9928	-98	-0.0004	98	0.020751	0.02298	M	1	0.941752	0.94181
3	0.890313	0.999179	0.870888	0.9921	0.9928	-90.5401	-37.5034	98.00008	0.019426	0.021353	M	1	0.941752	0.94181
3	0.865153	0.999179	0.844266	0.9922	0.9928	-69.2962	-69.2967	97.99998	0.020887	0.023573	M	1	0.941752	0.94181
3	0.848723	0.999111	0.825691	0.9923	0.9928	-37.5026	-90.5404	98.00005	0.023031	0.026419	M	1	0.941752	0.94181
3	0.890018	0.999248	0.87214	0.9922	0.9929	0.0004	-98	98	0.017878	0.019692	M	1	0.941752	0.94181
3	0.886408	0.999179	0.867906	0.9922	0.9929	37.5034	-90.5401	98.00008	0.018502	0.020446	M	1	0.941752	0.94181

Slot ID	N-Dep	N-DpRl	N-Sput	DpGOF	SpGOF	X	Y	Radius	N-Delta	N-SD	Zone	N-LF	N-HF	N-Du
3	0.930344	0.999385	0.916483	0.992	0.993	90.5404	-37.5026	98.00005	0.013861	0.014681	M	1	0.941752	0.94181
3	0.906284	0.999316	0.88828	0.9922	0.993	98	0.0004	98	0.018004	0.019479	M	1	0.941752	0.94181
3	0.915217	0.999521	0.89816	0.9921	0.993	90.5401	37.5034	98.00008	0.017058	0.018297	M	1	0.941752	0.94181
3	0.942693	0.999316	0.927384	0.9918	0.9929	69.2961	69.2968	97.99998	0.01531	0.015981	M	1	0.941752	0.94181
3	0.907775	0.999385	0.888775	0.9921	0.993	37.5026	90.5404	98.00005	0.019	0.020501	M	1	0.941752	0.94181
3	0.832151	0.999043	0.828135	0.9924	0.9927	-0.0006	147	147	0.004015	0.004802	O	1	0.941752	0.94181
3	0.811092	0.998837	0.805025	0.9923	0.9924	-38.047	141.991	147.0001	0.006066	0.007424	O	1	0.941752	0.94181
3	0.803045	0.998837	0.796549	0.9923	0.9923	-73.5004	127.3055	147	0.006497	0.008025	O	1	0.941752	0.94181
3	0.810998	0.998701	0.80729	0.9922	0.9923	-103.945	103.9443	146.9999	0.003708	0.004551	O	1	0.941752	0.94181
3	0.839234	0.998632	0.840368	0.9919	0.9923	-127.306	73.4996	147	-0.00113	-0.00135	O	1	0.941752	0.94181
3	0.800221	0.998632	0.797763	0.9919	0.992	-141.991	38.0458	147	0.002458	0.003062	O	1	0.941752	0.94181
3	0.786993	0.998564	0.781735	0.9919	0.9921	-147	-0.0006	147	0.005258	0.006637	O	1	0.941752	0.94181
3	0.782044	0.998564	0.777028	0.992	0.9922	-141.991	-38.047	147.0001	0.005015	0.006372	O	1	0.941752	0.94181
3	0.80479	0.998701	0.804092	0.992	0.992	-127.305	-73.5004	146.9999	0.000698	0.000866	O	1	0.941752	0.94181
3	0.774776	0.998564	0.770924	0.9917	0.992	-103.944	-103.945	147.0001	0.003852	0.004947	O	1	0.941752	0.94181
3	0.768713	0.998769	0.761567	0.9919	0.9922	-73.4994	-127.306	146.9999	0.007146	0.009211	O	1	0.941752	0.94181
3	0.779408	0.998974	0.774064	0.9924	0.9925	-38.0458	-141.991	147	0.005345	0.006811	O	1	0.941752	0.94181
3	0.79532	0.999248	0.79063	0.9929	0.9928	0.0006	-147	147	0.00469	0.005863	O	1	0.941752	0.94181
3	0.805446	0.999179	0.80214	0.9923	0.9924	38.047	-141.991	147.0001	0.003307	0.004088	O	1	0.941752	0.94181
3	0.82943	0.999453	0.825735	0.9926	0.9928	73.5006	-127.305	147	0.003695	0.004436	O	1	0.941752	0.94181
3	0.821727	0.999658	0.81814	0.993	0.993	103.9452	-103.944	147.0001	0.003588	0.004347	O	1	0.941752	0.94181
3	0.816565	0.99959	0.813796	0.993	0.993	127.3061	-73.4994	147	0.002769	0.003379	O	1	0.941752	0.94181
3	0.799923	0.999521	0.795472	0.993	0.9929	141.9913	-38.0458	147	0.00445	0.005532	O	1	0.941752	0.94181
3	0.786421	0.999385	0.778135	0.993	0.9929	147	0.0006	147	0.008285	0.010426	O	1	0.941752	0.94181
3	0.783426	0.999453	0.775507	0.993	0.993	141.991	38.047	147.0001	0.007919	0.010006	O	1	0.941752	0.94181
3	0.814615	0.999453	0.81072	0.9931	0.993	127.3054	73.5006	147	0.003895	0.004759	O	1	0.941752	0.94181
3	0.798932	0.999385	0.792571	0.9929	0.9928	103.9443	103.9452	147.0001	0.006361	0.007899	O	1	0.941752	0.94181
3	0.79632	0.999248	0.787004	0.9928	0.9927	73.4994	127.3061	147	0.009316	0.011563	O	1	0.941752	0.94181
3	0.795398	0.99959	0.787167	0.9926	0.9926	38.0458	141.9913	147	0.00823	0.010241	O	1	0.941752	0.94181

Slot ID	N-Dep	N-DpRI	N-Sput	DpGOF	SpGOF	X	Y	Radius	N-Delta	N-SD	Zone	N-LF	N-HF	N-Du
4	0.943295	0.999111	0.904825	0.9887	0.9916	-0.0001	49	49	0.03847	0.039185	I	0.941748	1	1
4	0.934773	0.998974	0.895297	0.9886	0.9914	-34.6483	34.648	48.99988	0.039477	0.04052	I	0.941748	1	1
4	0.923145	0.998906	0.882663	0.989	0.9915	-49	-0.0001	49	0.040482	0.04201	I	0.941748	1	1
4	0.915792	.	0.87546	0.9893	0.9915	-34.648	-34.6483	48.99988	0.040332	0.042183	I	0.941748	1	1
4	0.93075	0.999043	0.893389	0.9889	0.9915	0.0001	-49	49	0.037361	0.038591	I	0.941748	1	1
4	0.939731	0.999111	0.904543	0.9888	0.9915	34.6483	-34.648	48.99988	0.035187	0.036093	I	0.941748	1	1
4	0.952793	0.999179	0.919243	0.9886	0.9914	49	0.0001	49	0.033551	0.034015	I	0.941748	1	1
4	0.953442	0.999179	0.918023	0.9885	0.9914	34.648	34.6483	48.99988	0.035419	0.035818	I	0.941748	1	1
4	0.9105	0.999179	0.867657	0.9894	0.9914	-0.0003	98	98	0.042844	0.044941	M	0.941748	1	1
4	0.902869	0.999111	0.859009	0.9894	0.9914	-37.5034	90.5401	98.00008	0.04386	0.046328	M	0.941748	1	1
4	0.900377	0.999179	0.856472	0.9893	0.9913	-69.2967	69.2962	97.99998	0.043905	0.046495	M	0.941748	1	1
4	0.897239	0.999179	0.853352	0.9896	0.9914	-90.5404	37.5026	98.00005	0.043887	0.046633	M	0.941748	1	1
4	0.862238	0.999043	0.814872	0.9902	0.9913	-98	-0.0004	98	0.047366	0.052073	M	0.941748	1	1
4	0.868305	0.999111	0.822565	0.99	0.9913	-90.5401	-37.5034	98.00008	0.04574	0.050041	M	0.941748	1	1
4	0.845485	0.999111	0.798659	0.9903	0.9913	-69.2962	-69.2967	97.99998	0.046827	0.052478	M	0.941748	1	1
4	0.830809	0.999111	0.783068	0.9907	0.9914	-37.5026	-90.5404	98.00005	0.047741	0.054341	M	0.941748	1	1
4	0.866769	0.999179	0.824148	0.9902	0.9912	0.0004	-98	98	0.042621	0.046867	M	0.941748	1	1
4	0.866167	0.999043	0.82327	0.9901	0.9914	37.5034	-90.5401	98.00008	0.042897	0.047188	M	0.941748	1	1
4	0.869394	0.999179	0.827519	0.99	0.9912	69.2968	-69.2962	98.00005	0.041875	0.045953	M	0.941748	1	1
4	0.905083	0.999248	0.866131	0.9896	0.9914	90.5404	-37.5026	98.00005	0.038951	0.041261	M	0.941748	1	1
4	0.886915	0.999179	0.845177	0.9899	0.9913	98	0.0004	98	0.041738	0.044945	M	0.941748	1	1
4	0.894098	0.999316	0.852192	0.9899	0.9914	90.5401	37.5034	98.00008	0.041905	0.04477	M	0.941748	1	1
4	0.918931	0.999111	0.877474	0.9892	0.9914	69.2961	69.2968	97.99998	0.041457	0.043167	M	0.941748	1	1
4	0.889378	0.999179	0.844692	0.9898	0.9914	37.5026	90.5404	98.00005	0.044686	0.04784	M	0.941748	1	1
4	0.82031	0.998837	0.795239	0.9904	0.991	-0.0006	147	147	0.02507	0.029656	O	0.941748	1	1
4	0.798542	0.998769	0.771144	0.9902	0.991	-38.047	141.991	147.0001	0.027398	0.033171	O	0.941748	1	1
4	0.790506	0.998906	0.761728	0.9899	0.9908	-73.5004	127.3055	147	0.028778	0.035126	O	0.941748	1	1
4	0.791962	0.998769	0.765814	0.9898	0.9906	-103.945	103.9443	146.9999	0.026148	0.031961	O	0.941748	1	1
4	0.820557	0.998769	0.799675	0.9895	0.99	-127.306	73.4996	147	0.020882	0.024817	O	0.941748	1	1

Slot ID	N-Dep	N-DpRl	N-Sput	DpGOF	SpGOF	X	Y	Radius	N-Delta	N-SD	Zone	N-LF	N-HF	N-Du
4	0.771557	0.999043	0.745391	0.9894	0.9906	-147	-0.0006	147	0.026167	0.032802	O	0.941748	1	1
4	0.763213	0.998837	0.736232	0.9894	0.9909	-141.991	-38.047	147.0001	0.026981	0.034145	O	0.941748	1	1
4	0.785575	0.999043	0.763138	0.9894	0.9902	-127.305	-73.5004	146.9999	0.022437	0.027768	O	0.941748	1	1
4	0.754279	0.999179	0.728551	0.9892	0.9909	-103.944	-103.945	147.0001	0.025728	0.032985	O	0.941748	1	1
4	0.754101	0.999453	0.727122	0.9891	0.9908	-73.4994	-127.306	146.9999	0.026979	0.03454	O	0.941748	1	1
4	0.759428	0.999248	0.733046	0.99	0.9913	-38.0458	-141.991	147	0.026382	0.033573	O	0.941748	1	1
4	0.774563	0.999248	0.749026	0.991	0.9917	0.0006	-147	147	0.025537	0.031917	O	0.941748	1	1
4	0.781463	0.999248	0.757622	0.9901	0.9911	38.047	-141.991	147.0001	0.023841	0.029605	O	0.941748	1	1
4	0.803955	0.999316	0.779871	0.9906	0.9911	73.5006	-127.305	147	0.024084	0.029086	O	0.941748	1	1
4	0.797898	0.999316	0.774574	0.9913	0.9916	103.9452	-103.944	147.0001	0.023323	0.028401	O	0.941748	1	1
4	0.794786	0.999316	0.77195	0.9915	0.9917	127.3061	-73.4994	147	0.022836	0.02793	O	0.941748	1	1
4	0.777167	0.999385	0.751694	0.9914	0.9919	141.9913	-38.0458	147	0.025473	0.031737	O	0.941748	1	1
4	0.768902	0.999316	0.739902	0.9913	0.992	147	0.0006	147	0.029	0.036346	O	0.941748	1	1
4	0.765591	0.999316	0.736553	0.9912	0.9921	141.991	38.047	147.0001	0.029037	0.036542	O	0.941748	1	1
4	0.795791	0.999248	0.770542	0.9914	0.9917	127.3054	73.5006	147	0.025249	0.030753	O	0.941748	1	1
4	0.782917	0.999248	0.755005	0.9911	0.9917	103.9443	103.9452	147.0001	0.027912	0.034424	O	0.941748	1	1
4	0.779948	0.999179	0.749182	0.9909	0.9916	73.4994	127.3061	147	0.030766	0.037949	O	0.941748	1	1
4	0.776693	0.999521	0.74655	0.9906	0.9914	38.0458	141.9913	147	0.030143	0.03736	O	0.941748	1	1
5	0.978199	0.999248	0.978849	0.9911	0.9923	0	0	0	-0.00065	-0.00066	C	1	0.941752	1
5	0.989877	0.999248	0.985471	0.9912	0.9924	-0.0001	49	49	0.004406	0.004431	I	1	0.941752	1
5	0.97987	0.999043	0.97389	0.9911	0.9923	-34.6483	34.648	48.99988	0.00598	0.006065	I	1	0.941752	1
5	0.969056	0.999043	0.961259	0.9912	0.9925	-49	-0.0001	49	0.007798	0.007982	I	1	0.941752	1
5	0.958828	0.999932	0.950833	0.9914	0.9926	-34.648	-34.6483	48.99988	0.007995	0.008269	I	1	0.941752	1
5	0.975811	0.999179	0.970861	0.9912	0.9924	0.0001	-49	49	0.00495	0.005047	I	1	0.941752	1
5	0.984412	0.999248	0.981704	0.9912	0.9924	34.6483	-34.648	48.99988	0.002708	0.002743	I	1	0.941752	1
5	1	0.999316	1	0.9911	0.9923	49	0.0001	49	0	0	I	1	0.941752	1
5	0.999435	0.999316	0.997836	0.9911	0.9924	34.648	34.6483	48.99988	0.001599	0.001597	I	1	0.941752	1
5	0.943998	0.999385	0.931872	0.992	0.993	-0.0003	98	98	0.012126	0.012682	M	1	0.941752	1
5	0.933802	0.999316	0.920148	0.9921	0.9931	-37.5034	90.5401	98.00008	0.013654	0.014412	M	1	0.941752	1

Slot ID	N-Dep	N-DpRl	N-Sput	DpGOF	SpGOF	X	Y	Radius	N-Delta	N-SD	Zone	N-LF	N-HF	N-Du
5	0.931142	0.999316	0.918228	0.9921	0.993	-90.5404	37.5026	98.00005	0.012914	0.013679	M	1	0.941752	1
5	0.889401	0.999248	0.871882	0.9923	0.993	-98	-0.0004	98	0.017519	0.019317	M	1	0.941752	1
5	0.897121	0.999248	0.881479	0.9922	0.993	-90.5401	-37.5034	98.00008	0.015642	0.017137	M	1	0.941752	1
5	0.872438	0.999248	0.854496	0.9923	0.9929	-69.2962	-69.2967	97.99998	0.017942	0.020151	M	1	0.941752	1
5	0.855526	0.999111	0.835871	0.9924	0.9929	-37.5026	-90.5404	98.00005	0.019655	0.022458	M	1	0.941752	1
5	0.89778	0.999316	0.883482	0.9921	0.9929	0.0004	-98	98	0.014298	0.015676	M	1	0.941752	1
5	0.892686	0.999248	0.878003	0.9921	0.993	37.5034	-90.5401	98.00008	0.014683	0.016182	M	1	0.941752	1
5	0.898555	0.999316	0.884275	0.9921	0.9929	69.2968	-69.2962	98.00005	0.01428	0.015644	M	1	0.941752	1
5	0.940525	0.999521	0.930652	0.9919	0.9929	90.5404	-37.5026	98.00005	0.009873	0.010388	M	1	0.941752	1
5	0.915203	0.999385	0.901458	0.9921	0.993	98	0.0004	98	0.013744	0.014796	M	1	0.941752	1
5	0.926006	0.99959	0.912754	0.9921	0.993	90.5401	37.5034	98.00008	0.013252	0.014109	M	1	0.941752	1
5	0.950474	0.999453	0.939016	0.9919	0.9929	69.2961	69.2968	97.99998	0.011457	0.011911	M	1	0.941752	1
5	0.915525	0.999385	0.899952	0.9921	0.9931	37.5026	90.5404	98.00005	0.015573	0.016725	M	1	0.941752	1
5	0.835227	0.999111	0.833709	0.9926	0.9928	-0.0006	147	147	0.001518	0.001814	O	1	0.941752	1
5	0.812101	0.998974	0.808649	0.9925	0.9926	-38.047	141.991	147.0001	0.003453	0.004234	O	1	0.941752	1
5	0.805371	0.998906	0.801092	0.9925	0.9926	-73.5004	127.3055	147	0.004279	0.005285	O	1	0.941752	1
5	0.811103	0.998906	0.80929	0.9925	0.9926	-103.945	103.9443	146.9999	0.001813	0.00223	O	1	0.941752	1
5	0.837429	0.998837	0.840224	0.9923	0.9926	-127.306	73.4996	147	-0.00279	-0.00335	O	1	0.941752	1
5	0.799909	0.998769	0.799754	0.9922	0.9924	-141.991	38.0458	147	0.000155	0.000194	O	1	0.941752	1
5	0.789293	0.998701	0.786338	0.9923	0.9924	-147	-0.0006	147	0.002955	0.00373	O	1	0.941752	1
5	0.784551	0.998837	0.78235	0.9924	0.9925	-141.991	-38.047	147.0001	0.002201	0.002798	O	1	0.941752	1
5	0.804704	0.998837	0.806436	0.9922	0.9924	-127.305	-73.5004	146.9999	-0.00173	-0.00216	O	1	0.941752	1
5	0.774833	0.998632	0.772774	0.9919	0.9921	-103.944	-103.945	147.0001	0.00206	0.002651	O	1	0.941752	1
5	0.775308	0.998906	0.771444	0.992	0.9922	-73.4994	-127.306	146.9999	0.003864	0.004959	O	1	0.941752	1
5	0.779436	0.999111	0.776278	0.9925	0.9925	-38.0458	-141.991	147	0.003158	0.004036	O	1	0.941752	1
5	0.799471	0.999316	0.797672	0.9929	0.9928	0.0006	-147	147	0.001799	0.002245	O	1	0.941752	1
5	0.804829	0.999248	0.804248	0.9925	0.9925	38.047	-141.991	147.0001	0.000582	0.000722	O	1	0.941752	1
5	0.832869	0.999521	0.831919	0.9925	0.9927	73.5006	-127.305	147	0.00095	0.001139	O	1	0.941752	1
5	0.826668	0.99959	0.825935	0.9928	0.9929	103.9452	-103.944	147.0001	0.000733	0.000886	O	1	0.941752	1

Slot ID	N-Dep	N-DpRl	N-Sput	DpGOF	SpGOF	X	Y	Radius	N-Delta	N-SD	Zone	N-LF	N-HF	N-Du
5	0.801635	0.999521	0.800067	0.9929	0.9928	141.9913	-38.0458	147	0.001568	0.001952	O	1	0.941752	1
5	0.792924	0.999385	0.788011	0.9929	0.9928	147	0.0006	147	0.004913	0.006158	O	1	0.941752	1
5	0.791544	0.999385	0.786684	0.9929	0.9929	141.991	38.047	147.0001	0.00486	0.006102	O	1	0.941752	1
5	0.823644	0.999453	0.823032	0.9929	0.993	127.3054	73.5006	147	0.000612	0.000743	O	1	0.941752	1
5	0.80839	0.999453	0.804901	0.9928	0.9928	103.9443	103.9452	147.0001	0.003488	0.004297	O	1	0.941752	1
5	0.798585	0.999316	0.791642	0.9928	0.9928	73.4994	127.3061	147	0.006943	0.008619	O	1	0.941752	1
5	0.798228	0.99959	0.792101	0.9927	0.9927	38.0458	141.9913	147	0.006127	0.007618	O	1	0.941752	1
6	0.948598	0.999043	0.930681	0.9901	0.992	0	0	0	0.017917	0.018538	C	0.970874	0.970795	0.969828
6	0.958683	0.999043	0.934595	0.9902	0.9921	-0.0001	49	49	0.024088	0.02451	I	0.970874	0.970795	0.969828
6	0.949123	0.998837	0.924204	0.99	0.992	-34.6483	34.648	48.99988	0.024918	0.025583	I	0.970874	0.970795	0.969828
6	0.938465	0.998906	0.912029	0.9903	0.9922	-49	-0.0001	49	0.026436	0.027397	I	0.970874	0.970795	0.969828
6	0.931256	0.999726	0.905208	0.9905	0.9922	-34.648	-34.6483	48.99988	0.026049	0.027211	I	0.970874	0.970795	0.969828
6	0.948176	0.999043	0.925308	0.9901	0.9922	0.0001	-49	49	0.022869	0.023551	I	0.970874	0.970795	0.969828
6	0.954961	0.999043	0.933683	0.9902	0.9921	34.6483	-34.648	48.99988	0.021278	0.021796	I	0.970874	0.970795	0.969828
6	0.970146	0.999111	0.9508	0.99	0.992	49	0.0001	49	0.019346	0.019551	I	0.970874	0.970795	0.969828
6	0.969092	0.999179	0.948375	0.9901	0.992	34.648	34.6483	48.99988	0.020717	0.02093	I	0.970874	0.970795	0.969828
6	0.924733	0.999043	0.895288	0.9905	0.9922	-0.0003	98	98	0.029445	0.030859	M	0.970874	0.970795	0.969828
6	0.915622	0.998974	0.88488	0.9906	0.9922	-37.5034	90.5401	98.00008	0.030742	0.032484	M	0.970874	0.970795	0.969828
6	0.911175	0.999111	0.880264	0.9906	0.9922	-69.2967	69.2962	97.99998	0.030911	0.032811	M	0.970874	0.970795	0.969828
6	0.910778	0.998974	0.880004	0.9908	0.9922	-90.5404	37.5026	98.00005	0.030774	0.032684	M	0.970874	0.970795	0.969828
6	0.871714	0.998974	0.837226	0.9912	0.992	-98	-0.0004	98	0.034488	0.038058	M	0.970874	0.970795	0.969828
6	0.879281	0.998974	0.845969	0.991	0.9921	-90.5401	-37.5034	98.00008	0.033312	0.036503	M	0.970874	0.970795	0.969828
6	0.855383	0.999043	0.8215	0.9913	0.992	-69.2962	-69.2967	97.99998	0.033883	0.038102	M	0.970874	0.970795	0.969828
6	0.841746	0.998906	0.806566	0.9914	0.992	-37.5026	-90.5404	98.00005	0.03518	0.040117	M	0.970874	0.970795	0.969828
6	0.879159	0.999043	0.848601	0.9911	0.9921	0.0004	-98	98	0.030558	0.03359	M	0.970874	0.970795	0.969828
6	0.876296	0.999043	0.8459	0.9911	0.992	37.5034	-90.5401	98.00008	0.030396	0.033524	M	0.970874	0.970795	0.969828
6	0.880073	0.999111	0.850346	0.991	0.992	69.2968	-69.2962	98.00005	0.029726	0.032673	M	0.970874	0.970795	0.969828
6	0.919302	0.999179	0.89305	0.9908	0.9923	90.5404	-37.5026	98.00005	0.026253	0.027764	M	0.970874	0.970795	0.969828
6	0.898417	0.999179	0.868932	0.991	0.9923	98	0.0004	98	0.029485	0.031776	M	0.970874	0.970795	0.969828

Slot ID	N-Dep	N-DpRI	N-Sput	DpGOF	SpGOF	X	Y	Radius	N-Delta	N-SD	Zone	N-LF	N-HF	N-Du
6	0.93163	0.999111	0.903304	0.9904	0.9922	69.2961	69.2968	97.99998	0.028325	0.029507	M	0.970874	0.970795	0.969828
6	0.900209	0.999111	0.868278	0.9908	0.9922	37.5026	90.5404	98.00005	0.031931	0.034256	M	0.970874	0.970795	0.969828
6	0.829354	0.998701	0.814972	0.9912	0.9917	-0.0006	147	147	0.014381	0.017045	O	0.970874	0.970795	0.969828
6	0.806618	0.998632	0.790167	0.991	0.9914	-38.047	141.991	147.0001	0.016451	0.019987	O	0.970874	0.970795	0.969828
6	0.797896	0.998701	0.78074	0.9911	0.9913	-73.5004	127.3055	147	0.017156	0.021049	O	0.970874	0.970795	0.969828
6	0.803403	0.998496	0.788183	0.991	0.9912	-103.945	103.9443	146.9999	0.01522	0.018592	O	0.970874	0.970795	0.969828
6	0.82936	0.998496	0.818323	0.9909	0.9913	-127.306	73.4996	147	0.011036	0.013132	O	0.970874	0.970795	0.969828
6	0.792405	0.998496	0.778291	0.9907	0.9911	-141.991	38.0458	147	0.014114	0.0175	O	0.970874	0.970795	0.969828
6	0.779469	0.998632	0.762411	0.991	0.9914	-147	-0.0006	147	0.017058	0.021416	O	0.970874	0.970795	0.969828
6	0.77437	0.998632	0.757973	0.9909	0.9915	-141.991	-38.047	147.0001	0.016397	0.020735	O	0.970874	0.970795	0.969828
6	0.795324	0.998564	0.78363	0.9905	0.9909	-127.305	-73.5004	146.9999	0.011694	0.01449	O	0.970874	0.970795	0.969828
6	0.765626	0.998496	0.750943	0.9904	0.9911	-103.944	-103.945	147.0001	0.014682	0.018816	O	0.970874	0.970795	0.969828
6	0.765321	0.998701	0.748257	0.9903	0.9911	-73.4994	-127.306	146.9999	0.017064	0.021811	O	0.970874	0.970795	0.969828
6	0.769541	0.998769	0.754134	0.9908	0.9914	-38.0458	-141.991	147	0.015407	0.019628	O	0.970874	0.970795	0.969828
6	0.788352	0.999111	0.773611	0.9919	0.9921	0.0006	-147	147	0.01474	0.018355	O	0.970874	0.970795	0.969828
6	0.793994	0.999043	0.780575	0.9912	0.9915	38.047	-141.991	147.0001	0.013418	0.016619	O	0.970874	0.970795	0.969828
6	0.81656	0.999248	0.802971	0.9917	0.9918	73.5006	-127.305	147	0.013588	0.016369	O	0.970874	0.970795	0.969828
6	0.811608	0.999316	0.798653	0.992	0.9921	103.9452	-103.944	147.0001	0.012955	0.015711	O	0.970874	0.970795	0.969828
6	0.806229	0.999248	0.793512	0.9923	0.9923	127.3061	-73.4994	147	0.012717	0.015529	O	0.970874	0.970795	0.969828
6	0.787103	0.999316	0.771681	0.9921	0.9923	141.9913	-38.0458	147	0.015423	0.019217	O	0.970874	0.970795	0.969828
6	0.778128	0.999248	0.759384	0.9922	0.9923	147	0.0006	147	0.018743	0.023521	O	0.970874	0.970795	0.969828
6	0.775489	0.999248	0.756861	0.9921	0.9924	141.991	38.047	147.0001	0.018628	0.023457	O	0.970874	0.970795	0.969828
6	0.807651	0.999248	0.793071	0.9923	0.9922	127.3054	73.5006	147	0.014579	0.017732	O	0.970874	0.970795	0.969828
6	0.792114	0.999043	0.774751	0.9919	0.9921	103.9443	103.9452	147.0001	0.017363	0.02145	O	0.970874	0.970795	0.969828
6	0.787333	0.999043	0.767099	0.9918	0.992	73.4994	127.3061	147	0.020234	0.025055	O	0.970874	0.970795	0.969828
6	0.787312	0.999248	0.767933	0.9915	0.9918	38.0458	141.9913	147	0.019379	0.024023	O	0.970874	0.970795	0.969828
7	0.939974	0.999111	0.919435	0.9899	0.992	0	0	0	0.020539	0.021383	C	0.941748	0.941752	0.94181
7	0.95004	0.999043	0.923416	0.99	0.9921	-0.0001	49	49	0.026624	0.02726	I	0.941748	0.941752	0.94181
7	0.940003	0.998906	0.912353	0.99	0.992	-34.6483	34.648	48.99988	0.027651	0.028575	I	0.941748	0.941752	0.94181

Slot ID	N-Dep	N-DpRl	N-Sput	DpGOF	SpGOF	X	Y	Radius	N-Delta	N-SD	Zone	N-LF	N-HF	N-Du
7	0.922938	0.999726	0.894743	0.9905	0.9922	-34.648	-34.6483	48.99988	0.028195	0.029644	I	0.941748	0.941752	0.94181
7	0.938962	0.998974	0.913689	0.9901	0.9921	0.0001	-49	49	0.025273	0.02621	I	0.941748	0.941752	0.94181
7	0.945771	0.999111	0.92181	0.9902	0.9921	34.6483	-34.648	48.99988	0.023961	0.024709	I	0.941748	0.941752	0.94181
7	0.960508	0.999111	0.938511	0.9899	0.9919	49	0.0001	49	0.021997	0.022389	I	0.941748	0.941752	0.94181
7	0.959725	0.999179	0.936165	0.99	0.992	34.648	34.6483	48.99988	0.02356	0.023961	I	0.941748	0.941752	0.94181
7	0.921799	0.999111	0.890471	0.9905	0.9922	-0.0003	98	98	0.031327	0.032868	M	0.941748	0.941752	0.94181
7	0.913709	0.998974	0.881773	0.9905	0.9921	-37.5034	90.5401	98.00008	0.031935	0.033771	M	0.941748	0.941752	0.94181
7	0.909045	0.999043	0.876788	0.9906	0.9921	-69.2967	69.2962	97.99998	0.032257	0.034268	M	0.941748	0.941752	0.94181
7	0.907794	0.999043	0.875731	0.9907	0.9921	-90.5404	37.5026	98.00005	0.032063	0.034114	M	0.941748	0.941752	0.94181
7	0.873455	0.998906	0.837981	0.9909	0.9919	-98	-0.0004	98	0.035474	0.039028	M	0.941748	0.941752	0.94181
7	0.879179	0.998974	0.845123	0.991	0.9919	-90.5401	-37.5034	98.00008	0.034055	0.037291	M	0.941748	0.941752	0.94181
7	0.852075	0.999043	0.816816	0.9915	0.9921	-69.2962	-69.2967	97.99998	0.035259	0.039736	M	0.941748	0.941752	0.94181
7	0.840551	0.998974	0.8042	0.9915	0.9919	-37.5026	-90.5404	98.00005	0.036351	0.041454	M	0.941748	0.941752	0.94181
7	0.880169	0.998974	0.84822	0.9909	0.9919	0.0004	-98	98	0.031949	0.035027	M	0.941748	0.941752	0.94181
7	0.876947	0.999043	0.845403	0.991	0.9919	37.5034	-90.5401	98.00008	0.031544	0.034722	M	0.941748	0.941752	0.94181
7	0.879324	0.998974	0.84781	0.991	0.992	69.2968	-69.2962	98.00005	0.031514	0.034599	M	0.941748	0.941752	0.94181
7	0.917568	0.999248	0.889239	0.9907	0.9922	90.5404	-37.5026	98.00005	0.028329	0.02995	M	0.941748	0.941752	0.94181
7	0.896929	0.999111	0.865429	0.9908	0.9921	98	0.0004	98	0.0315	0.033928	M	0.941748	0.941752	0.94181
7	0.904711	0.999248	0.873215	0.9909	0.9921	90.5401	37.5034	98.00008	0.031496	0.033642	M	0.941748	0.941752	0.94181
7	0.929891	0.999043	0.899355	0.9904	0.9922	69.2961	69.2968	97.99998	0.030536	0.031795	M	0.941748	0.941752	0.94181
7	0.899222	0.999111	0.865546	0.9908	0.9921	37.5026	90.5404	98.00005	0.033676	0.036098	M	0.941748	0.941752	0.94181
7	0.823414	0.998837	0.80641	0.9917	0.9919	-0.0006	147	147	0.017004	0.020232	O	0.941748	0.941752	0.94181
7	0.81046	0.998632	0.792539	0.9911	0.9914	-38.047	141.991	147.0001	0.017921	0.021633	O	0.941748	0.941752	0.94181
7	0.80325	0.998701	0.785213	0.9911	0.9912	-73.5004	127.3055	147	0.018037	0.021962	O	0.941748	0.941752	0.94181
7	0.804652	0.998564	0.788798	0.9909	0.9912	-103.945	103.9443	146.9999	0.015854	0.019322	O	0.941748	0.941752	0.94181
7	0.835161	0.998496	0.823952	0.9904	0.991	-127.306	73.4996	147	0.011209	0.013243	O	0.941748	0.941752	0.94181
7	0.794183	0.998496	0.779793	0.9907	0.991	-141.991	38.0458	147	0.01439	0.017796	O	0.941748	0.941752	0.94181
7	0.781725	0.998701	0.764979	0.9907	0.9912	-147	-0.0006	147	0.016746	0.020972	O	0.941748	0.941752	0.94181
7	0.774477	0.998632	0.757835	0.9909	0.9915	-141.991	-38.047	147.0001	0.016642	0.021036	O	0.941748	0.941752	0.94181

Slot ID	N-Dep	N-DpRl	N-Sput	DpGOF	SpGOF	X	Y	Radius	N-Delta	N-SD	Zone	N-LF	N-HF	N-Du
7	0.766565	0.998632	0.750782	0.9904	0.9911	-103.944	-103.945	147.0001	0.015783	0.020174	O	0.941748	0.941752	0.94181
7	0.763574	0.998769	0.745665	0.9904	0.9912	-73.4994	-127.306	146.9999	0.017909	0.022917	O	0.941748	0.941752	0.94181
7	0.767856	0.998906	0.750755	0.991	0.9917	-38.0458	-141.991	147	0.017101	0.021786	O	0.941748	0.941752	0.94181
7	0.787327	0.999111	0.771384	0.992	0.9921	0.0006	-147	147	0.015943	0.019847	O	0.941748	0.941752	0.94181
7	0.790824	0.999043	0.775565	0.9913	0.9916	38.047	-141.991	147.0001	0.015259	0.018929	O	0.941748	0.941752	0.94181
7	0.815057	0.999248	0.799456	0.9916	0.9917	73.5006	-127.305	147	0.015602	0.018782	O	0.941748	0.941752	0.94181
7	0.811777	0.999248	0.796935	0.9918	0.9919	103.9452	-103.944	147.0001	0.014842	0.017955	O	0.941748	0.941752	0.94181
7	0.808111	0.999316	0.79377	0.9922	0.9922	127.3061	-73.4994	147	0.014341	0.017436	O	0.941748	0.941752	0.94181
7	0.788766	0.999316	0.773012	0.9921	0.9921	141.9913	-38.0458	147	0.015754	0.019582	O	0.941748	0.941752	0.94181
7	0.779264	0.999179	0.760079	0.9921	0.9922	147	0.0006	147	0.019185	0.024028	O	0.941748	0.941752	0.94181
7	0.777021	0.999248	0.757911	0.9919	0.9922	141.991	38.047	147.0001	0.01911	0.024004	O	0.941748	0.941752	0.94181
7	0.809397	0.999316	0.794215	0.9922	0.992	127.3054	73.5006	147	0.015182	0.018411	O	0.941748	0.941752	0.94181
7	0.794684	0.999248	0.776638	0.9919	0.9919	103.9443	103.9452	147.0001	0.018046	0.022204	O	0.941748	0.941752	0.94181
7	0.792256	0.999043	0.770395	0.9918	0.992	73.4994	127.3061	147	0.021861	0.026852	O	0.941748	0.941752	0.94181
7	0.791681	0.999248	0.770777	0.9916	0.9917	38.0458	141.9913	147	0.020904	0.025725	O	0.941748	0.941752	0.94181
8	0.955389	0.998974	0.937828	0.9894	0.9916	0	0	0	0.017561	0.01805	C	0.941748	0.941752	1
8	0.962466	0.998974	0.939235	0.9895	0.9918	-0.0001	49	49	0.02323	0.023568	I	0.941748	0.941752	1
8	0.953214	0.998906	0.928644	0.9894	0.9918	-34.6483	34.648	48.99988	0.02457	0.025128	I	0.941748	0.941752	1
8	0.9425	0.998906	0.916707	0.9897	0.9919	-49	-0.0001	49	0.025793	0.026638	I	0.941748	0.941752	1
8	0.934294	.	0.908863	0.99	0.992	-34.648	-34.6483	48.99988	0.025431	0.026498	I	0.941748	0.941752	1
8	0.94936	0.998906	0.926493	0.9896	0.9919	0.0001	-49	49	0.022867	0.02352	I	0.941748	0.941752	1
8	0.959532	0.998974	0.939199	0.9893	0.9917	34.6483	-34.648	48.99988	0.020334	0.020752	I	0.941748	0.941752	1
8	0.972435	0.999043	0.953354	0.9892	0.9917	49	0.0001	49	0.019081	0.019244	I	0.941748	0.941752	1
8	0.971395	0.999179	0.951022	0.9894	0.9917	34.648	34.6483	48.99988	0.020374	0.020543	I	0.941748	0.941752	1
8	0.928264	0.999043	0.89977	0.9901	0.992	-0.0003	98	98	0.028493	0.029781	M	0.941748	0.941752	1
8	0.921166	0.998906	0.892004	0.9901	0.992	-37.5034	90.5401	98.00008	0.029162	0.030686	M	0.941748	0.941752	1
8	0.915115	0.999111	0.885216	0.9901	0.992	-69.2967	69.2962	97.99998	0.029899	0.031639	M	0.941748	0.941752	1
8	0.915256	0.999043	0.885684	0.9903	0.9919	-90.5404	37.5026	98.00005	0.029573	0.031299	M	0.941748	0.941752	1
8	0.878961	0.998974	0.845887	0.9907	0.9918	-98	-0.0004	98	0.033074	0.036264	M	0.941748	0.941752	1

Slot ID	N-Dep	N-DpRl	N-Sput	DpGOF	SpGOF	X	Y	Radius	N-Delta	N-SD	Zone	N-LF	N-HF	N-Du
8	0.862655	0.998974	0.829915	0.9907	0.9916	-69.2962	-69.2967	97.99998	0.03274	0.036565	M	0.941748	0.941752	1
8	0.846702	0.998906	0.812672	0.9911	0.9918	-37.5026	-90.5404	98.00005	0.03403	0.038638	M	0.941748	0.941752	1
8	0.884101	0.999043	0.854889	0.9907	0.9919	0.0004	-98	98	0.029212	0.031984	M	0.941748	0.941752	1
8	0.881935	0.998974	0.853269	0.9906	0.9918	37.5034	-90.5401	98.00008	0.028666	0.03148	M	0.941748	0.941752	1
8	0.886086	0.999043	0.857515	0.9906	0.9918	69.2968	-69.2962	98.00005	0.028571	0.031236	M	0.941748	0.941752	1
8	0.923236	0.999248	0.898056	0.9903	0.992	90.5404	-37.5026	98.00005	0.025181	0.02655	M	0.941748	0.941752	1
8	0.904045	0.999043	0.875668	0.9905	0.9919	98	0.0004	98	0.028378	0.030434	M	0.941748	0.941752	1
8	0.911598	0.999248	0.883557	0.9904	0.992	90.5401	37.5034	98.00008	0.028041	0.029842	M	0.941748	0.941752	1
8	0.936741	0.999043	0.909591	0.99	0.992	69.2961	69.2968	97.99998	0.02715	0.028167	M	0.941748	0.941752	1
8	0.906768	0.999179	0.876373	0.9905	0.992	37.5026	90.5404	98.00005	0.030395	0.032433	M	0.941748	0.941752	1
8	0.831962	0.998701	0.817957	0.9909	0.9913	-0.0006	147	147	0.014005	0.016555	O	0.941748	0.941752	1
8	0.810878	0.998564	0.795009	0.9908	0.9911	-38.047	141.991	147.0001	0.015869	0.019195	O	0.941748	0.941752	1
8	0.803792	0.998701	0.787073	0.9909	0.9911	-73.5004	127.3055	147	0.016719	0.020376	O	0.941748	0.941752	1
8	0.807904	0.998496	0.794033	0.9905	0.9907	-103.945	103.9443	146.9999	0.01387	0.016878	O	0.941748	0.941752	1
8	0.834289	0.998427	0.824338	0.9901	0.9907	-127.306	73.4996	147	0.009951	0.011787	O	0.941748	0.941752	1
8	0.795817	0.998496	0.78309	0.9905	0.9907	-141.991	38.0458	147	0.012727	0.015741	O	0.941748	0.941752	1
8	0.786244	0.998496	0.771496	0.9902	0.9907	-147	-0.0006	147	0.014748	0.018412	O	0.941748	0.941752	1
8	0.774862	0.998496	0.759749	0.9906	0.9912	-141.991	-38.047	147.0001	0.015114	0.019132	O	0.941748	0.941752	1
8	0.797579	0.998701	0.786931	0.9905	0.9907	-127.305	-73.5004	146.9999	0.010648	0.013175	O	0.941748	0.941752	1
8	0.766731	0.998701	0.752505	0.9902	0.9911	-103.944	-103.945	147.0001	0.014227	0.018217	O	0.941748	0.941752	1
8	0.766367	0.998769	0.750547	0.9901	0.9909	-73.4994	-127.306	146.9999	0.015819	0.020225	O	0.941748	0.941752	1
8	0.76695	0.998906	0.751579	0.9908	0.9915	-38.0458	-141.991	147	0.015371	0.019648	O	0.941748	0.941752	1
8	0.788254	0.999043	0.774428	0.9916	0.9918	0.0006	-147	147	0.013826	0.017238	O	0.941748	0.941752	1
8	0.792414	0.999043	0.779675	0.9911	0.9914	38.047	-141.991	147.0001	0.01274	0.015823	O	0.941748	0.941752	1
8	0.814505	0.999179	0.801903	0.9914	0.9916	73.5006	-127.305	147	0.012602	0.015236	O	0.941748	0.941752	1
8	0.812639	0.999248	0.801049	0.9915	0.9917	103.9452	-103.944	147.0001	0.01159	0.014062	O	0.941748	0.941752	1
8	0.809088	0.999248	0.797251	0.992	0.992	127.3061	-73.4994	147	0.011837	0.014419	O	0.941748	0.941752	1
8	0.790877	0.999248	0.77625	0.9919	0.992	141.9913	-38.0458	147	0.014627	0.018159	O	0.941748	0.941752	1
8	0.78216	0.999179	0.764289	0.9919	0.9921	147	0.0006	147	0.01787	0.022337	O	0.941748	0.941752	1

Slot ID	N-Dep	N-DpRI	N-Sput	DpGOF	SpGOF	X	Y	Radius	N-Delta	N-SD	Zone	N-LF	N-HF	N-Du
8	0.809769	0.999179	0.795423	0.992	0.9921	127.3054	73.5006	147	0.014346	0.017408	O	0.941748	0.941752	1
8	0.796512	0.999111	0.779715	0.9918	0.992	103.9443	103.9452	147.0001	0.016797	0.020653	O	0.941748	0.941752	1
8	0.793373	0.999043	0.77385	0.9917	0.9918	73.4994	127.3061	147	0.019523	0.024016	O	0.941748	0.941752	1
8	0.792566	0.999248	0.774115	0.9913	0.9915	38.0458	141.9913	147	0.018452	0.022751	O	0.941748	0.941752	1
9	0.93064	0.999111	0.895573	0.989	0.9915	0	0	0	0.035068	0.036313	C	0.941748	1	0.94181
9	0.940441	0.999111	0.898501	0.9889	0.9917	-0.0001	49	49	0.041941	0.042693	I	0.941748	1	0.94181
9	0.929757	0.998974	0.886573	0.9891	0.9917	-34.6483	34.648	48.99988	0.043184	0.044385	I	0.941748	1	0.94181
9	0.920421	0.998974	0.87622	0.9893	0.9916	-49	-0.0001	49	0.044201	0.045822	I	0.941748	1	0.94181
9	0.914815		0.87169	0.9893	0.9915	-34.648	-34.6483	48.99988	0.043125	0.045018	I	0.941748	1	0.94181
9	0.929694	0.999043	0.889064	0.9891	0.9916	0.0001	-49	49	0.04063	0.041873	I	0.941748	1	0.94181
9	0.937649	0.999111	0.898987	0.989	0.9916	34.6483	-34.648	48.99988	0.038662	0.0396	I	0.941748	1	0.94181
9	0.951931	0.999179	0.915021	0.9887	0.9915	49	0.0001	49	0.036911	0.037327	I	0.941748	1	0.94181
9	0.950379	0.999111	0.911315	0.9887	0.9916	34.648	34.6483	48.99988	0.039064	0.03948	I	0.941748	1	0.94181
9	0.912778	0.999179	0.866043	0.9895	0.9916	-0.0003	98	98	0.046734	0.048706	M	0.941748	1	0.94181
9	0.904974	0.999043	0.857447	0.9897	0.9915	-37.5034	90.5401	98.00008	0.047528	0.049898	M	0.941748	1	0.94181
9	0.901726	0.999179	0.854203	0.9893	0.9913	-69.2967	69.2962	97.99998	0.047523	0.050064	M	0.941748	1	0.94181
9	0.899468	0.999043	0.85223	0.9898	0.9916	-90.5404	37.5026	98.00005	0.047238	0.049897	M	0.941748	1	0.94181
9	0.864969	0.999179	0.814899	0.9903	0.9914	-98	-0.0004	98	0.05007	0.054719	M	0.941748	1	0.94181
9	0.870756	0.999043	0.8223	0.9902	0.9914	-90.5401	-37.5034	98.00008	0.048457	0.052715	M	0.941748	1	0.94181
9	0.84782	0.999179	0.79814	0.9906	0.9915	-69.2962	-69.2967	97.99998	0.04968	0.055354	M	0.941748	1	0.94181
9	0.835374	0.999043	0.78454	0.9907	0.9915	-37.5026	-90.5404	98.00005	0.050834	0.057361	M	0.941748	1	0.94181
9	0.872224	0.999179	0.826063	0.99	0.9912	0.0004	-98	98	0.046161	0.050263	M	0.941748	1	0.94181
9	0.868775	0.999111	0.822692	0.9902	0.9913	37.5034	-90.5401	98.00008	0.046082	0.050371	M	0.941748	1	0.94181
9	0.872092	0.999179	0.82634	0.9901	0.9914	69.2968	-69.2962	98.00005	0.045752	0.049847	M	0.941748	1	0.94181
9	0.909616	0.999248	0.86693	0.9897	0.9916	90.5404	-37.5026	98.00005	0.042687	0.044825	M	0.941748	1	0.94181
9	0.890301	0.999179	0.84463	0.9899	0.9914	98	0.0004	98	0.045671	0.048796	M	0.941748	1	0.94181
9	0.897488	0.999248	0.851504	0.9899	0.9915	90.5401	37.5034	98.00008	0.045984	0.048739	M	0.941748	1	0.94181
9	0.921107	0.999111	0.875981	0.9893	0.9914	69.2961	69.2968	97.99998	0.045126	0.046703	M	0.941748	1	0.94181
9	0.891117	0.999179	0.842568	0.9898	0.9914	37.5026	90.5404	98.00005	0.048548	0.051665	M	0.941748	1	0.94181

Slot ID	N-Dep	N-DpRl	N-Sput	DpGOF	SpGOF	X	Y	Radius	N-Delta	N-SD	Zone	N-LF	N-HF	N-Du
9	0.801506	0.998906	0.770966	0.9902	0.991	-38.047	141.991	147.0001	0.03054	0.036705	O	0.941748	1	0.94181
9	0.797136	0.998837	0.766513	0.99	0.9908	-73.5004	127.3055	147	0.030624	0.036996	O	0.941748	1	0.94181
9	0.797802	0.998701	0.769478	0.9902	0.9908	-103.945	103.9443	146.9999	0.028324	0.034285	O	0.941748	1	0.94181
9	0.828533	0.998769	0.805925	0.9895	0.9901	-127.306	73.4996	147	0.022607	0.026561	O	0.941748	1	0.94181
9	0.78893	0.998769	0.763108	0.9897	0.9905	-141.991	38.0458	147	0.025822	0.031693	O	0.941748	1	0.94181
9	0.775956	0.998906	0.74772	0.9899	0.991	-147	-0.0006	147	0.028236	0.035111	O	0.941748	1	0.94181
9	0.767439	0.998769	0.738347	0.99	0.9912	-141.991	-38.047	147.0001	0.029092	0.036523	O	0.941748	1	0.94181
9	0.7914	0.999043	0.767685	0.9901	0.9904	-127.305	-73.5004	146.9999	0.023715	0.029094	O	0.941748	1	0.94181
9	0.760834	0.998974	0.733878	0.9892	0.9908	-103.944	-103.945	147.0001	0.026957	0.034218	O	0.941748	1	0.94181
9	0.758084	0.999179	0.728841	0.9895	0.991	-73.4994	-127.306	146.9999	0.029243	0.037142	O	0.941748	1	0.94181
9	0.761104	0.999179	0.733063	0.9898	0.9911	-38.0458	-141.991	147	0.028041	0.035534	O	0.941748	1	0.94181
9	0.787841	0.999179	0.761983	0.9907	0.9913	0.0006	-147	147	0.025858	0.031778	O	0.941748	1	0.94181
9	0.78646	0.999248	0.760161	0.9904	0.9912	38.047	-141.991	147.0001	0.026299	0.032358	O	0.941748	1	0.94181
9	0.809004	0.999316	0.781862	0.9908	0.9912	73.5006	-127.305	147	0.027141	0.03246	O	0.941748	1	0.94181
9	0.805065	0.999248	0.778511	0.991	0.9914	103.9452	-103.944	147.0001	0.026554	0.031931	O	0.941748	1	0.94181
9	0.803614	0.999385	0.777724	0.9914	0.9916	127.3061	-73.4994	147	0.02589	0.031211	O	0.941748	1	0.94181
9	0.784872	0.999316	0.757577	0.9914	0.9917	141.9913	-38.0458	147	0.027295	0.033607	O	0.941748	1	0.94181
9	0.774725	0.999248	0.743974	0.9912	0.9919	147	0.0006	147	0.030751	0.038177	O	0.941748	1	0.94181
9	0.772132	0.999248	0.741371	0.9913	0.9918	141.991	38.047	147.0001	0.03076	0.038312	O	0.941748	1	0.94181
9	0.803171	0.999111	0.776035	0.9914	0.9916	127.3054	73.5006	147	0.027136	0.032682	O	0.941748	1	0.94181
9	0.789065	0.999248	0.757914	0.9912	0.9916	103.9443	103.9452	147.0001	0.03115	0.037978	O	0.941748	1	0.94181
9	0.787465	0.999179	0.75346	0.991	0.9916	73.4994	127.3061	147	0.034005	0.041396	O	0.941748	1	0.94181
9	0.785148	0.999453	0.751924	0.9906	0.9913	38.0458	141.9913	147	0.033224	0.040598	O	0.941748	1	0.94181
10	0.950978	0.999111	0.932685	0.9899	0.992	0	0	0	0.018293	0.018873	C	0.970874	0.970795	0.969828
10	0.961075	0.999043	0.93668	0.9899	0.992	-0.0001	49	49	0.024395	0.024755	I	0.970874	0.970795	0.969828
10	0.95148	0.998906	0.925947	0.9899	0.992	-34.6483	34.648	48.99988	0.025533	0.026133	I	0.970874	0.970795	0.969828
10	0.940919	0.998906	0.914177	0.9902	0.9922	-49	-0.0001	49	0.026742	0.027635	I	0.970874	0.970795	0.969828
10	0.932857	.	0.906228	0.9904	0.9922	-34.648	-34.6483	48.99988	0.02663	0.027754	I	0.970874	0.970795	0.969828
10	0.949022	0.998974	0.925274	0.9901	0.9921	0.0001	-49	49	0.023748	0.024413	I	0.970874	0.970795	0.969828

Slot ID	N-Dep	N-DpRl	N-Sput	DpGOF	SpGOF	X	Y	Radius	N-Delta	N-SD	Zone	N-LF	N-HF	N-Du
10	0.971952	0.999111	0.951779	0.9899	0.9919	49	0.0001	49	0.020173	0.020333	I	0.970874	0.970795	0.969828
10	0.971169	0.999111	0.949734	0.9898	0.992	34.648	34.6483	48.99988	0.021435	0.021594	I	0.970874	0.970795	0.969828
10	0.925624	0.999111	0.8958	0.9905	0.9921	-0.0003	98	98	0.029824	0.031214	M	0.970874	0.970795	0.969828
10	0.916776	0.998974	0.885301	0.9905	0.9922	-37.5034	90.5401	98.00008	0.031475	0.033193	M	0.970874	0.970795	0.969828
10	0.913654	0.999111	0.882406	0.9905	0.9921	-69.2967	69.2962	97.99998	0.031248	0.03307	M	0.970874	0.970795	0.969828
10	0.912991	0.998974	0.881572	0.9905	0.9921	-90.5404	37.5026	98.00005	0.03142	0.033269	M	0.970874	0.970795	0.969828
10	0.874978	0.998906	0.839984	0.9909	0.992	-98	-0.0004	98	0.034995	0.038457	M	0.970874	0.970795	0.969828
10	0.880842	0.998974	0.847213	0.991	0.992	-90.5401	-37.5034	98.00008	0.033628	0.036774	M	0.970874	0.970795	0.969828
10	0.857146	0.998974	0.822421	0.9912	0.9919	-69.2962	-69.2967	97.99998	0.034725	0.038935	M	0.970874	0.970795	0.969828
10	0.844671	0.998906	0.808892	0.9913	0.9919	-37.5026	-90.5404	98.00005	0.035779	0.040637	M	0.970874	0.970795	0.969828
10	0.883116	0.998974	0.852162	0.9908	0.992	0.0004	-98	98	0.030953	0.033863	M	0.970874	0.970795	0.969828
10	0.878123	0.998974	0.846955	0.991	0.992	37.5034	-90.5401	98.00008	0.031169	0.034278	M	0.970874	0.970795	0.969828
10	0.881951	0.999043	0.851572	0.9911	0.9921	69.2968	-69.2962	98.00005	0.030379	0.033299	M	0.970874	0.970795	0.969828
10	0.922116	0.999179	0.89525	0.9907	0.9922	90.5404	-37.5026	98.00005	0.026866	0.028311	M	0.970874	0.970795	0.969828
10	0.899855	0.999111	0.869583	0.9909	0.9922	98	0.0004	98	0.030272	0.032546	M	0.970874	0.970795	0.969828
10	0.910035	0.999248	0.88033	0.9906	0.9921	90.5401	37.5034	98.00008	0.029705	0.03161	M	0.970874	0.970795	0.969828
10	0.933755	0.999043	0.904406	0.9904	0.9922	69.2961	69.2968	97.99998	0.029349	0.030473	M	0.970874	0.970795	0.969828
10	0.902597	0.999111	0.87025	0.9908	0.9922	37.5026	90.5404	98.00005	0.032347	0.034598	M	0.970874	0.970795	0.969828
10	0.828343	0.998632	0.813461	0.9911	0.9915	-0.0006	147	147	0.014881	0.017648	O	0.970874	0.970795	0.969828
10	0.807095	0.998632	0.790704	0.9908	0.9911	-38.047	141.991	147.0001	0.01639	0.019904	O	0.970874	0.970795	0.969828
10	0.798877	0.998632	0.781175	0.9911	0.9913	-73.5004	127.3055	147	0.017702	0.021679	O	0.970874	0.970795	0.969828
10	0.805286	0.998496	0.789462	0.991	0.9913	-103.945	103.9443	146.9999	0.015825	0.019272	O	0.970874	0.970795	0.969828
10	0.832658	0.998427	0.822052	0.9907	0.9912	-127.306	73.4996	147	0.010606	0.012577	O	0.970874	0.970795	0.969828
10	0.792552	0.998769	0.778724	0.9908	0.9911	-141.991	38.0458	147	0.013828	0.017149	O	0.970874	0.970795	0.969828
10	0.78069	0.998427	0.764227	0.9908	0.9913	-147	-0.0006	147	0.016463	0.020652	O	0.970874	0.970795	0.969828
10	0.774018	0.998564	0.757708	0.9908	0.9913	-141.991	-38.047	147.0001	0.01631	0.020637	O	0.970874	0.970795	0.969828
10	0.797428	0.998427	0.785652	0.9908	0.991	-127.305	-73.5004	146.9999	0.011776	0.014553	O	0.970874	0.970795	0.969828
10	0.763638	0.998564	0.748143	0.9904	0.9911	-103.944	-103.945	147.0001	0.015495	0.019887	O	0.970874	0.970795	0.969828
10	0.766803	0.998632	0.749704	0.9903	0.9911	-73.4994	-127.306	146.9999	0.0171	0.021814	O	0.970874	0.970795	0.969828

Slot ID	N-Dep	N-DpRl	N-Sput	DpGOF	SpGOF	X	Y	Radius	N-Delta	N-SD	Zone	N-LF	N-HF	N-Du
10	0.798536	0.998906	0.785955	0.9912	0.9913	0.0006	-147	147	0.012581	0.015511	O	0.970874	0.970795	0.969828
10	0.795487	0.998974	0.781964	0.9912	0.9914	38.047	-141.991	147.0001	0.013522	0.016715	O	0.970874	0.970795	0.969828
10	0.819501	0.999179	0.805641	0.9915	0.9917	73.5006	-127.305	147	0.01386	0.016631	O	0.970874	0.970795	0.969828
10	0.81436	0.999248	0.801043	0.9918	0.9919	103.9452	-103.944	147.0001	0.013317	0.01609	O	0.970874	0.970795	0.969828
10	0.811044	0.999316	0.798298	0.9921	0.9922	127.3061	-73.4994	147	0.012746	0.015473	O	0.970874	0.970795	0.969828
10	0.789855	0.999179	0.773666	0.9921	0.9922	141.9913	-38.0458	147	0.01619	0.020086	O	0.970874	0.970795	0.969828
10	0.779965	0.999111	0.76049	0.992	0.9922	147	0.0006	147	0.019475	0.024361	O	0.970874	0.970795	0.969828
10	0.779774	0.999179	0.760729	0.9919	0.9922	141.991	38.047	147.0001	0.019045	0.023842	O	0.970874	0.970795	0.969828
10	0.809238	0.999111	0.793738	0.9921	0.9921	127.3054	73.5006	147	0.0155	0.018794	O	0.970874	0.970795	0.969828
10	0.794094	0.999111	0.776155	0.9919	0.9919	103.9443	103.9452	147.0001	0.017939	0.022091	O	0.970874	0.970795	0.969828
10	0.793442	0.999043	0.773018	0.9917	0.9919	73.4994	127.3061	147	0.020424	0.025095	O	0.970874	0.970795	0.969828
10	0.790356	0.999316	0.770955	0.9915	0.9916	38.0458	141.9913	147	0.019401	0.023959	O	0.970874	0.970795	0.969828

Table 6. Summary Data:

Slot Id	N-LF	N-HF	N-Du	N Rows	Mean N-Dep	Mean N-DpRI	Mean N-Delta	Mean N-SD	Std N-Dep	Std N-DpRI	Std N-Delta	Std N-SD
1	1	1	0.94181	49	0.85134954	0.99905542	0.02028318	0.02277897	0.063051	0.00023422	0.009285	0.009449
2	1	1	1	49	0.85580385	0.99903562	0.01932017	0.02177791	0.071772	0.00027434	0.007331	0.007322
3	1	0.9418	0.94181	49	0.86514352	0.99919333	0.00974501	0.01089066	0.069591	0.00031585	0.006425	0.006877
4	0.9417	1	1	49	0.84358619	0.99913521	0.03377059	0.03814712	0.065798	0.00017363	0.008414	0.007499
5	1	0.9418	1	49	0.87216141	0.99924217	0.0065045	0.00719008	0.073978	0.00026626	0.00611	0.006634
6	0.9709	0.9708	0.96983	49	0.85532706	0.99899236	0.02185316	0.02461995	0.06753	0.0002633	0.007321	0.007149
7	0.9417	0.9418	0.94181	49	0.85386763	0.9990105	0.02330925	0.02624019	0.064311	0.00024621	0.007552	0.007251
8	0.9417	0.9418	1	49	0.85906521	0.99895712	0.02091248	0.02345723	0.068257	0.00023201	0.007172	0.006956
9	0.9417	1	0.94181	49	0.84708939	0.99910386	0.03663108	0.04107272	0.062798	0.00016646	0.008996	0.007905
10	0.9709	0.9708	0.96983	49	0.85760453	0.99894572	0.02221193	0.02493569	0.067449	0.00024386	0.007542	0.007345

The terms “Std” are standard deviation terms derived from the entire data set and “N Rows” is the term which represents the point of measurement taken from the set of 49 data points collected from a single wafer.

Chapter 4

Uncertainties of the models:

In this study, not only can the three main factors affect the entire model, oxygen gas, argon gas, chamber pressure, the calibration of each parameter and several other factors affect the process. Some of those points are discussed here.

The hardware setup is one of the most important factors in microelectronic fabrication. For this thesis, the experimental setup is shown in Figure 57. The cleaning of chambers, loadlocks, transfer modules, the hardware replacements, the injectors, their radius of apertures etc. are some of the factors that really affect process indirectly or directly. A power generator replacement can also cause calibration issues. In this study, it was discovered that the cleaning of injectors and their apertures is very important. The gas injectors are shown in Figure 58. This does not exclude cleaning of the main process chamber.

There is always a hardware cleaning cycle for cleaning out the deposition of silicon dioxide in entire process chamber after every 12 product wafers get processed. Its achieved by coating the particles with a thick coat of oxide or by etching the layers of oxide and cleaning the chamber of particles and previous layers.

Such regular cleaning cycles normally use ceramic or bare test wafers and the cleaning process is performed after the process chamber is ready for manufacturing. Hence on the basis of continuous monitoring, the process tool can be analyzed for its behavior over a duration of months especially during any process excursion. Also, a

similar monitoring approach can address for future issues as well when such an occurrence is observed again.

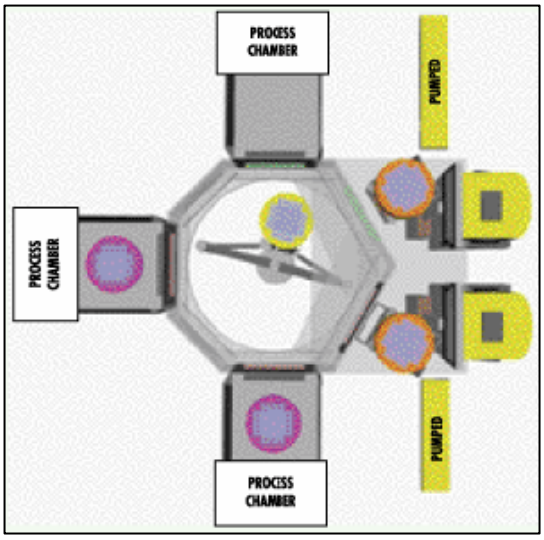

Figure 56. The internal set up of process chambers and the loadlocks along with transfer module.

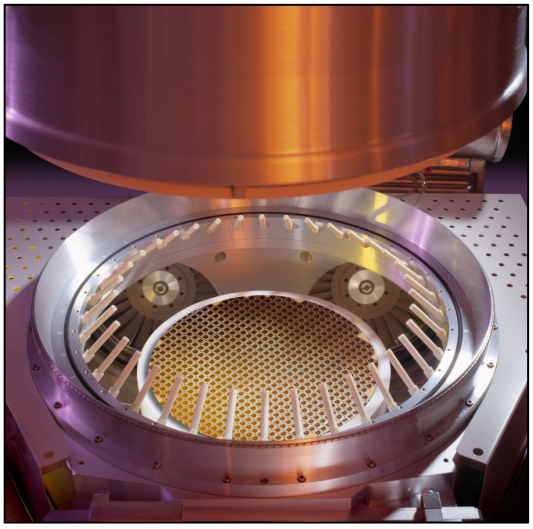

Figure 58. Another figure showing the actual process chamber with its gas injectors all focusing in the centre.

Overall, there can be many other hardware factors affecting the process tool without even changing drastically or without even getting noticed on a normal course. Hence for such research for a particular process issue, up to date monitoring and history of the tool is required and an account of such hardware changes, calibration changes, overall process shifts or parameter value change can make a huge impact and can also imbalance the study of such experiments and hence they have to be accounted as well during such a detailed study. Thus, by making sure that all the factors have been noticed and firmly accounted, one can make better judgment from the data obtained from such design of experiments.

Chapter 5

Conclusion

The low frequency and high frequency powers do affect the process deposition rates and the sputtering rates as well. As shown in the data and model, the effect of HF and LF is completely opposite to one another. Therefore increasing the biasing would not increase the deposition rates and sputtering rates. Appropriate biasing and the proper balance between the two is critical in this. Also, sputter to deposition ratio needs to be under a certain value according to the process recipe for the particular geometry, as high sputter to deposition ratio would not only cause etch-outs or voids, but they also harm the structures irreversibly. Hence sputter to deposition ratios, total power, LF power and HF power and a proper balance of sputtering gas flows are important during manufacturing. From this work, in later stages, a thicker layer of HDP is recommended (100Å or more thicker) so that the HPD layer can be deposited without issues. As a result, the tunneling effect of the NAND cells would be improved with enhanced quality in trench isolation. These recommendations would be create more reliable products that also last longer.

REFERENCES

[1] Gordon Moore, "*Cramming more components onto integrated circuits*", Electronics, Volume 38, Number 8, April 1965.

[2] Roberto Bez, Emilio Camerlenghi, Alberto Modelli, Angelo Visconti, "*Introduction to Flash Memory*", Proc. IEEE, Vol. 91, No. 4, April 2003

[3] Communication and resources from CVD dept, Micron Technology, Virginia, 2006-2007.

[4] Eric W. Law, "*Structures of silicates*", Introduction to Mineralogy, Muskingum College.

[5] S. Eliezer and Y. Eliezer, "*The Fourth State of Matter, an Introduction to Plasma Science*", second edition 2001.

[6] Stephen A. Campbell, "*The Science and Engineering of Microelectronic Fabrication*", second edition.

[7] W. R. Grove, *Philos. Trans. Faraday Soc*. 87 (1852).

[8] I. Langmuir, *General Electric Rev*. 26:731(1923).

[9] M. Armacost, P.D. Hoh, R. Wise, W. Yan, J.J. Brown, J.H. Keller, G.A. Kaplita, S.D. Halle, K.P. Muller, M.D. Naeem, S. Srinivasan, H.Y. Ng, M. Gutsche, A. Gutmann, B. Spuler, "*Plasma-etching processes for ULSI semiconductor circuits*", IBM Journal of Research and Development.

[10] G. K. Wehner, *Adv. Electron. Electron Phys.* **VII**:253 (1955).

[11] M. L. Tarng and G. K. Wehner, "Alloy Sputtering Studies with in-situ Auger Electron Spectroscopy," *J. Appl. Phys.* **42**:2449 (1971).

[12] L. I. Maissel and R. Glang, eds., Handbook of Thin Film Technology, McGraw-Hill, New York, 1970, pp. 3-23.

[13] Hua Ji, "*HDP CVD Process for void-free gap fill of a high aspect ratio trench*", United States Patent # 20030162363, (2003).

[14] M.M. Moslehi, K.C. Sarawat, IEEE-ED 32 (1985) 106.

[15] C.S. Pai, Mater. Chem. Phys. 44 (1995) 1.

[16] Chuan Jie Zhong, Hiroaki Tanaka, Shigetoshi Sugawa, Tadahiro Ohmi, "*Improvement of the electrical properties of PECVD silicon oxide using high-density and low-ion-energy plasma post-treatment*", Journal of Non-Crystalline Solids 351 (2005) 2232–2237.

[17] J. Isidorović, "*Paschen Curves and spatial distribution of emitted light of glow discharge in the air*", Acta Phys. Pol. A 88 Supplement, S-37 (1995).

[18] K. Frank, J. Christiansen, "*The Fundamentals of the Pseudospark and Its Applications*", IEEE Transactions on Plasma Science, Vol. 17 No. 5, October 1989.

[19] Friedrich Paschen, "*Ueber die zum Funkenübergang in Luft, Wasserstoff und Kohlensäure bei verschiedenen Drucken erforderliche Potentialdifferenz*", Wied. Ann., 37, 69, 1889.

[20] Resources from Intel Corporation, 2007.